QUEOS,
a Simulation-Experiment
of the Premixing Phase of
a Steam Explosion with
Hot Spheres in Water
Base Case Experiments

L. Meyer, G. Schumacher

Institut für Neutronenphysik und Reaktortechnik
Projekt Nukleare Sicherheitsforschung

April 1996

QUEOS, a Simulation-Experiment of the Premixing Phase of a Steam Explosion with Hot Spheres in Water Base Case Experiments

L. Meyer, G. Schumacher

Institut für Neutronenphysik und Reaktortechnik
Projekt Nukleare Sicherheitsforschung

ABSTRACT

This report describes the QUEOS facility and gives the results of the first test series performed up to 6/1995.

The premixing phase of a steam explosion is investigated experimentally with simulant materials. The transient three-dimensional multi-component interaction of molten corium with water is studied using a large number of small solid spheres at temperatures up to 2300 °C. The objective of the experiments is to establish a data base for testing the models of heat and momentum transfer in multi-fluid codes as well as the code's capability to correctly describe multiphase flows. The experiments have the advantage that the diameter of the 'coarse melt fragments' are known and that detailed measurements can be performed without the danger of a steam explosion.

In this first series of experiments up to 10 kg of spheres (max. 24000 pieces) were used. The spheres, made of molybdenum or zirconia, were heated to temperatures up to 2000 °C and are discharged into 0.5 m^3 of saturated water. High speed films are taken, pressures, temperatures and the steaming rate are measured.

QUEOS, ein Simulationsexperiment der Vorvermischungsphase einer Dampfexplosion mit heißen Kugeln in Wasser

ZUSAMMENFASSUNG

Dieser Bericht beschreibt die QUEOS Anlage und die Ergebnisse der ersten Versuchsserie, die bis 6/1995 durchgeführt wurde.

Die Vorvermischungsphase einer Dampfexplosion wird experimentell mit Simulationsmaterialien untersucht. Die transiente dreidimensionale Multikomponenten-Wechselwirkung von geschmolzenem Corium mit Wasser wird mit einer großen Anzahl von kleinen festen Kugeln mit einer Temperatur von bis zu 2300 °C studiert. Das Ziel der Experimente ist die Erstellung einer Datenbasis zum Testen der Modelle zum Wärme- und Impulsaustausch in Multifluid-Rechenprogrammen, als auch der Fähigkeit der Programme Mehrphasenströmungen richtig zu beschreiben. Die Experimente haben den Vorteil, daß der Durchmesser der 'Schmelzetropfen' bekannt ist und detaillierte Messungen ohne die Gefahr einer Dampfexplosion durchgeführt werden können.

In dieser ersten Serie von Experimenten wurden bis zu 10 kg Kugeln (max 24000 Stück) verwendet. Die Kugeln aus Molybdän oder Zirkondioxid wurden auf Temperaturen bis zu 2000°C aufgeheizt und in 0.5 m^3 gesättigtes Wasser geschüttet. Es wurden Hochgeschwindigkeitsfilme gemacht und Drücke, Temperaturen und Dampfraten gemessen.

Acknowledgments:

CONTENTS

1. BACKGROUND

In the frame of the Light-Water-Reactor safety studies it has been recognized that an energetic steam explosion might occur in the case of a core melt accident and threaten the integrity of the reactor containment. In general a steam explosion can happen when two liquids at very different temperatures come into intimate contact. During a fuel-coolant-interaction (FCI) the hot liquid (fuel) fragments and transfers its internal energy to the colder more volatile liquid (coolant, water). The rate of energy transfer between the fuel and the water determines if the FCI becomes explosive in nature, e.g. a steam explosion. An overview of the state of experimental and analytical work done in this field up to 1993 is compiled in the proceedings of the CSNI specialist meeting on FCI [1] and in a special issue of Nuclear Engineering and Design [2].

A steam explosion is considered to develop through four major phases:
- *premixing*, break up of liquid fuel streams in water into droplets which are surrounded by a water-vapor film;
- *triggering*, destabilization and collapse of the vapor film by a triggering event (shock wave ?), fragmentation of fuel droplets and rapid increase of the surface area and thereby of the heat transfer and vapor production;
- *propagation*, the pressure wave due to the rapid vapor production travels throughout the fuel-water mixture extending the fragmentation and rapid vapor production to a large volume;
- *expansion*, pressure build up, expansion of vapor transforming internal energy into kinetic energy.

Experiments have been and are being performed for each of these stages. In the phase of premixing, the conditions are formed which determine the strength of a potential steam explosion. To study the premixing phase, multi-phase multi-component hydrodynamics computer codes with three velocity fields are used to describe the separate motions of melt, liquid water and steam as well as the heat and mass transfer between them. The most well-known are TEXAS [3], PM-ALPHA [4], CHYMES [5], IFCI [6], MC-3D formerly TRIO-MC [7] and IVA-KA [8] developed as IVA-3 [9]. These codes must be validated against separate effects- and more prototypical experiments.

In one group of experiments molten metal-oxide is poured into water (FARO [10], KRO-TOS [11], MIXA [12], ALPHA [13], PREMIX [14]), in the other group hot solid spheres are used instead of molten material (MAGICO [15], BILLEAU [16] and QUEOS). The use of solid spheres has the advantage that the shape, size and surface area of the hot

material are known and can be varied in a systematic way. Additionally the temperature and material properties can be easily varied. Thus, the models for heat transfer and multi-phase drag can be verified. Because of the large effect of radiation the temperature of the solid spheres should be as high or as close as possible to the temperature of the prototypical melt, which is assumed to have temperatures between 2000 and 3000 K.

The MAGICO experiment involves the pouring of up to ten kilograms of mm-sized steel or zirconiumoxide (ZrO_2) spheres at temperatures of up to 1000 °C or 1500°C, respectively, into an open water-pool at various subcoolings. In the BILLEAU experiment up to 500 steel, aluminum or ZrO_2-spheres with diameters between 5 and 15 millimeter of up to 1000°C are poured into an open water-pool. The BILLEAU geometry in most cases is two-dimensional, i.e. the spheres fall into a water pool arranged in a plane. The pool is only slightly wider than the diameter of the spheres. Both experiments are planned to reach sphere temperatures of 2000°C or 2200°C, respectively.

In the QUEOS-experiment a large quantity of spheres (up to 40 kg or 7000 cm^3) will be heated up to 2300°C and poured into a pool of water at saturation temperature or with subcooling at atmospheric pressure. Up to now charges of 10 kg have been employed. Three types of spheres are used, with two different diameters (4-5 and 10 mm) and two different materials (molybdenum and zirconiumoxide).

The objective of these experiments is to determine, under a variety of conditions:
- the distribution of spheres, water and steam during the mixing process
- the heat transfer rate from hot spheres in water
- the steam generation rate

In this report the test facility, test procedure and a first series of experiments is described.

2. SYSTEM DESCRIPTION

The QUEOS facility (Fig. 2.1) consist of four main parts, the furnace, the intersection valves unit, the release vessel and the venting pipe. Not shown in the scheme are the rectifier for the electric power supply and the heating system for the water.

2.1 Furnace

Figures 2.2 and 2.3 show photographs of the furnace. The layout of the radiation furnace is shown schematically in Figure 2.4. The spheres are heated in a vertical tungsten tube (I.D. 126 mm, O.D. 134 mm, height 1000 mm). The axial zone with a uniform temperature is approximately 55 cm long which amounts to a maximum heated volume of 7000 cm^3. The bottom of this volume is formed by a cone shaped support for the spheres that is monted on a tungsten rod which can be moved down to release the spheres. For the release of the heated spheres a pneumatic system pushes the rod and the bottom into a lower position (Festo DNU-63-650, 1760 N at 6 bar). The tungsten tube is surrounded by four stripes made of tungsten mesh, which are electrically heated by direct current (max., 40 VDC / 2500 A). Ten radiation shields made of tungsten (4), molybdenum (4) and steel (2) sheet metal are positioned around the heating elements and axially at the top and bottom of the tungsten cylinder. This aggregate is contained in an air tight stainless steel box (380 x 380 mm, 1270 mm height), which is water cooled at its outside. A total of 12 separate cooling circuits is used for various parts of the furnace.

For the tests at 1000°C NiCr-Ni thermocouples (type K) and at 1500°C Pt-Rh thermocouples (type B) are used, respectively, to monitor the temperatures of the spheres and of the tungsten cylinder during the heating phase. Figure 2.5 shows typical temperature histories. Based on these data the heating phase of the tests with temperatures ≥1500°C is controlled by a pyrometer measurement of the outside temperature of the tungsten cylinder only. Additionally the flow rate and the inlet and outlet temperature of the cooling water is monitored at several important cooling circuits. The atmosphere in the furnace is argon with 5% hydrogen.

2.2 Valves unit

To separate the furnace atmosphere from the steam atmosphere of the mixing vessel three pneumatic sliding door valves (KAMMERER) are employed (Fig. 2.6 and 2.3). The upper and lower valve are gas tight. The middle valve is designed to hold the hot spheres for several seconds or in case of malfunctions indefinitely. In that case a water cooling would set in. The space between the upper and the lower valve initially contains

the inert atmosphere. During the heating of the spheres all three valves are closed. Before the release of the spheres the upper valve opens, the spheres fall onto the middle valve and are kept there until the upper valve is closed and the lower valve is open. The middle valve has two sliding doors which open symmetrically within 40 ms. The distance between this valve and the water level is 130 cm. After the release of the spheres from the middle valve the lower valve closes again (for the times see Fig. 3.4). All inner surfaces of the intersection valves unit, which is made of stainless steel, are protected against the high temperature spheres by inserts of molybdenum sheet metal. The insert above the middle valve has a diameter of 180 mm and the segments below have a diameter of 200 mm. Consequently the diameter of the sphere stream yields 180 mm after the discharge and the spheres fall freely without touching any walls.

2.3 Water vessel

The water vessel is made of stainless steel frames and glass with an inner cross section of ca. 70 x 70 cm and a height of 138 cm (Fig. 2.7). The exact horizontal cross section is 5250 cm². Three walls have glass windows, made of hardened ESG-Borosilicate-glass (Pyrex®), 32 mm thick, polished for good optical quality and high thermal and mechanical load endurance. The glass has high and uniform transmission properties in the visible and infrared domain. The field of view is 50 cm wide and 113.5 cm high. A reference grid of 10 x 10 cm is mounted close to the inside of each of the windows, consisting of steel wire with 2 mm diameter (Fig.2.8). The fourth wall is the instrumentation wall made of steel (Fig.2.9). It has provisions for 12 thermocouples, 9 pressure transducers and one pyrometer. Additionally three panels can be taken off and can be equipped with other probes or instruments. At the upper end there are two openings, with diameters of 100 and 200 mm respectively, connected to the steam venting pipes (Fig.2.10). These pipes are guard-heated and insulated. During an experiment only one of the pipes is used, the other one is closed at the instrumentation wall. The bottom of the vessel, which has a man-hole, is covered with 49 (a matrix of 7x7) square boxes (10x10x5 cm) for determining the final distribution of the spheres.

The water is heated externally by an electric heater (max. 36 kW). It enters the vessel through two openings in the instrumentation panel near the center and leaves it through two holes near the bottom. All sides of the vessel, including the top and the bottom, are heated from outside by a large number of infrared-radiators with a total maximum power of 10 kW. By controlling all heaters automatically an almost uniform temperature of the water and the vessel walls is obtained. All inner and outer steel-surfaces of the vessel are painted with a hot-water resistant black paint to minimize light reflection.

2.4 Steam vent pipe

The vent pipe (Fig. 2.10) restricts the outflow of the steam from the vessel and there-fore the pressure increase in the vessel is both a function of the steaming rate and the flow resistance of the steam pipe. The pressure loss coefficient is defined as

$$\zeta = \Delta p / (\rho w^2 / 2) \tag{2.1}$$

The flow resistance was measured with a steady state air flow. The total resistance is made up of several parts. The main contribution comes from the orifice plate, the hon-eycomb straightener and the vortex flow meter. The different contributions are:

the orifice plate and honeycomb straightener	$\zeta = 1.76$
the vortex flow meter	$\zeta = 1.73$
the tube (5 m)	$\zeta = 0.60$
three 90 degree pipe turns	$\zeta = 0.45$

that gives a total coefficient of	$\zeta_{total} = 4.54$.

2.5 Instrumentation

The quantities measured are the temperatures of the spheres and water, the pressures in the vessel and in the venting pipe, the steam mass flow rates in the venting pipe, the water level swell and the distribution of the spheres at the vessel bottom. In future test series the local void fraction in the cloud of spheres will be measured also. Of course, the most important instruments are the video and high speed film cameras.

2.5.1 Temperature Measurements

The release temperature of the spheres is monitored by high temperature thermocou-ples or a pyrometer as described in Section 2.1. The temperature of the spheres just before they enter the water is measured by a MAURER-Infrared-Pyrometer with a re-mote glass fiber optic. Its response time is 1 ms, the spectral range is 0,8-1,1 μm and the temperature range is 1200-2400°C. The measurement of the temperature of the spheres during they fall through the water has not been realized yet and will be de-scribed in a later report. The temperatures of the water and steam are measured by Ni-CrNi-thermocouples with a diameter of 0.35 mm. Their positions are shown in Figs. 2.9 and 2.10.

2.5.2 Pressure Measurements

Six KISTLER pressure transducers (Type 4043/43 A1, piezoresistive, max. 2 bar absolute, 14 kHz eigen-frequency) measure the vessel pressure. They are installed at the positions indicated in Fig.2.9 within shielding tubes, which extend 20 mm into the water. In the steam venting pipe the pressure is measured by two miniature piezoresistive transducers (KULITE XTC, max. 0.35 bar differential) with a diameter of 3.7 mm. One of those is mounted flush to the pipe wall, the other one is mounted in a guiding tube extending into the center of the pipe, to measure the total head.

2.5.3 Steaming Rate

The steaming rate is measured by vortex flowmeters (Endress+Hauser, Swingwirl II) which work on the principle of vortex shedding. The frequency of the vortices which are created by the flow passing a strut within the pipe, is unaffected by changes in temperature or pressure, but is strictly proportional to the flow velocity at Reynolds numbers $Re > 2 \cdot 10^4$. The pressure pulsations due to the vortex shedding are measured, counted and transformed into frequency signals, which are proportional to the volume flow rate. The range for saturated steam at 1 bar is 80-700 dm³/s for the 100 mm type, and 300-2500 dm³/s for the 200 mm type.

2.5.4 Water Level

The water level is measured by up to four level meters (Endress+Hauser, Multicap) mounted in the four corners of the vessel cover plate. They consist of a long rod submerged partially into the water and work on the principle of the impedance change of a condenser due to the change of the surrounding medium. In a mixture of water and steam they measure the collapsed height of the water. The time constant is in the order of 20 ms, depending on the water level. For protection against the hot spheres the rods are inside of a open tube. As for the vortex mass flow meter the output signal has a frequency which is proportional to the water level height.

2.5.5 Image taking

Pictures from the experiment are taken from two sides (90°) by two high speed film cameras (LOCAM II and PHOTO SONICS 1PL) and two video cameras (CCD-Color SDT-CS5131). The film cameras are 16 mm, pin-registered, intermittent transport cameras with operating speeds from 2 to 500 frames per second. The speed was set to 500 f/s, the video cameras take 50 frames per second at shutter speeds ≤ 1/1000 second. The positions of the cameras relative to the vessel are shown in Fig. 2.8. The main direction has a long focal distance to reduce the perspective distortion. The background is lighted by a HIGH-S-LIGHT 4000/8000 W BOOST, with a short pass filter of 650 nm cutoff wavelength. The second position of picture taking is against the black background

of the instrumentation panel. Because the windows are 50 cm wide there is a 10 cm wide space on both sides which cannot fully be seen, depending on the camera position. Also the bottom cannot be seen, it is 10 cm below the lower edge of the windows.

2.6 Data acquisition

The data acquisition equipment is contained in an electromagnetic shielded cabin. All sensor cables are shielded and are fed through special plugs into this cabin. The conditioned and amplified signals are then digitized by two DT2839-boards running on two DOS-computers with Turbo Lab® as acquisition software. Table 2.1 lists all pertaining information.

Table 2.1 Instrumentation and data acquisition

Purpose	Location	Instrument	Range	Quantity	Chan. No.	sample freq. [kHz]
pressure, absolute	vessel	piezoresistive (Kistler)	0 - 2 [bar]	6	1-6	1
pressure, differential	vent pipe	piezoresistive (Kulite)	0.35 [bar]	2	7-8	1
temperature	vessel / water	K-thermocouples	0-200 [°C]	8	23-30	1
temperature	vent pipe / steam	K-thermocouple	0-200 [°C]	1	33	1
temperature at impact	vessel / spheres	pyrometer	1200 - 2400 °C	1	17	1
steaming rate	vent pipe	Swingwirl ,impulses (Endres & Hauser)	80-700 [dm³/s]	2	11-12	30
water level	vessel	level meter, impulses (Endres & Hauser)		4	13-16	30

6 m ▽

Pneumatic Release
Mechanism

High-Temperature
Furnace (2600 K)

Argon-atmosphere

Steam-
Flowmeter

SLUICE

Fast Acting-
Valves

3 m ▽

steam-atmosphere

Pyrometer

High-speed-
Camera

Video-
Camera

Heated
Water

0 m ▽
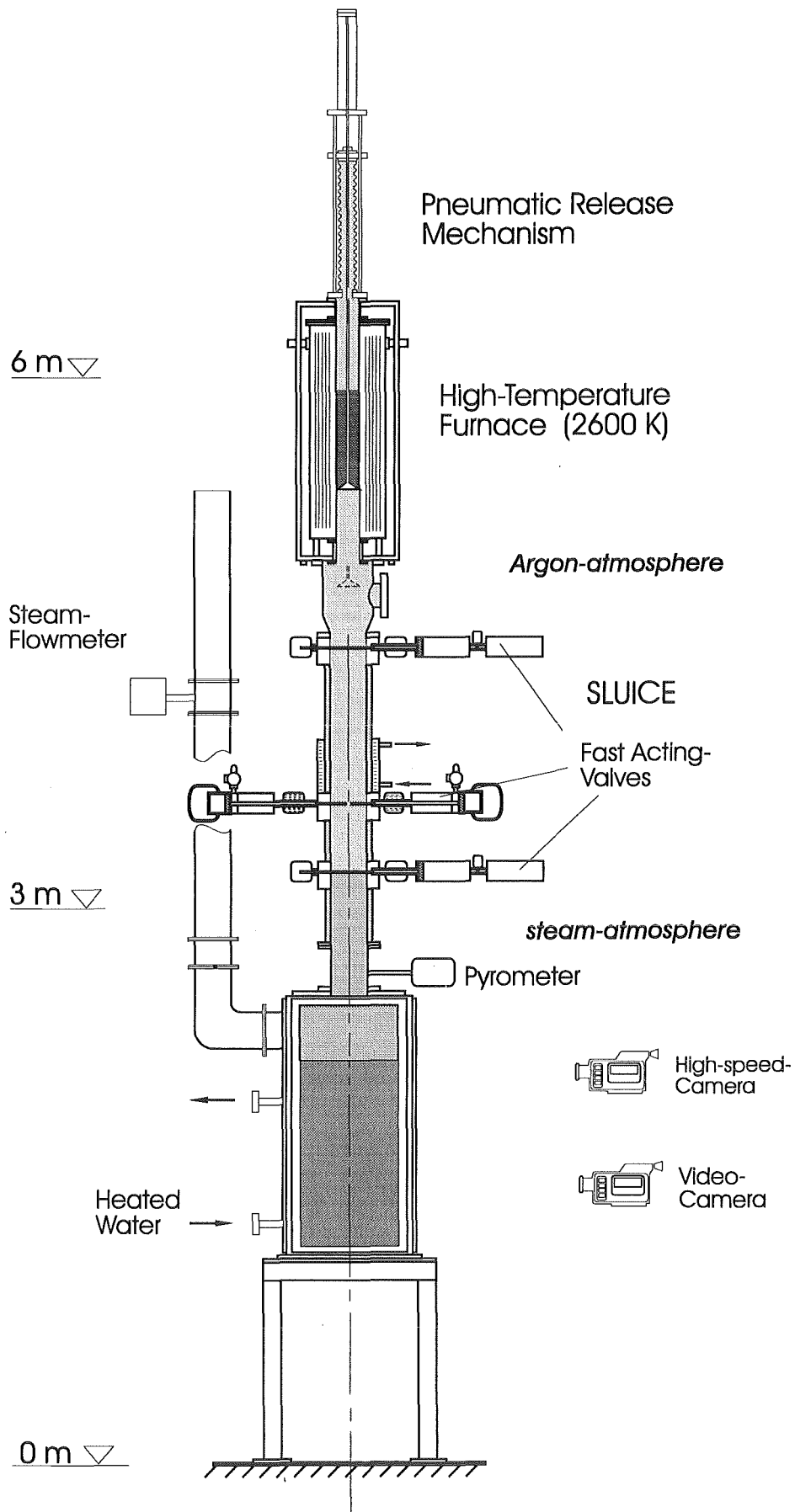
Fig. 2.1   Scheme of the QUEOS facility
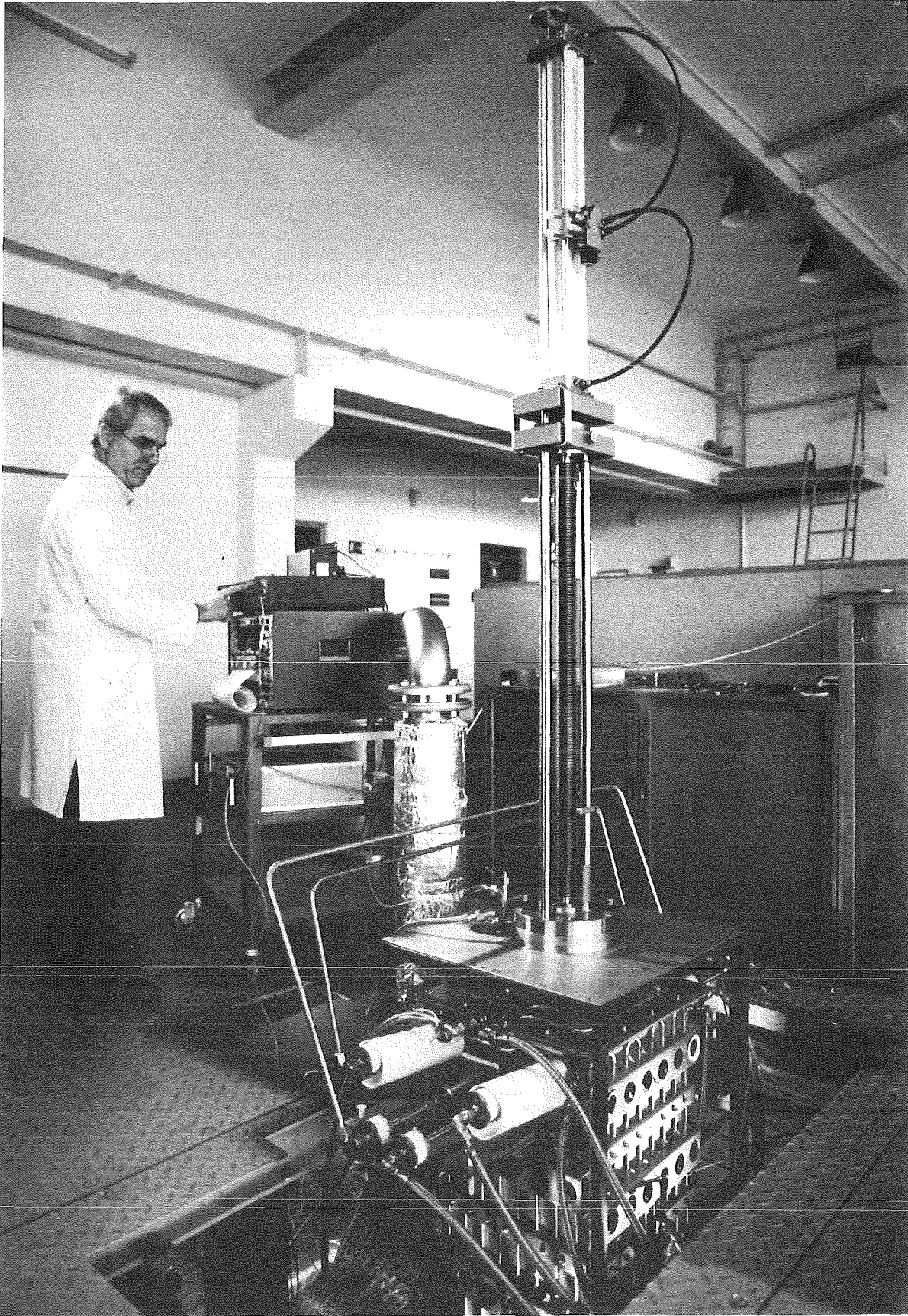
Fig. 2.2 The high temperature furnace with the pneumatic release mechanism
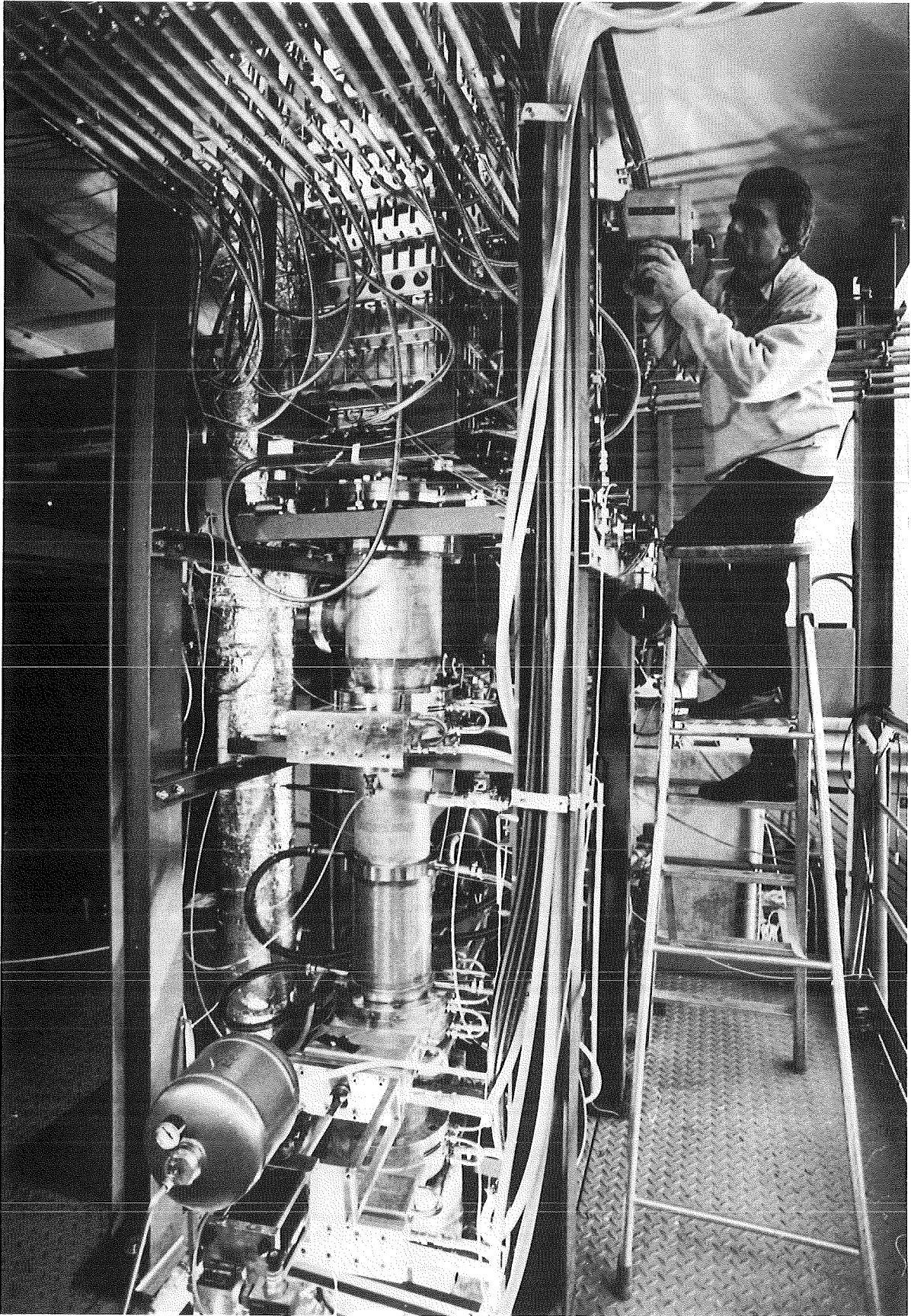
Fig. 2.3 The high temperature furnace and the sliding door valve section
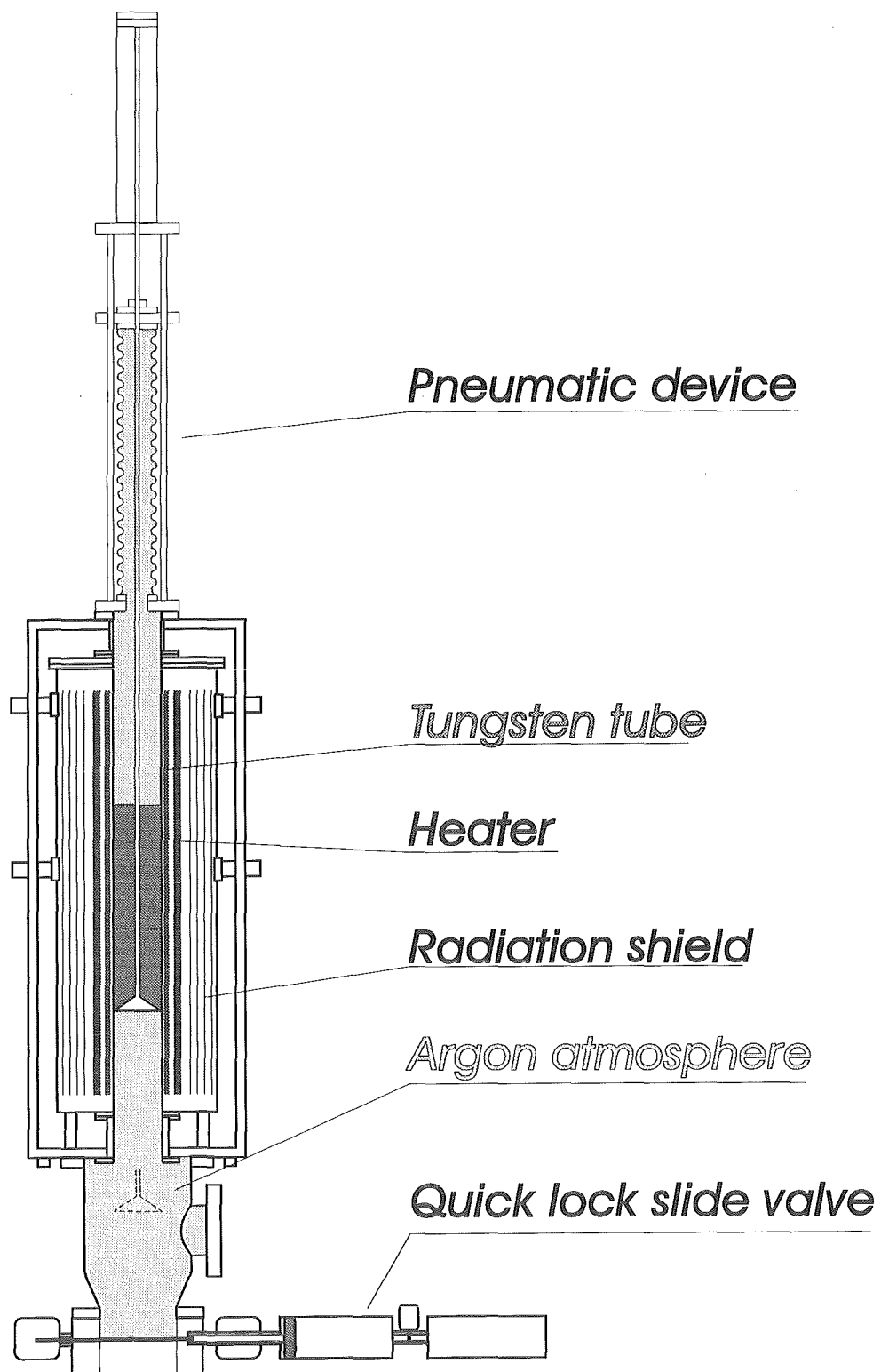
Fig. 2.4   Scheme of radiation furnace
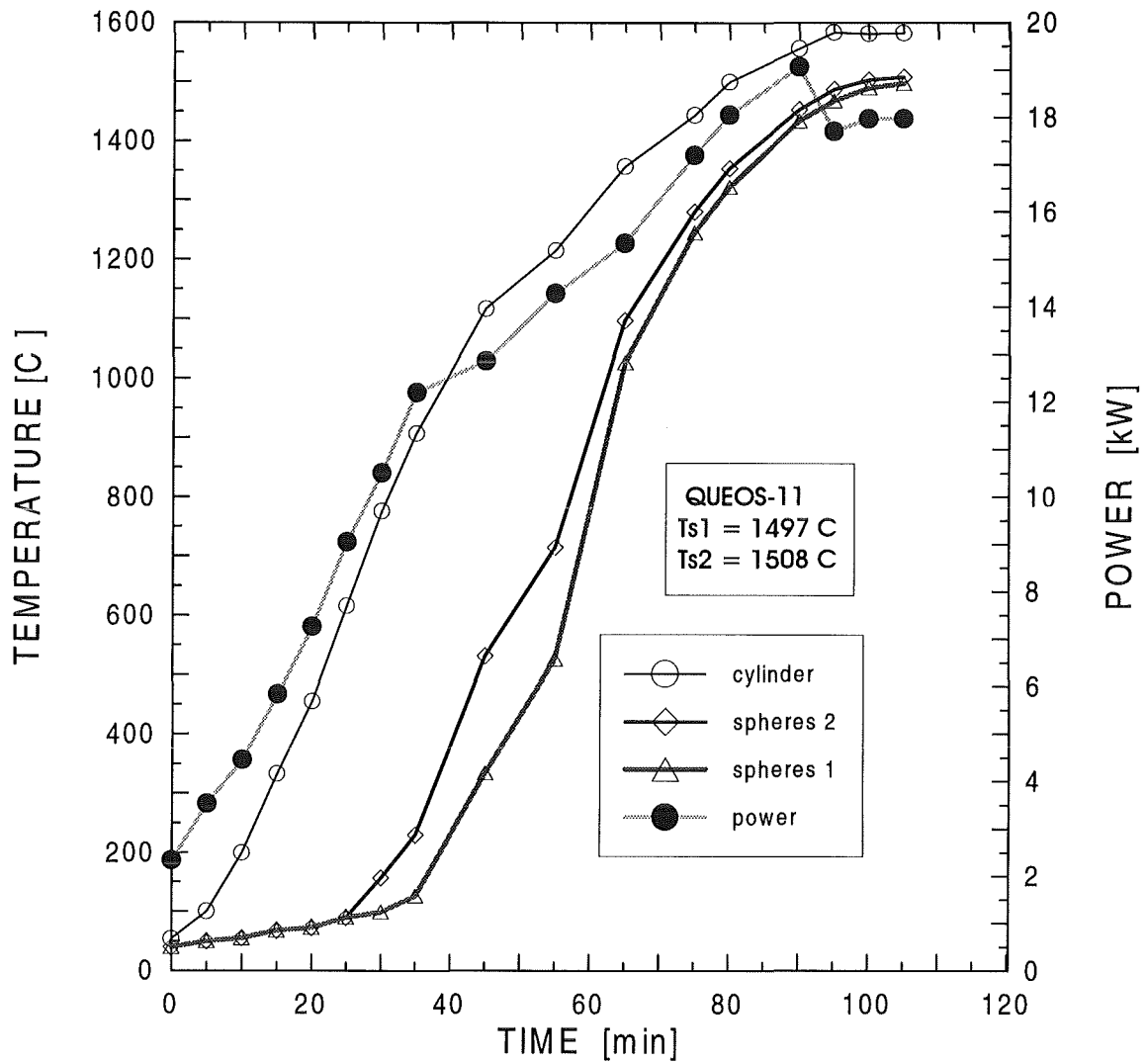
Fig. 2.5 Heating power and temperatures during the heating phase of the spheres

Furnace

Spring- Bellow

Argon - Inlet

Argon - Outlet

Sliding Door Valve 1

875

875

Cooling Water - Inlet

Cooling Water - Outlet

Sliding Door Valve 2

375

Thermocouple

0,35 Ni Cr / Ni

330

Sliding Door Valve 3

215

Argon - Inlet

Ø 207

Ø 215
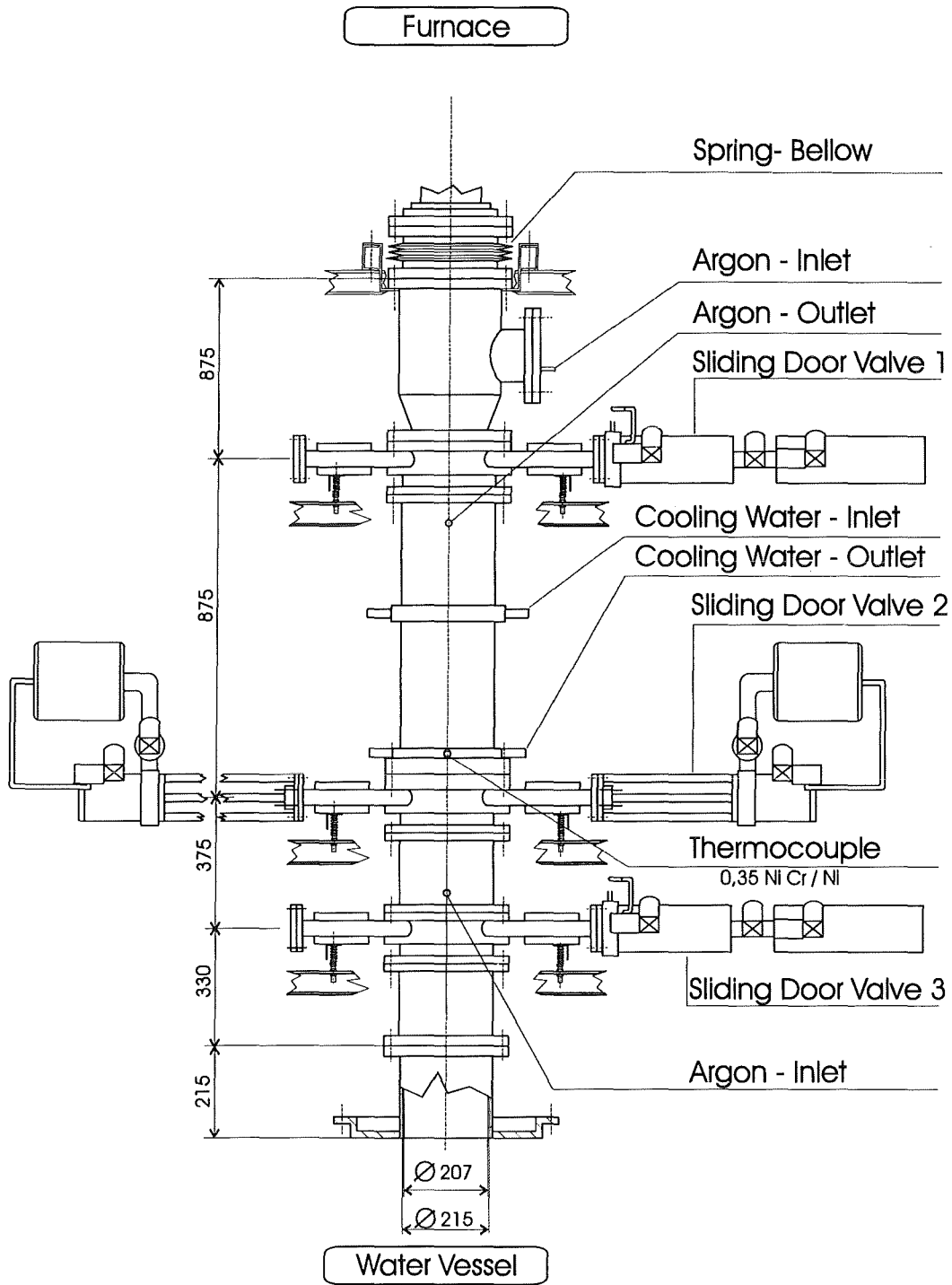
Water Vessel

Fig. 2.6 The fast acting sliding door valve arrangement
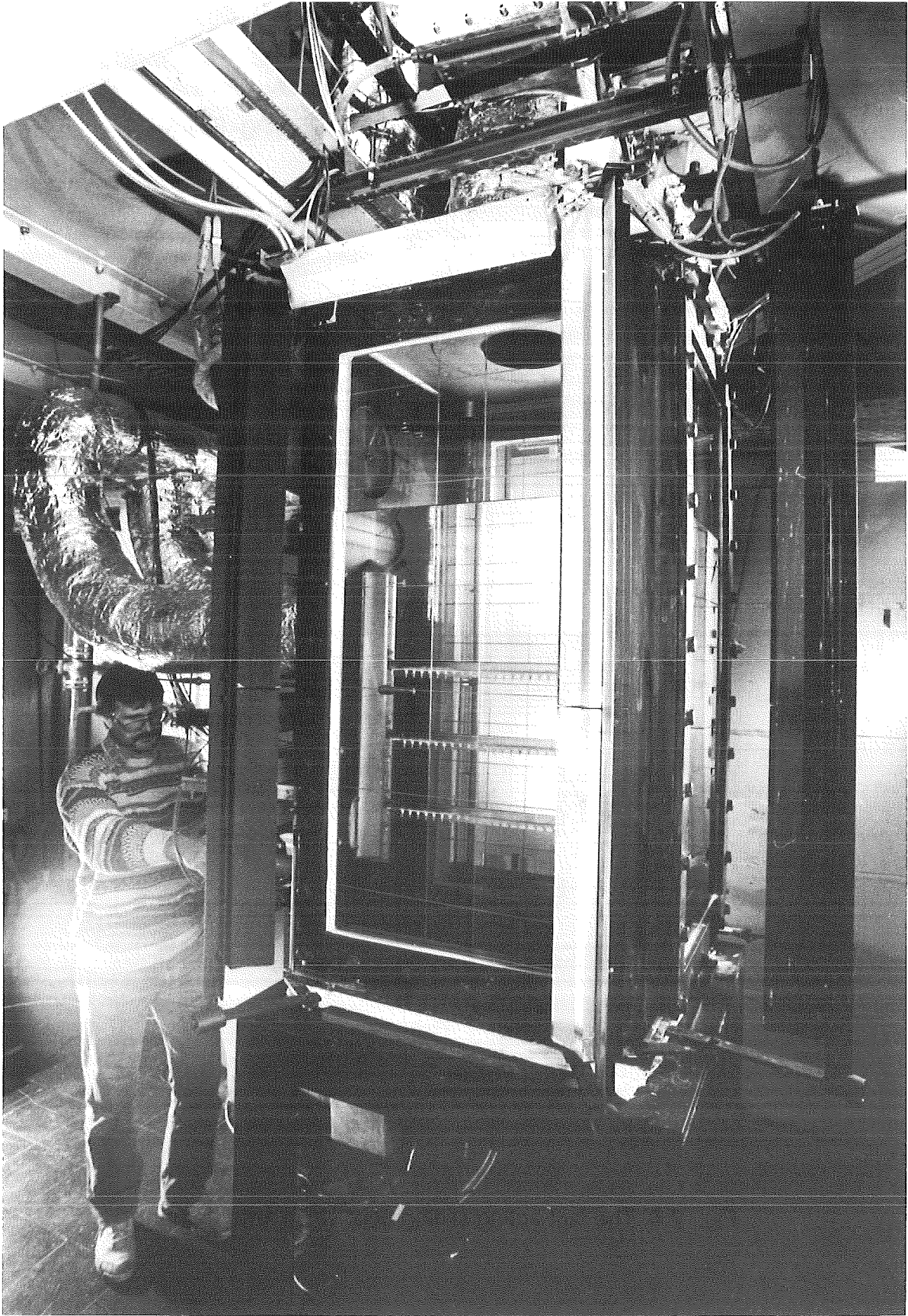
Fig. 2.7   The QUEOS water vessel

WEST (dark background)

Camera

Distance   3,16 m

NORTH (backlighted)

Camera

Distance   6,415 m

BACK WINDOW   FRONT WINDOW
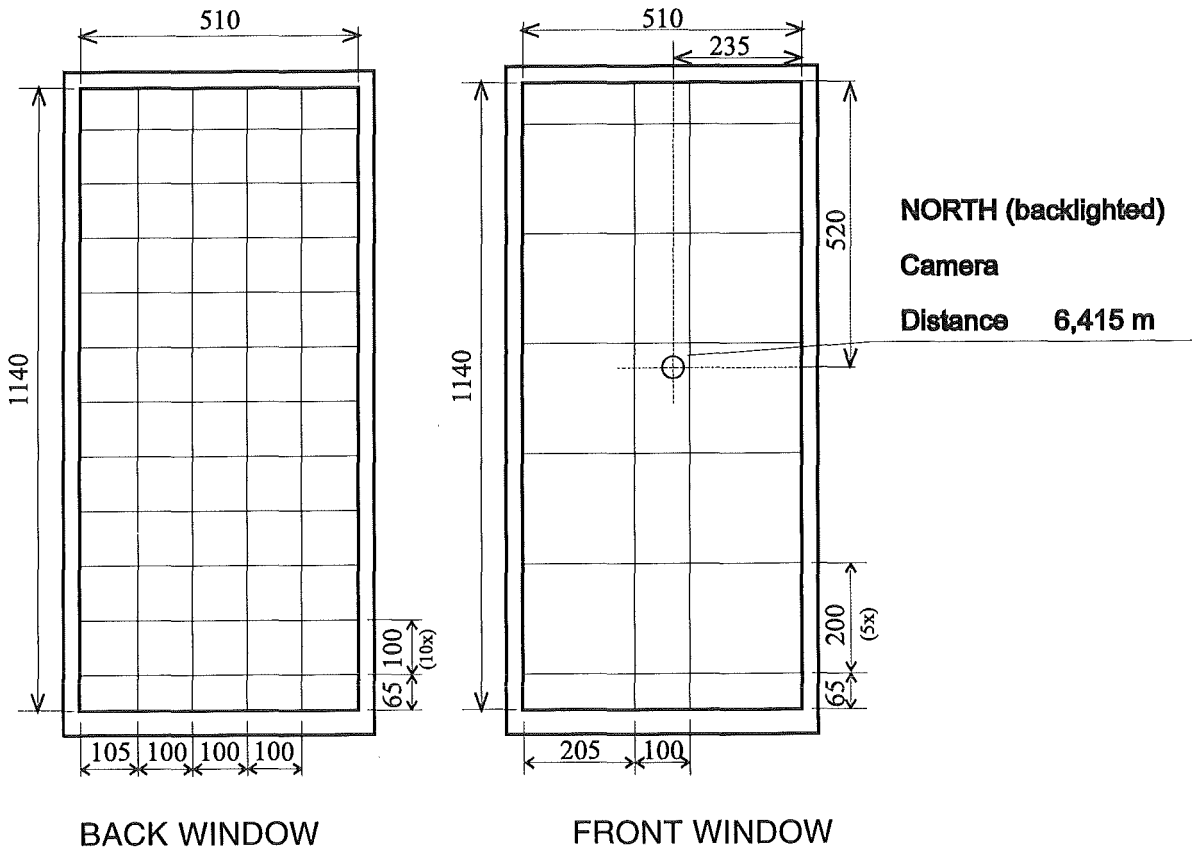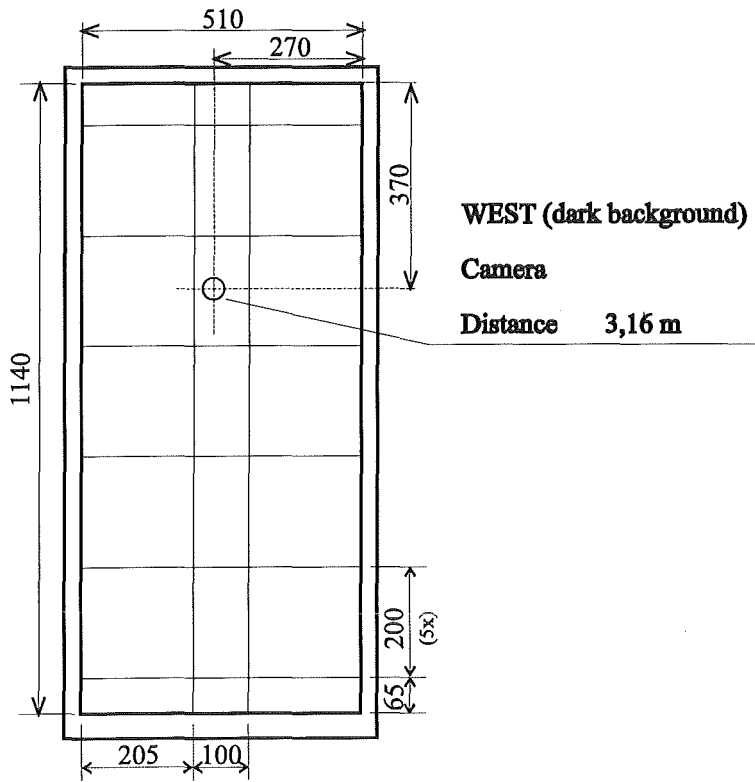
Fig. 2.8 The reference grid of the windows and the camera positions
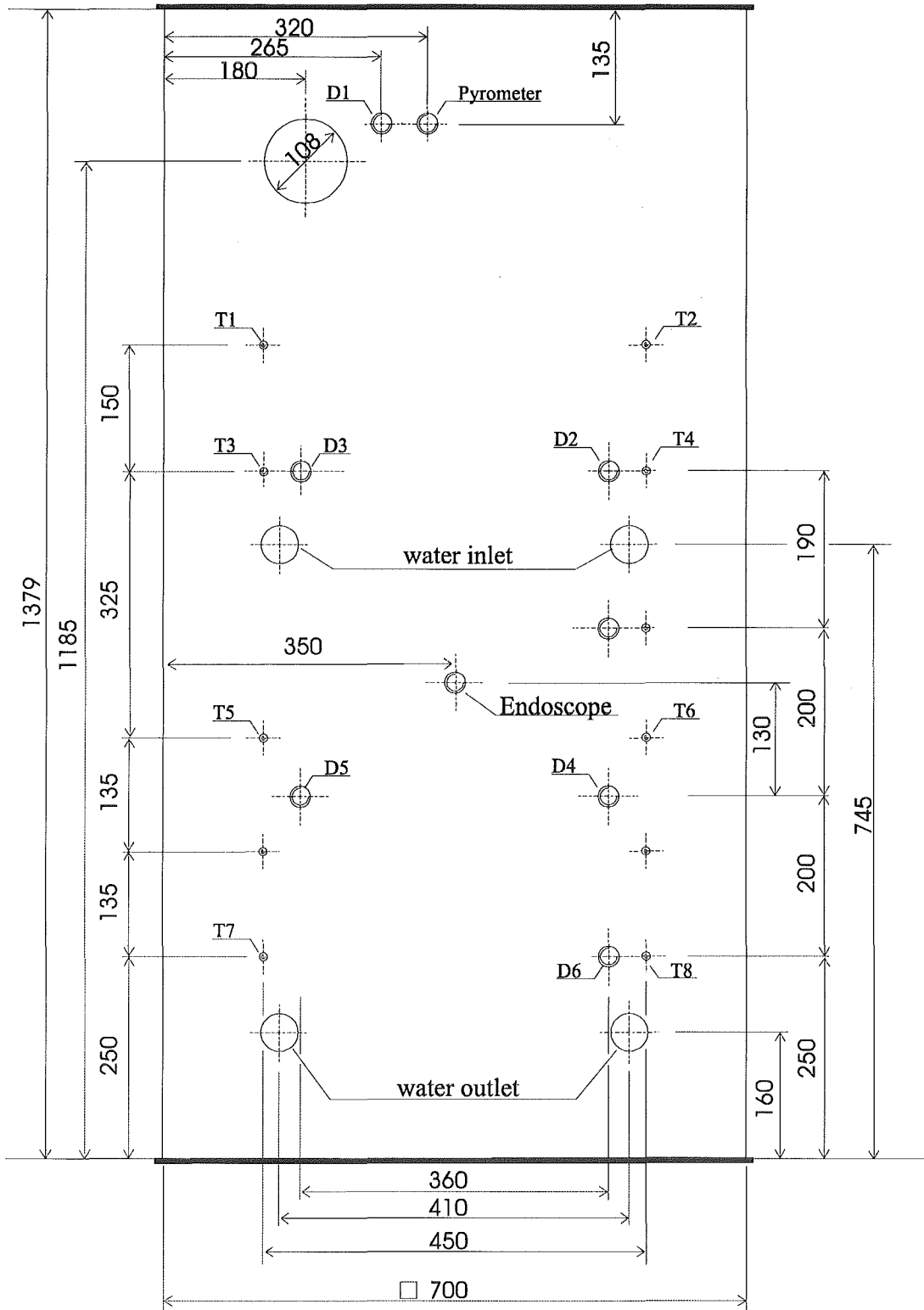
Fig. 2.9 Instrumentation panel in the water vessel, water level is at 1000 mm,
T: thermocouples, D: pressures

Flow Direction

Vortex Flow Meter

Kulite - Pressure Transducer
Total - Head

Static - Pressure

Honeycomb
Ø of holes:	9 mm
Thickness:	0,1 mm
Length:	150 mm

Orificeplate
Ø of holes:	9 mm
Number of holes:	55
Aperture ratio	0,4715
Thickness of plate	10 mm

Thermocouple
0,35 NiCr/Ni

1580

475

1580

75

R 150

75

Ø 108
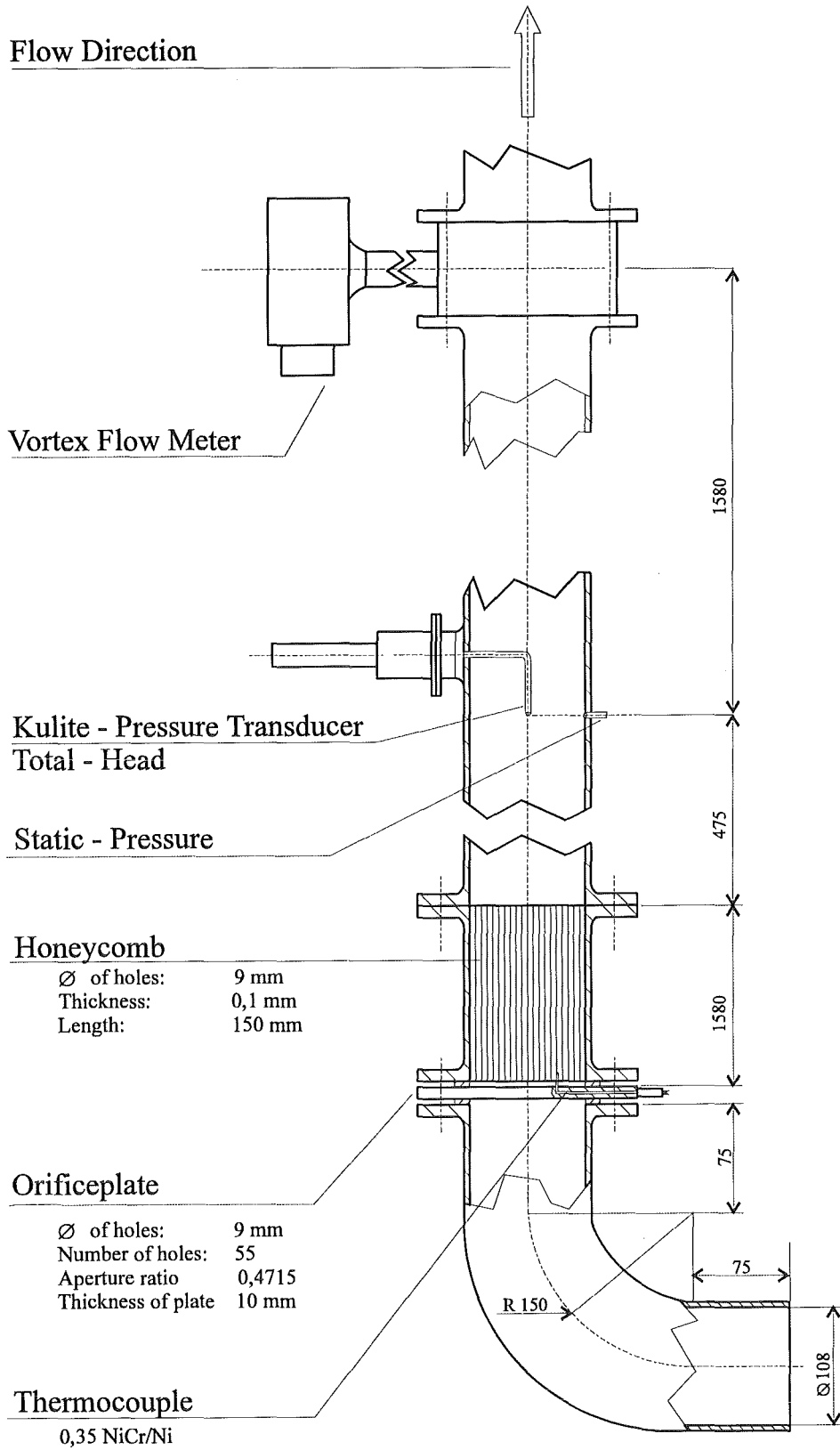
Fig. 2.10 Scheme of the steam venting pipe

3. TEST PROCEDURE

3.1 Pretest operations

One day before an experiment will be conducted the spheres are filled into the furnace through a small pipe, which is inserted into the tungsten cylinder at the top flange connecting the furnace to the bellows of the pneumatic release mechanism. When this flange is installed the furnace and the pipe that leads down to the lower sliding door valve is alternately evacuated and flushed with argon gas for several times. The flushing is continued at low overpressure until the next day. Demineralized water is filled into the test vessel also the day before the experiment will be performed.

Next day all guard heaters and the external water heater are started and are set to control the temperature of the water to 99.5°C and the temperature of the vent pipe and entrance section to the vessel to 104°C. It takes approximately three hours until all temperatures have reached their target value. During this time all systems are checked. The cameras and the video cameras are set into standby mode. A sample data set is acquired and checked for correctness.

Then the water cooling system is started and the circuits for the furnace are opened. Now the heating of the furnace begins and is manually controlled by setting the desired voltage (Fig.3.1 and 3.2). To minimize reactions between spheres and between wall and spheres the heat up time should be as short as possible. On the other hand there is the problem of different thermal expansion due to a radial temperature gradient. The tungsten cylinder heats up first and expands in diameter. The spheres can settle and fill the larger volume. Later the spheres expand and become jammed. Whereas the thermal expansion coefficients for tungsten and molybdenum are similar in the temperature range up to 2000 °C with 5.3×10^{-6} and 6.5×10^{-6}, respectively, the ZrO_2-spheres have an approximately 30% larger coefficient, which aggravates the problem of jamming.

In the experiments with sphere temperatures of 1500 °C and higher the jamming or adherence of spheres in the furnace is the main difficulty. To prevent any oxidization the buffer gas has been changed from pure argon to argon with 5% hydrogen. The Mo-spheres have been coated with a rhenium layer, because exploratory experiments had shown that Mo-spheres stuck together when heated to 2000°C. To prevent or diminish jamming several provisions have been made. The rod which carries the cone shaped bottom is tapered with the smaller diameter at the top end. So when it moves downward it increases the free volume available for the spheres. The experiment with ZrO_2-spheres employed a cone shaped insert holding the spheres, made of 0.5 mm thick

molybdenum sheet metal, which was slightly smaller than the tungsten cylinder at its lower end and decreased in its diameter to the top end. The expanding spheres could enlarge the thin sheet metal insert without damaging the tungsten cylinder. To push the spheres out of the furnace four rods where attached around the central rod with their lower tips just above the upper surface of the spheres fill. They are pushed down together with the central rod and loosen the jammed spheres. In spite of all these provisions a considerable number of spheres did not leave the furnace in some high temperature experiments. In the next test series further changes in the heating procedure are planned.

3.2 Test sequence

After the spheres have reached a nearly uniform temperature, which is monitored by two thermocouples at different radii within the sphere fill, the experiment is started. First the lights, which need a heat-up period of two minutes, are switched on and final adjustments of the backlight system (mirror adjustments) are performed. Then the mechanical lock is removed from the pneumatic release mechanism. When the video cameras are running and all systems are ready the SIMATIC-S5 control system is manually started. This is programmed to activate the release mechanism, the valves, the cameras and the data acquisition in a prescribed timing.

At the start all sliding door valves are closed. The first signal opens the upper valve, which is equipped with a pilot relay and sends a signal back to the SIMATIC when it is open. Now the pneumatic release mechanism, the high speed cameras and the data acquisition are activated. After 2.5 seconds the upper valve closes (closing time is 50 ms) and the lower valve opens, triggered by the pilot signal from the upper valve when it is closed. When the lower valve signals it is open, the middle valve, on which the hot spheres rest, opens symmetrically and releases the spheres to fall into the water. A diagram in Fig.3.3 shows the program structure of the SIMATIC control and Fig.3.4 shows the measured signals from the pilot relays at the valves. After the lower valve is closed again the water cooling circuits for the sliding door valves and the pipe section above the middle valve are opened.

The data are recorded for a period of 20 seconds, the high speed film cameras run for 10 seconds and the video cameras are stopped when the boiling ceases (ca. 40 seconds).

3.3 Posttest operations and data processing

The cooling and argon flushing of the furnace has to be continued for several hours. After the water has been drained from the vessel, the boxes from the vessel bottom are taken out and the spheres are weighed. The raw data are processed with Turbo Lab®, using macros for semi-automatic processing. Applying the calibrating constants the pressure and temperature data are converted into the respective dimensionalized data and are low pass filtered if appropriate. The frequency signals from the vortex mass flow meter and the level meters are transformed into the respective data with special programs written in C (s. Appendix A). The time base for all data is the same with time zero being the instant when the middle valve starts to open and discharges the spheres into the water. All data are available in ASCII format.
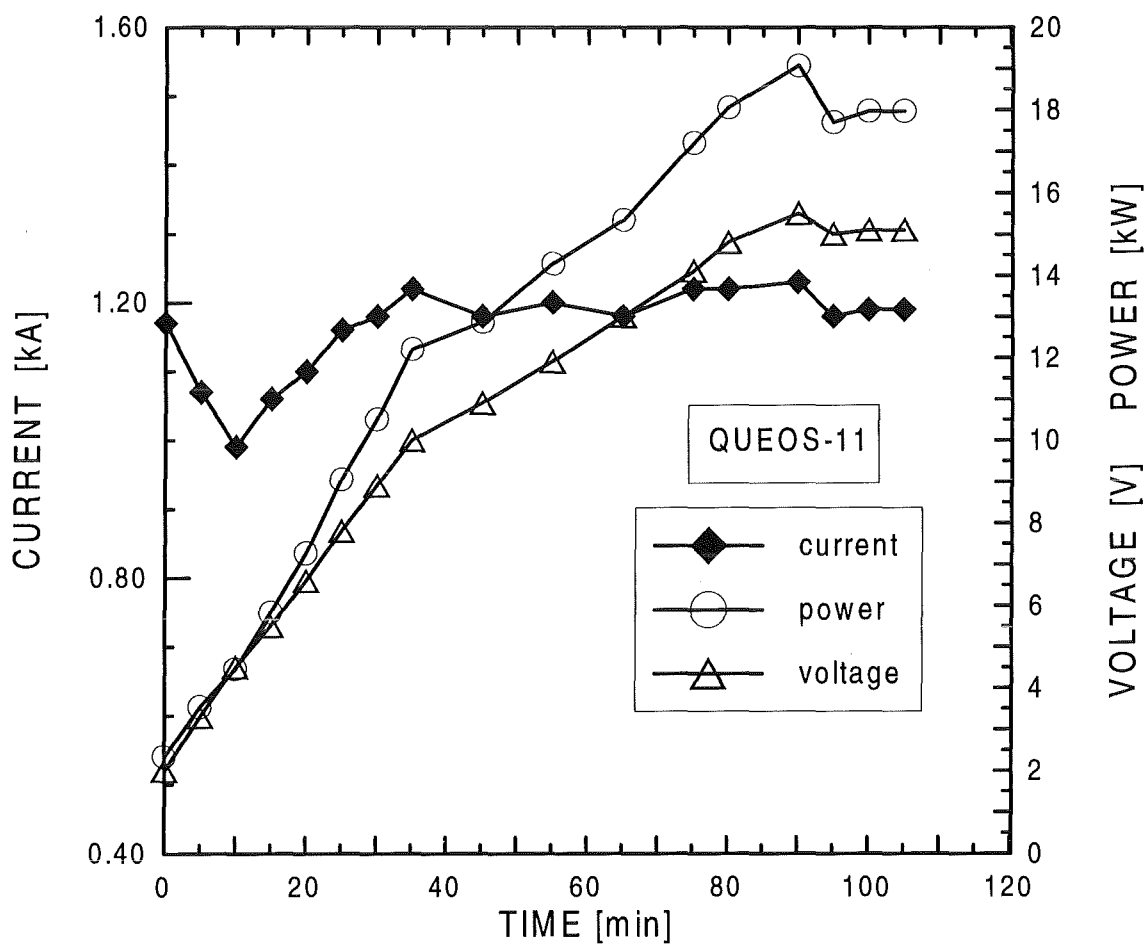
Fig. 3.1 Heating power in run Q-11
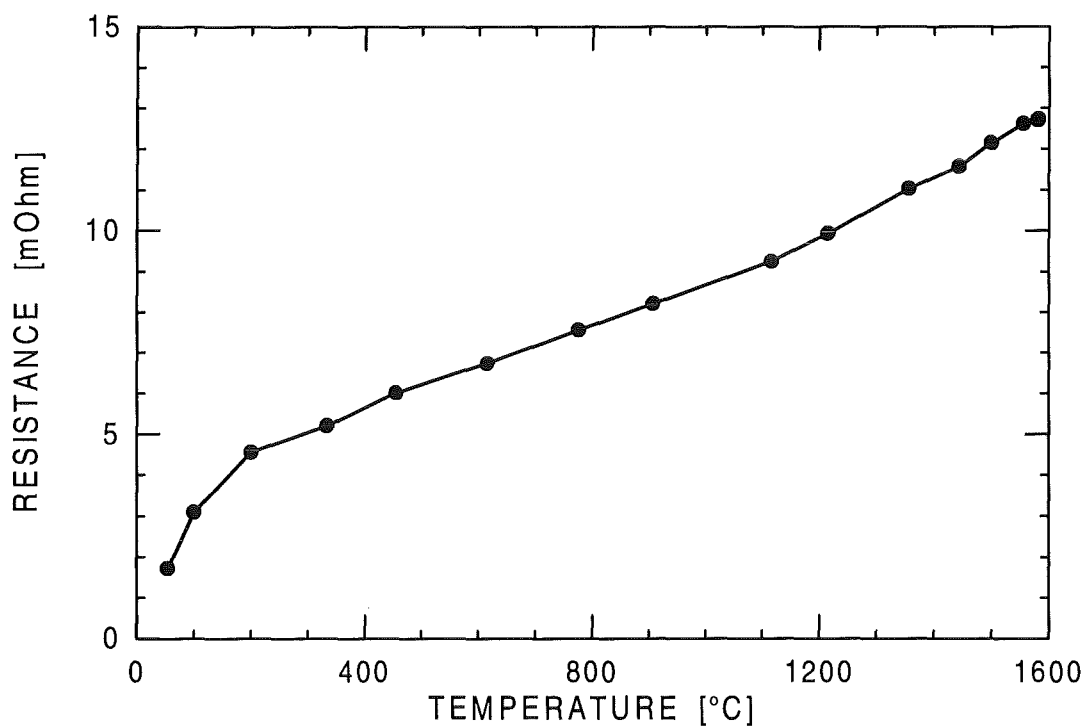
Fig. 3.2 Electric resistance of heater
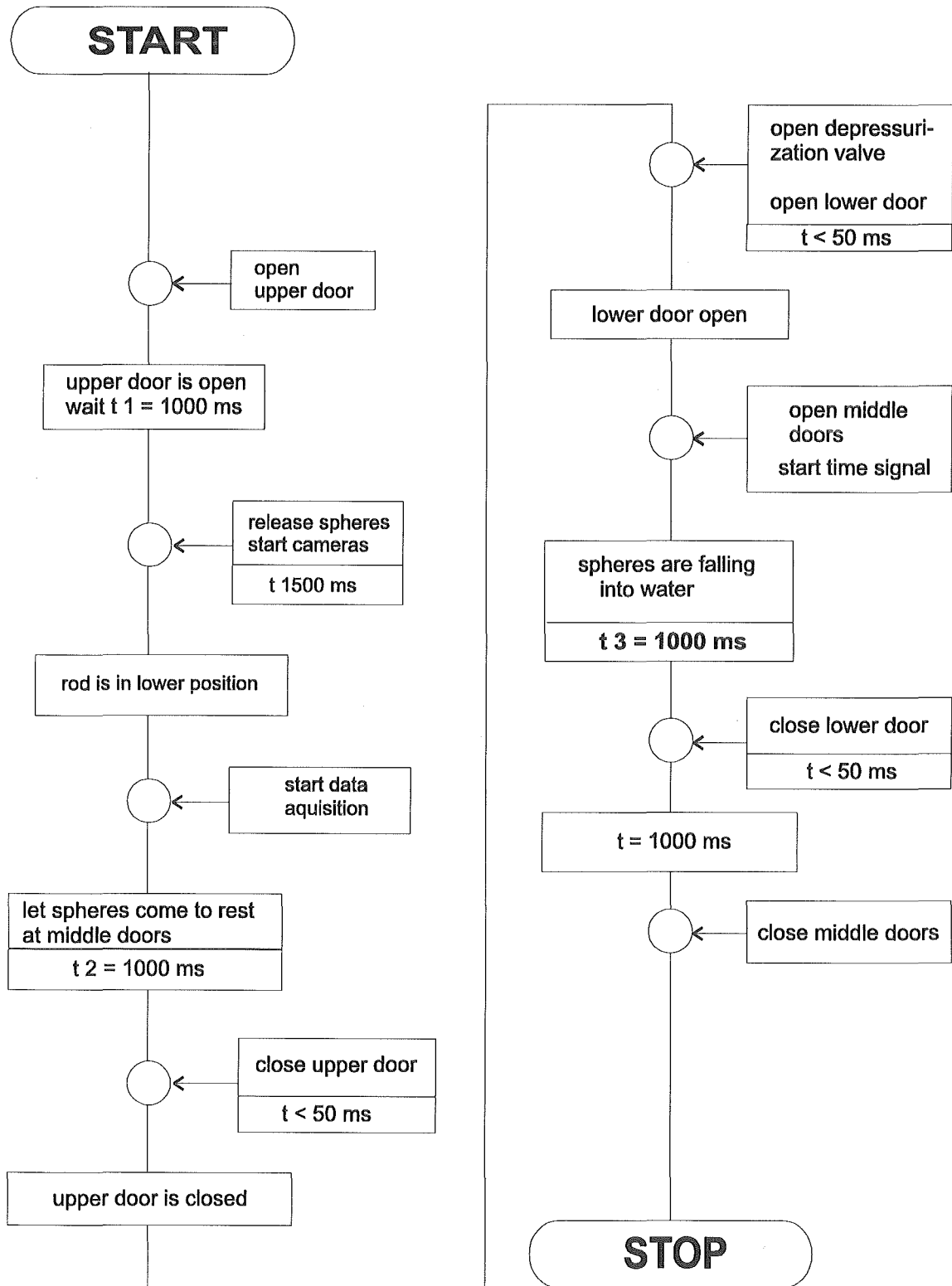
Fig. 3.3 Flow chart of the SIMATIC control of the experiment
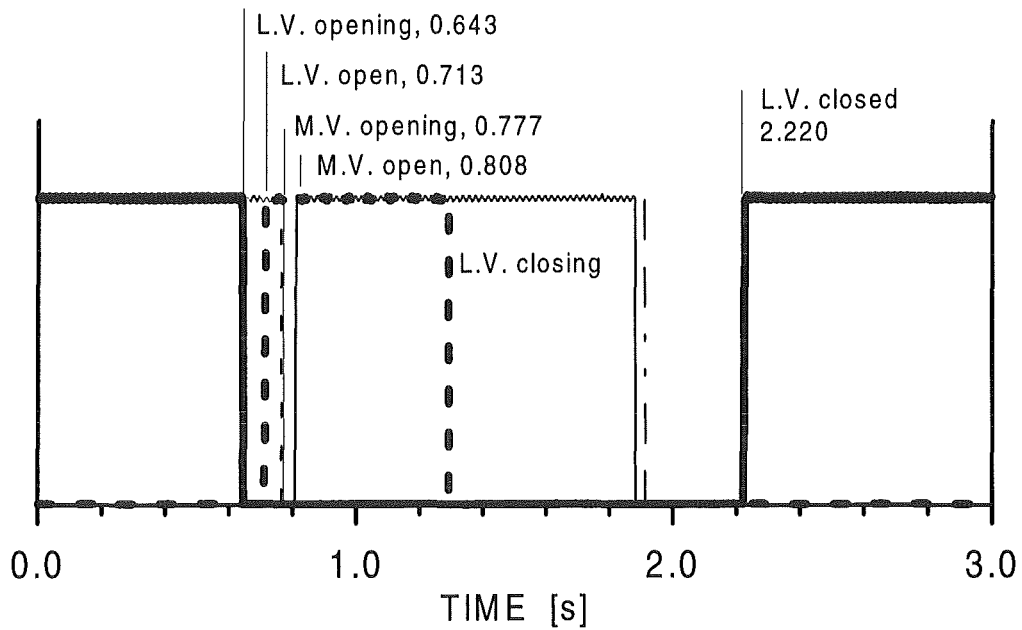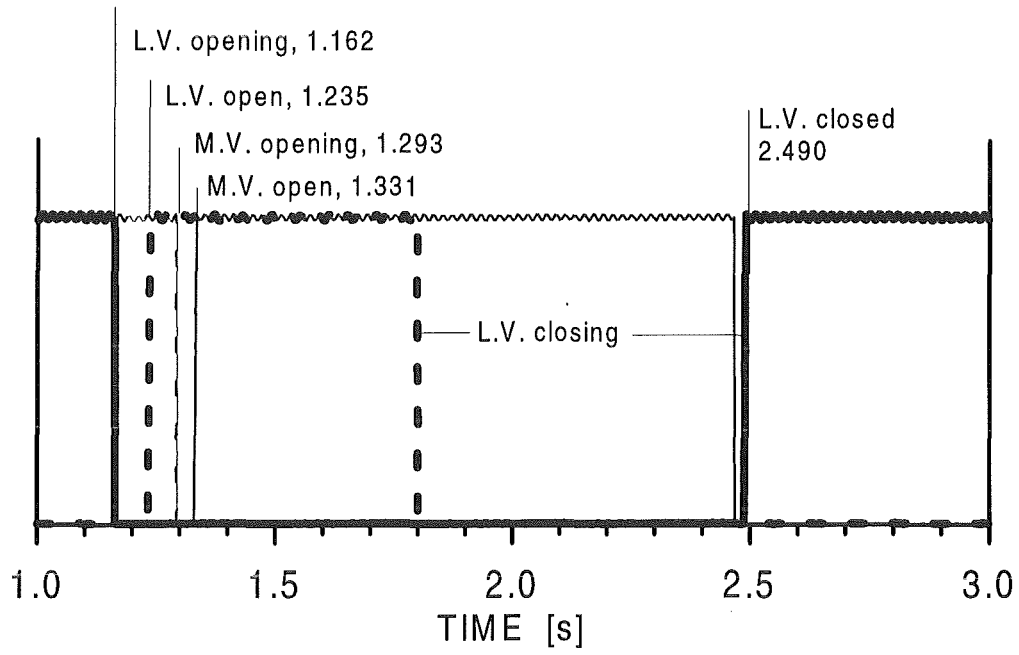
Fig. 3.4 Time signals from the lower (L.V.) and middle valve (M.V.);
time zero is start of the data acquisition; top: Q12, bottom: Q11

4. BASE CASE EXPERIMENTS

4.1 Test matrix and initial conditions

The experimental series was started with exploratory tests using steel spheres, which could not be used at temperatures of 1000°C because of a sintering process. The experiments with the three types of spheres were performed with a low mass and were started with cold spheres in each case.

Table 4.1 shows the data of the first test series. The experiments are arranged according to the type of spheres used and with increasing temperature. The temperature value stated is an approximate value, since the uncertainty is in the range of ±30 K. The volumes and numbers of spheres stated are approximate values also, only the mass data are exact. The quantity of spheres was selected according to the volume of 10 kg of molybdenum spheres. Thereby the heat content at similar sphere temperatures is similar in each experiment (see Table 4.2). Only in test No.1 was the volume twice as large. In the tests Nos.10, 11 and 12 not all the spheres left the furnace (see chapter 3.1).

The steel and zirconiumoxide spheres had a near ideal spherical shape with smooth polished surfaces. The molybdenum 'spheres', however, were pressed with semi-spherical parts at two sides and a small cylindrical 'belt' at the equator.

The volumes stated in Table 4.1 are the bulk volumes, the packing factor varies for the different sphere types between 0.55 for the Mo-spheres and 0.65 for the ZrO_2-spheres. For the code input the initial volume fraction at the time of impact on the water is an important parameter. This can be determined by image processing or theoretically with certain assumptions.

The opening time of the sliding door valve is approximately (s. Table 4.4)

$$t_{open} = 0.04 \text{ s} .$$

The volume of 2000 cm^3 spheres above the sliding door valve with a diameter of 0.18 m has a bulk height of

$$s_b = 0.08 \text{ m}.$$

We make the following assumptions supported by observation in special tests:

1. The first spheres start to fall at $t_1 = 0$ s   from the height $s_1 = 1.30$ m.
2. The last spheres start to fall at $t_2 = 0.04$ s from the height $s_2 = s_1 + s_b = 1.38$ m.

Times of free fall are $$\Delta t = \sqrt{\frac{2s}{g}}$$

which gives $\qquad \Delta t_1 = 0.515$ s

and $\qquad \Delta t_2 = 0.530$ s .

At $t_{w1} = 0.515$ s the first spheres reach the water level and at $t_{w2} = t_2 + \Delta t_2 = 0.570$ s the last spheres reach the water level.

The corresponding impact velocities $w = \sqrt{2sg}$ are $w_1 = 5.05$ m/s and $w_2 = 5.20$ m/s.

At the impact time of the first spheres, at $t_{w1} = 0.515$ s, the last spheres have traveled

$$s_2{}^* = \tfrac{1}{2} \, g \, (t_{w1} - t_{open})^2 = 1.10 \text{ m}$$

The apparent height of the sphere cloud at impact time is

$$h = s_1 + s_b - s_2{}^* = 0.28 \text{ m} .$$

Another way to determine this height is the following:

The time interval between impact of the first and last spheres is 0.055 s. The average velocity is 5.12 m/s, so the apparent length is $h = w \, t = 0.28$ m, which is the same as above.

Assuming that the shape is still cylindrical with the same radius of $r = 9$ cm, we get a volume $v_i = \pi \, r^2 \, h \approx 7000$ cm^3. Especially for the cold tests we find the height of 28 cm and the radius of 9 cm quite well confirmed by the images. Of course, at the front part there is a deformation of the cylindrical shape due to the two doors opening along one dimension and there is some non-uniformity in the density particularly at the front and top of the sphere cloud. Taking all this and the uncertainty of the assumptions 1 and 2 into account and the variable opening times of the doors, we think we can state an initial solid volume fraction with an uncertainty of $\pm 15\%$. This volume fraction is defined as $r_{vs} = (m_s/\rho_s) / v_i$ and is approximately 0.17. These numbers can be verified by the image processing in most cases.

In the tests with hot spheres an effect occurs which breaks up the front of the sphere cloud. While the spheres are resting upon the middle valve the pressure increases due to the heat up of the gas in the closed space between the upper and the lower valve. When the lower valve is opened a gas burst which disturbs the water surface can be observed. When the middle valve opens, there is still some overpressure above the spheres and gas is forced through the spheres accelerating the front spheres. In these tests always a small number of spheres are ahead of the bulk. Therefore a pressure relief valve was installed above the middle sliding door which opens together with the lower sliding door valve. This reduced this effect somewhat (starting with Q-10).

Table 4.1 Experimental conditions

No.	Material	⌀ [mm]	Mass [kg]	Volume [cm³]	Number of spheres	Temp. [K]
1	steel	4.7	20	4440	46000	300
2	steel	4.7	10	2220	23000	300
5	ZrO₂	5.0	7.0	1830	18000	300
9	ZrO₂	5.0	7.0	1880	18000	1300
6	ZrO₂	10.0	7.0	1900	2340	300
7	ZrO₂	10.0	7.0	1900	2340	1300
10	ZrO₂	10.0	6.3	1740	2100	1800
8	Mo	4.2	10	1800	24000	300
3	Mo	4.2	10	1800	24000	920
4	Mo	4.2	10	1800	24000	1300
11	Mo	4.2	5.7	1025	13700	1800
12	Mo	4.2	6.9	1183	16600	2300

Table 4.2 Properties of sphere and furnace material

Properties	W (20 -2000°C)	Steel	Mo (20-1500°C)	ZrO₂ (1200°C)
expansion coefficient K^{-1}	5.3×10^{-6}	8.5×10^{-6}	6.5×10^{-6}	$8\text{-}10\times10^{-6}$
thermal conductivity $Wm^{-1}K^{-1}$	129 - 100	15	142 -88	3.7
specific heat $kJ\,kg^{-1}\,K^{-1}$	0.14 - 0.2	0.5	0.25-0.44	0.71
content of heat $J\,cm^{-3}\,K^{-1}$		3.9	4.5	4.1
density $g\,cm^{-3}$	19.3	7.8	10.2	5.75
melting point °C	3410	1400	2620	2650
modulus of elasticity $kN\,mm^{-2}$	410 - 280	200 - 100	300 -150	

Table 4.3 Volumes and volume fractions of spheres

Material	diameter [mm]	solid density ρ_s [g/cm³]	mass [kg]	bulk volume V_b [cm³]	bulk density ρ_b [g/cm³]	ρ_b / ρ_s	impact solid fraction r_{vs}
steel	4.7	7.8	10.3	2220	4.64	0.595	0.17±.02
Mo	4.2	10.2	10.0	1800	5.55	0.545	0.17±.02
ZrO₂	5.0	5.75	7.0	1850	3.78	0.657	0.17±.02
ZrO₂	10.0	5.75	7.0	1900	3.68	0.640	0.17±.02

Table 4.4 Timing of the middle and lower sliding door valves

No.	MV open [s] *	LV closing [s]	LV closed [s]
4	-	0.600	1.557
5	-	0.505	2.005
6	0.040	0.552	1.877
7	0.041	0.490	1.398
8	0.035	0.480	1.092
9	0.036	0.485	1.248
10	0.037	0.539	1.449
11	0.031	0.515	1.443
12	0.038	0.507	1.197

* time zero is begin of opening of middle sliding door valve

4.2 Experimental Results

The results are presented grouped by the type of measurement rather than by experiment number. Within the groups the sequence is by the type of spheres and increasing temperature. Since this is the first series not all measurements were performed in all experiments. Table 4.5 shows which data are available for any particular test.

The time axis for the transient data has its origin (t = 0) at the start of the opening of the middle sliding door valve that releases the spheres. In the first experiments Nos.1 through 5 the signal of this valve was not recorded, therefore time zero has an uncertainty of ±20 ms for these tests.

Table 4.5 Available measurements

No.	Images		vessel press.	vent pipe press.	steam rate	water level	pyro. temp.	distr. on ground
	N	W						
1	V	-	-	-	-	-	-	X
2	V	-	-	-	-	-	-	X
5	X	V	-	-	-	X	-	X
9	X	V	X	X	X	X	-	X
6	X	V	X	-	-	X	-	X
7	X	V	X	X	X	-	-	X
10	X	X	X	X	X	X	-	X
8	X	V	X	-	-	X	-	X
3	V	V	X	-	-	-	-	X
4	X	V	X	X	X	X	-	X
11	X	X	X	X	X	X	X	X
12	X	X	X	X	X	X	X	X

V Video cameras only
X data available
- no data available

4.2.1 Images

Six characteristic images of each experiment are shown from the 'North' side (with back-lighting), and when available also from the 'West' side (with black background). These images shall give a qualitative impression of the process, for quantitative evaluation and comparison we refer to the results from image processing which will be published in a

later report. All images obtained during the period when the spheres are visible were digitized and are available as TIFF-files on CD-ROMs. Since in this first series the time signal was not recorded on film, the time of impact at the surface was evaluated from the images and set to t = 0.51 s. The uncertainty is in the order of 0.01 seconds. All images are shown in black and white although for all experiments with temperatures of 1000°C and higher color films are available, which contain more information.

Cold steel spheres (No1. and 2)

The characteristic feature of the first experiment, the only one with 20 kg mass, is the almost spherical shape of the three-phase region (spheres, water, gas) after the gas chimney closed (Fig.4.1). When the front of the sphere cloud has reached the bottom, a large gas bubble is released. In the second experiment with half the mass used (Fig.4.2), the shape of the multi-phase region is less spherical and the gas bubble rises earlier, before the spheres have reached the vessel bottom. Around the periphery of the multiphase region spheres surrounded only by water form the typical inverted mushroom shape.

Small ZrO$_2$ - spheres (No. 5 and 9)

The small zirconia spheres were more decelerated than steel spheres (Fig.4.3-4.6), which means that the sphere front reaches the vessel bottom later. The gas entrainment in the cold run (Q05) is similar to run Q02. Comparing the two views from the 90 degree different positions, the effect of the sliding doors can be seen. Looking from west against the black background (Fig. 4.4) the doors open sideways which causes the pointed front. In spite of this deformation of the sphere cloud at water impact its shape is closer to cylindrical geometry further down in the water pool. Hot spheres (Fig. 4.5 and 4.6, Q09, T = 1300 K) do not entrap a large gas bubble. The gas (vapor) release is by small bubbles, as can be seen in the last frame, also at later times.

Large ZrO$_2$ - spheres (No. 6, 7 and 10)

The gas entrainment is much less with large spheres. In the cold test No.6 (Fig. 4.7 - 4.9) there are very few spheres in the center of the sphere cloud. The dark cloud is air, as can be seen in the frames from the HS-film (Fig.4.8). At 1000°C (Fig.4.10 - 4.12, Q07) the gas chimney is wider and exists longer than with cold spheres of the same kind. Because of the elongated steam envelope around each sphere it is not possible to look into the multi-phase region; but the outer shape is quite similar to that of the cold test. Except for a somewhat larger steam production there is no significant difference in the shape of the sphere clouds between sphere temperatures of 1000°C and 1500°C (No.10, Fig.4.13 and 4.15). The brighter light of the hotter spheres makes it possible to better identify individual spheres.

Small Mo-spheres (No. 8, 3, 4, 11, and 12)

The pour of the cold Mo-spheres (Fig.4.16 - 4.18) looks similar to that of the steel spheres, again there is a large gas volume being dragged deep down into the water. The solid fraction at water impact is very close to its theoretical value which is not the case in test No.3 with moderately hot spheres (Fig.4.19 and 4.20). In this case the spheres rested for almost a minute on the middle valve and the pressure between the upper and lower valve must have risen above 2 bars. The effect of acceleration of spheres by a gas flow as described in 4.1 elongated the sphere stream and reduced the solid fraction. No large gas bubble can be observed in this experiment. This difference does not seem do depend on the temperature (at least not up to 1000°C) because in test No.4 a large bubble is present again (Fig.4.21- 4.24). The shape at 1500°C is quite different (Q11, Fig.4.25). The initial solid fraction is close to the theoretical one but the steam production changes the mixing process entirely. The lateral movement of the spheres is increased and the multi-phase front is split up in two peaks. The view from the other (west) side is shown in Fig.4.26. Here the spreading is less and the front is more uniform. In test Q12 with a sphere temperature of 2000°C the initial form of the sphere stream is elongated compared with the theoretical value (Fig. 4.27). The shape of the multi-phase region is not as wide as in the previous experiment and the sphere front has a single pointed tip in the north view.

It is obvious that besides of the three parameters of density, size and temperature of the spheres a fourth parameter, the initial form of the sphere cloud, plays an important role for the further development of the mixing zone.

4.2.2 Pressure

The figures 4.28 - 4.37 show the pressures measured in the vessel at different levels. Pressure No.1 was measured in the gas space above the water level and therefore shows the lowest static pressure signal. Because the transducers measure the absolute pressure it should give the barometric pressure. There was, however, a small offset in the order of 0.01 bar in most experiments. The transducers 2 to 6 were at different water depths and measured also the static head according to their position. With a total water height of 1000 mm, the transducers 2 and 3 at the position 838 mm above the bottom get a static head of 162 mm or 0.016 bar, the Nos. 4 an 5 at 450 mm get a head of 0.055 bar and No. 6 at 250 mm gets a static head of 0.075 bar.

The spheres enter the water at approximately t = 0.5 s (see Chapter 4.1) and reach the vessel bottom at t = 0.7 s. Measurements are available for two tests with cold spheres, Q06 and Q08 (Fig. 4.28 and 4.29). There is a slight pressure increase in the water when the spheres enter the water, lasting only 70 ms for Q08, then the pressure drops below

the static value. At t = 0.72 s it reaches a minimum and increases sharply. This pressure spike is highest deep down in the vessel. It coincides with the collapse of the gas chimney (see Fig. 4.17). The initial pressure increase is approximately concurrent to the increase of the static head due to the water level rise (Fig.4.38). However, the pressure increases less at the positions 4 and 5 close to the water surface, and the pressure drop sets in before the maximum water level rise has been reached. The high pressure peak reverberates several times with a frequency of 18 Hz and declining amplitude. The other experiment with cold spheres, Q6, shows similar pressure traces, however, there is a pressure decrease before the spheres enter the water, which we cannot explain (Fig. 4.29). The pressure oscillations have a frequency of 27 Hz.

The pressures for hot large Zirconia spheres are shown in Fig.4.30 (Q07, 1300 K) and 4.31 (Q10, 1800 K). The pressure increase at 1300 K is not higher than for cold spheres but the oscillations are almost not existent. At sphere temperatures of 1800 K the pressure increase is higher and the drop below the static pressure is smaller. For small Zirconia spheres the pressure rise is higher at 1300 K (Q09, Fig. 4.32), even higher than that of large spheres at 1800 K (Fig. 4.33).

The pressures for hot molybdenum spheres are shown in figures 4.34 to 4.37. Except for the noise in the signal the first part of the transient is similar for 900 K and for cold spheres (Q03 and Q08). The high peak and the oscillations are absent in experiments with hot spheres. With increasing temperature the initial pressure rise increases and the subsequent drop below the static pressure is smaller. In experiment Q12 with sphere temperatures of 2300 K there is still a small peak in the pressure signal of the transducers at lower positions, which is due to the collapse of the gas funnel at t = 0.7 s. Fig. 4.39 shows a comparison of the pressure rise at different sphere temperatures.

The figures 4.40 to 4.45 show the pressures measured in the vent pipe (see Fig. 2.6). It was planned to determine the steam velocity by measuring the static and the total head. However, the measurement of the total head was obviously faulty, probably because of water droplets or a defect transducer. The total head in many cases was smaller than the static pressure. The pressures shown are the static measurements. These data serve to check the mass flow measurements, because it was not known, how the vortex mass flow meter was reacting in highly transient flow. The comparison with the measured mass flow (see below) shows very good correspondence.

In chapter 2.4 the pressure loss coefficient ζ of the vent pipe was given with ζ_{total} = 4.54 for stationary flow. Up to the position of the pressure transducer it should be approximately ζ = 2.2. With the velocity in the vent pipe (Fig. 4.59) and the pressures in the vessel and vent pipe the true pressure loss coefficient can be determined by Eq. 2.1. The steam density was taken as ρ_{st} = 0.6 kgm^{-3}. The pressure difference is shown in

Fig. 4.46. Compared to stationary flow the pressure loss coefficient ζ (Fig. 4.47) is larger by a factor of two for accelerating flow and up to six times larger for decelerating flow.

4.2.3 Steam rate

The steam flow through the vent pipe (Fig. 4.48 - 4.53) corresponds to the pressure in the vessel. Only during the short time period when the spheres are falling through the water the steam production is strong enough to generate a measurable flow. The lower bound of the measuring range of the vortex flow meter is approximately 80 dm³/s. The steam generation for sphere temperatures below 2300 K is very moderate. From the volume flow rate steam velocities were determined with a pipe diameter of 108 mm (Fig. 4.54 - 4.59).

4.2.4 Water level

The water level was measured in the four corners of the vessel by two types of level meters with different lengths. Meters of the same type were installed in diagonally opposite corners. The two identical meters gave almost identical results each, while there was a difference between the long and the short type, especially at times after the first level rise. This is due to damping effects caused by the protection tube. Thus the short level meters are the more reliable ones and results obtained with these meters are shown in the figures 4.60 through 4.67 with full dark lines.

4.2.5 Temperature

Up to experiment Q11 the temperature of the spheres was measured in the furnace only. The figures 4.68 through 4.72 show the data of two thermocouples placed among the spheres, one near the center and one near the inner wall of the tungsten tube and one placed at the outer wall of the tube. Fig. 4.72 shows the pyrometer measurement of the tube temperature for comparison. In these experiments the spheres were released after the temperature had leveled off.

In the experiment Q12 (Fig. 4.73) the tungsten tube had reached a temperature of 2060 °C, but it was still rising. It was not possible to measure the temperature in the center of the sphere bed because no thermocouple was available for temperatures around 2000 °C. However an estimation of the temperature in the center is possible using the temperature of the tungsten tube, that is measured by a pyrometer, and the relations between the tube and the center temperatures measured in Q11 (Fig.4.72). For this estimation we have to extrapolate the temperature drop between tube and center of the bed

of Q11 (dashed horizontal lines in Fig.4.72) for the higher temperatures and steeper temperature rise in Q12 with

$$\Delta T_{Q12} = k\Delta T_{Q11}.$$

The factor k is calculated from the ratio of the heat that is transferred by radiation for Q12 and Q11:

$$k = \frac{Q_{12}}{Q_{11}} = \frac{T_{12}^4 \ (dT/dt)_{11}}{T_{11}^4 \ (dT/dt)_{12}}$$

A calculation using the data represented in Fig.4.72 and 4.73 yields at 2000 °C for Q12 a temperature drop $\Delta T_{12} = 75$ °C. Because radiation is the main heat transfer process at the considered temperatures, convection was neglected in the calculation.

The next two figures show the data from pyrometer measurements of the falling spheres 25 cm above the water level. Because the emissivity of rhenium coated molybdenum spheres changes when the spheres fall through a steam atmosphere, the pyrometer data have a large uncertainty in the order of 100 K. Also, the fraction of the radiation energy absorbed by steam is in the order of ten percent for the existing conditions. For Q11 the pyrometer gives 100 K more than expected and for Q12 ca. 80 K less than expected. In addition to the temperature these data show the exact time and length of the pour of spheres.

4.2.6 Time distribution of the measured data

Figures 4.76 through 4.78 show the chronological relation of the various signals for three experiments. The pressure rise, the mass flow and the water level rise start at the same instant when the first spheres enter the water.

4.2.6 Mass distribution on ground

The distribution of the spheres on the vessel bottom is given in a table, corresponding to the 7x7 boxes, and a 3-D plot (Fig. 4.79 - 4.90). The instrumentation of the vessel wall is situated at the top side of the matrix and at the left back side of the plot, respectively. The north camera would look from the left side and the west camera from the front or the right front in the plot. The sliding doors would open sideways in respect to the matrix. A clear effect of the sliding doors cannot be seen in the distribution.
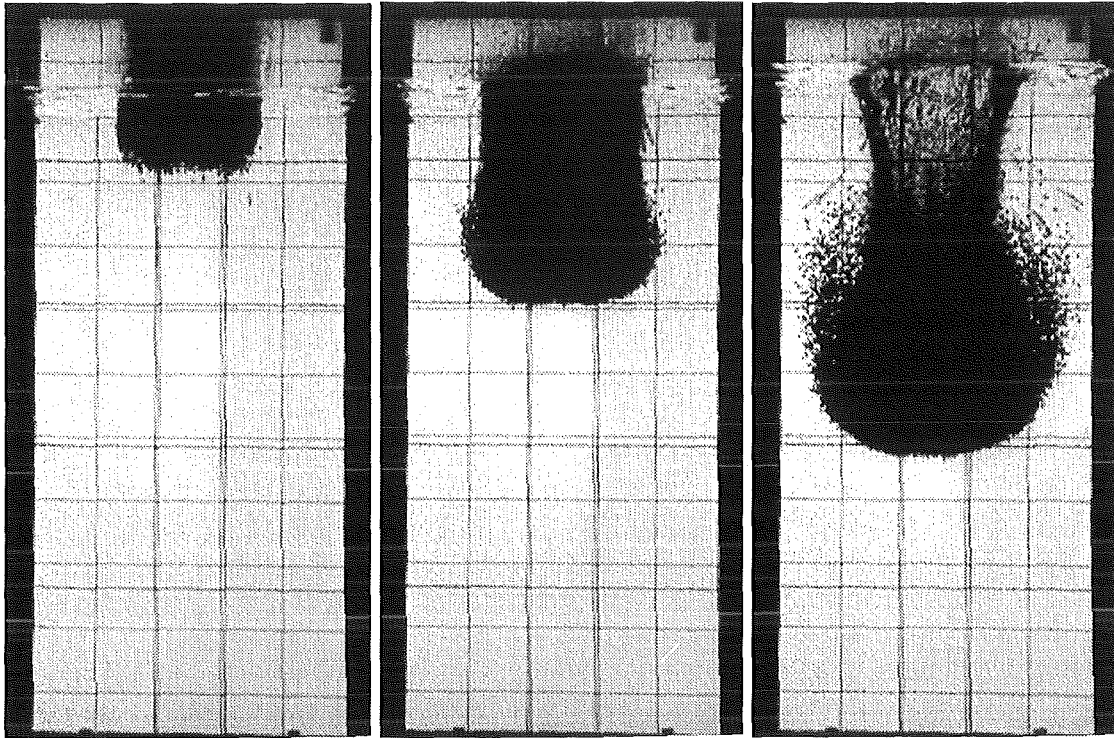
t = 0.500 s   0.560 s   0.620 s
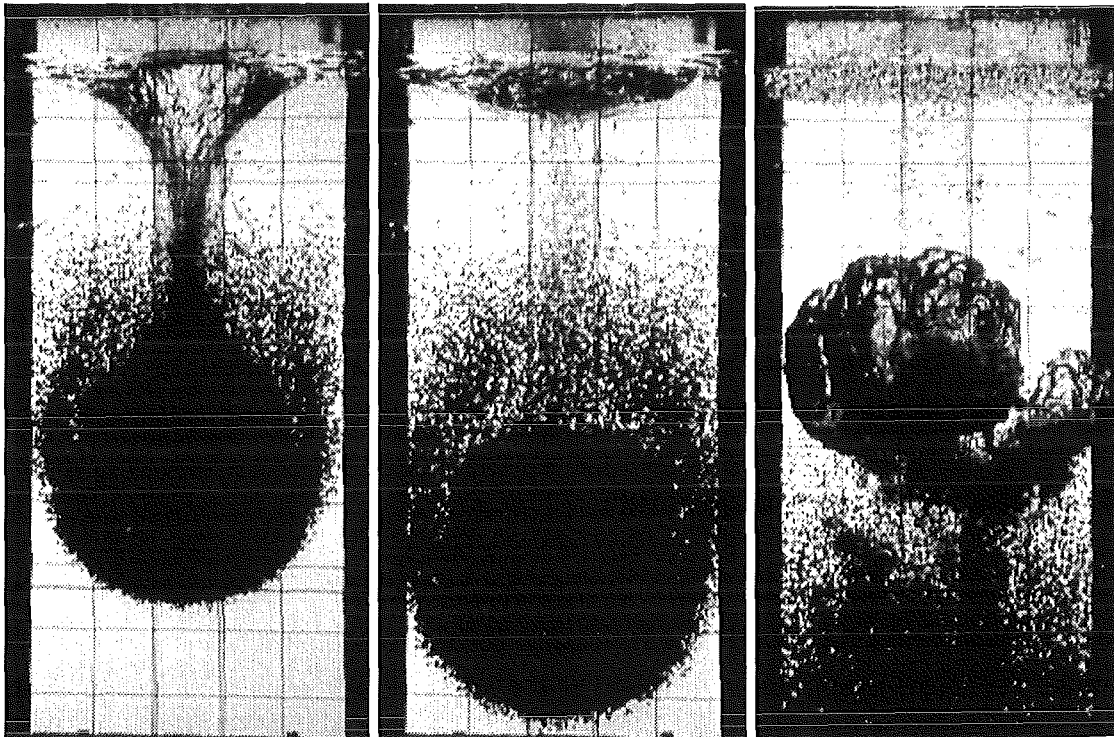
0.680 s   0.740 s   *1.040* s

Fig. 4.1 **Q01,** Video, Δt = 60 ms (*300 ms*)
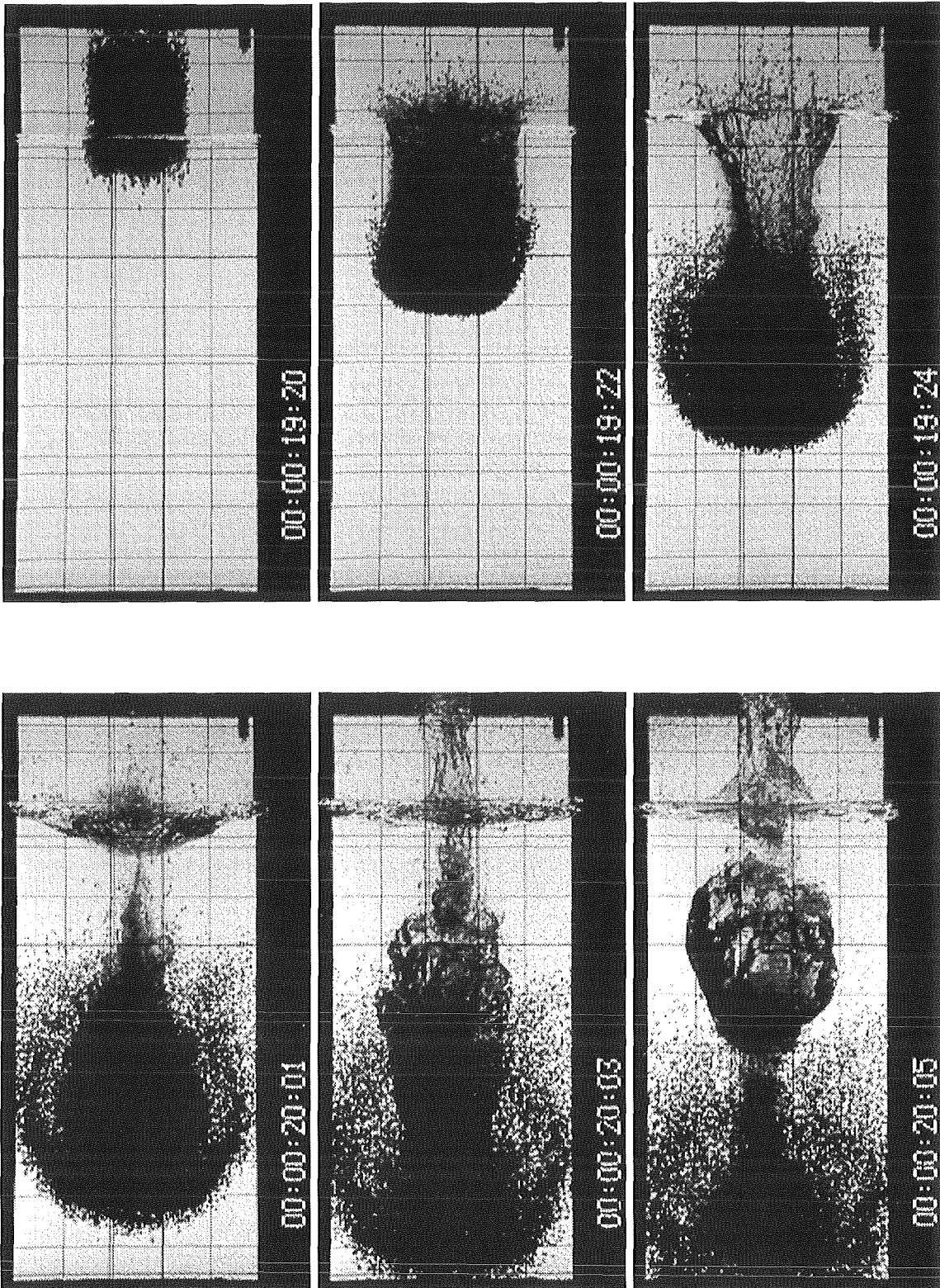
Fig. 4.2 **Q02**, Video, $\Delta t = 80$ ms
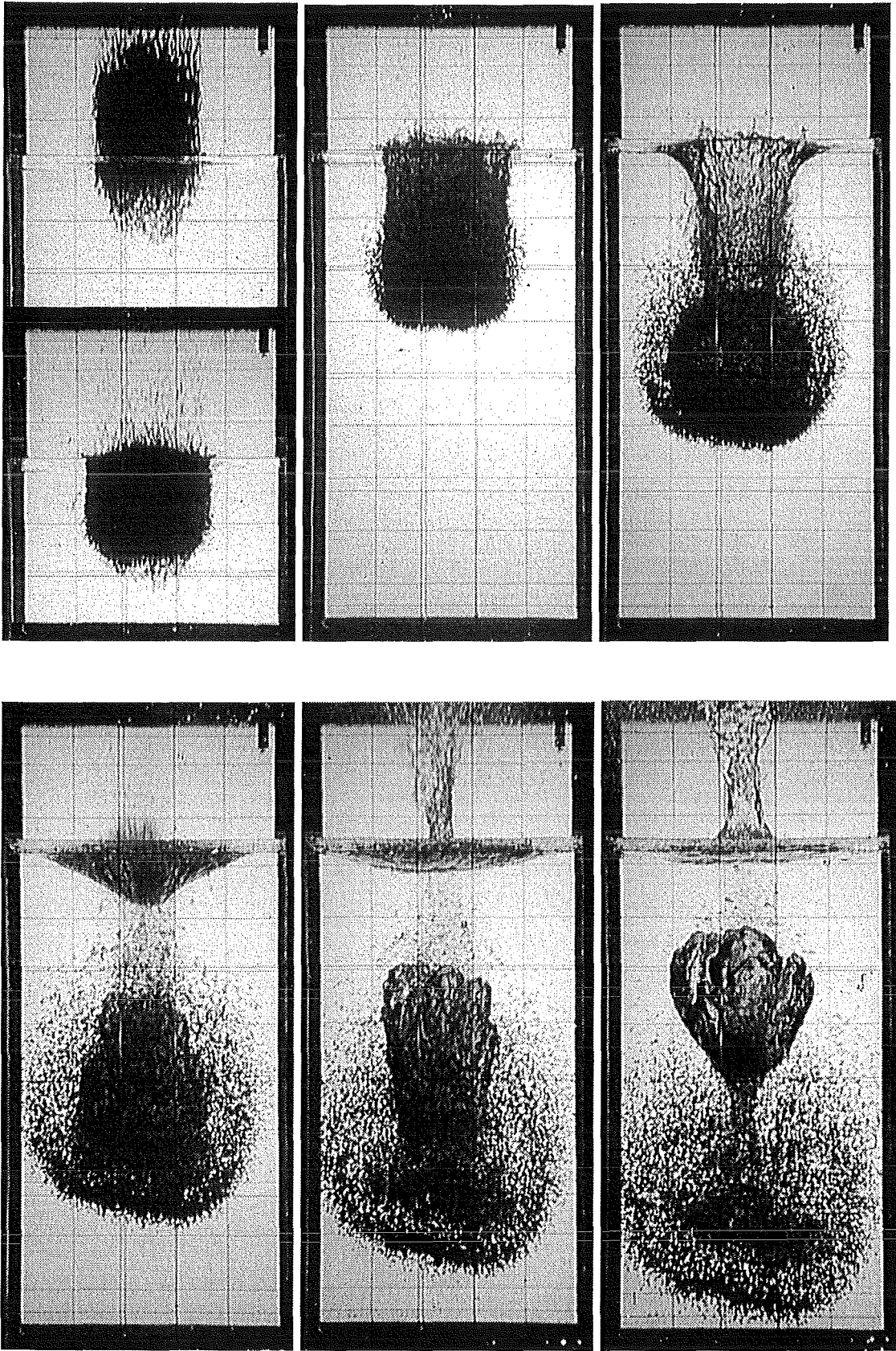
Fig. 4.3 **Q05,** PS, North, $\Delta t = 80$ ms
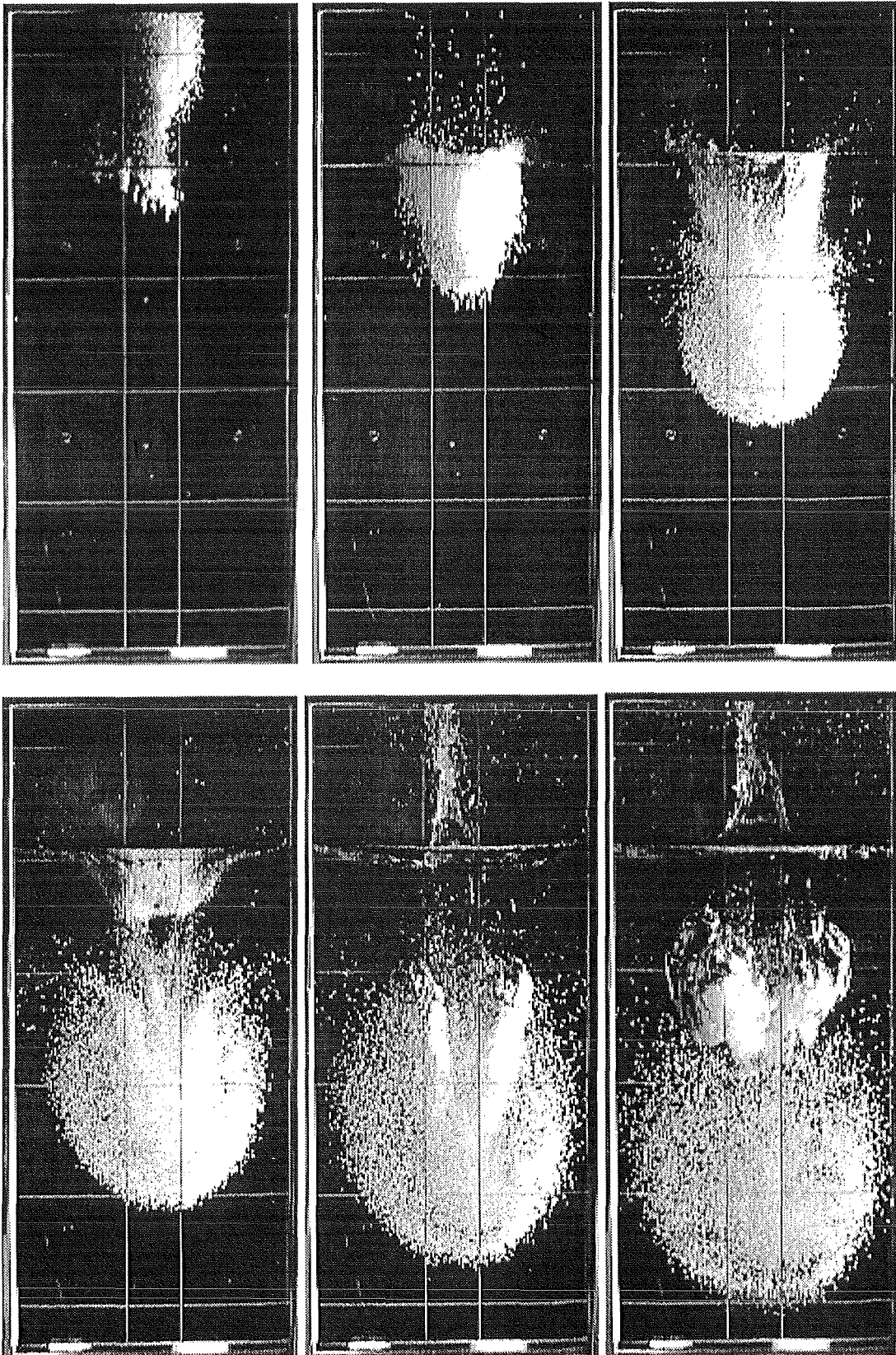
Fig. 4.4 **Q-05**, Video west, $\Delta t = 80$ ms
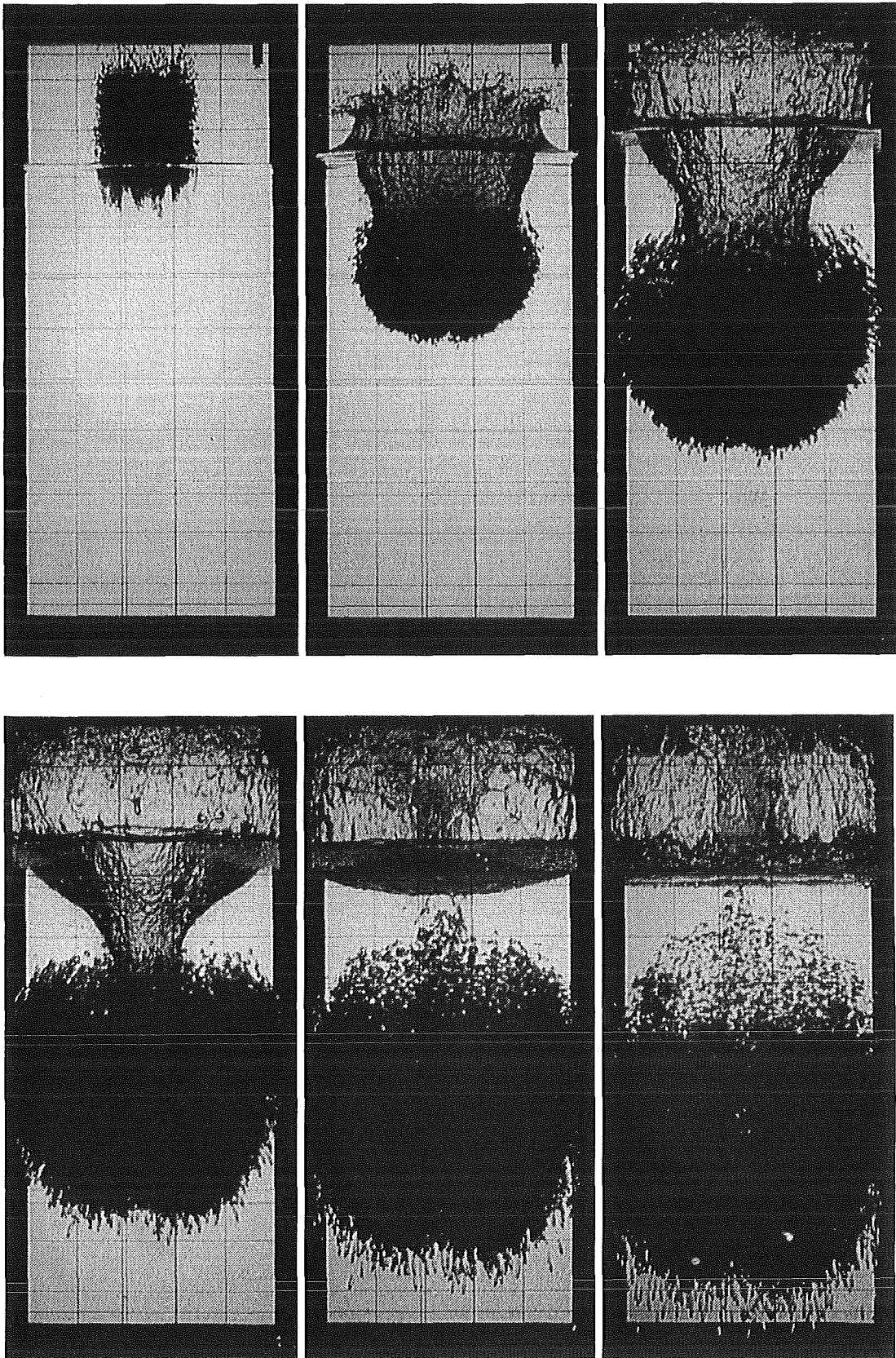
Fig. 4.5 **Q-09**, PS, north, $\Delta t = 80$ ms
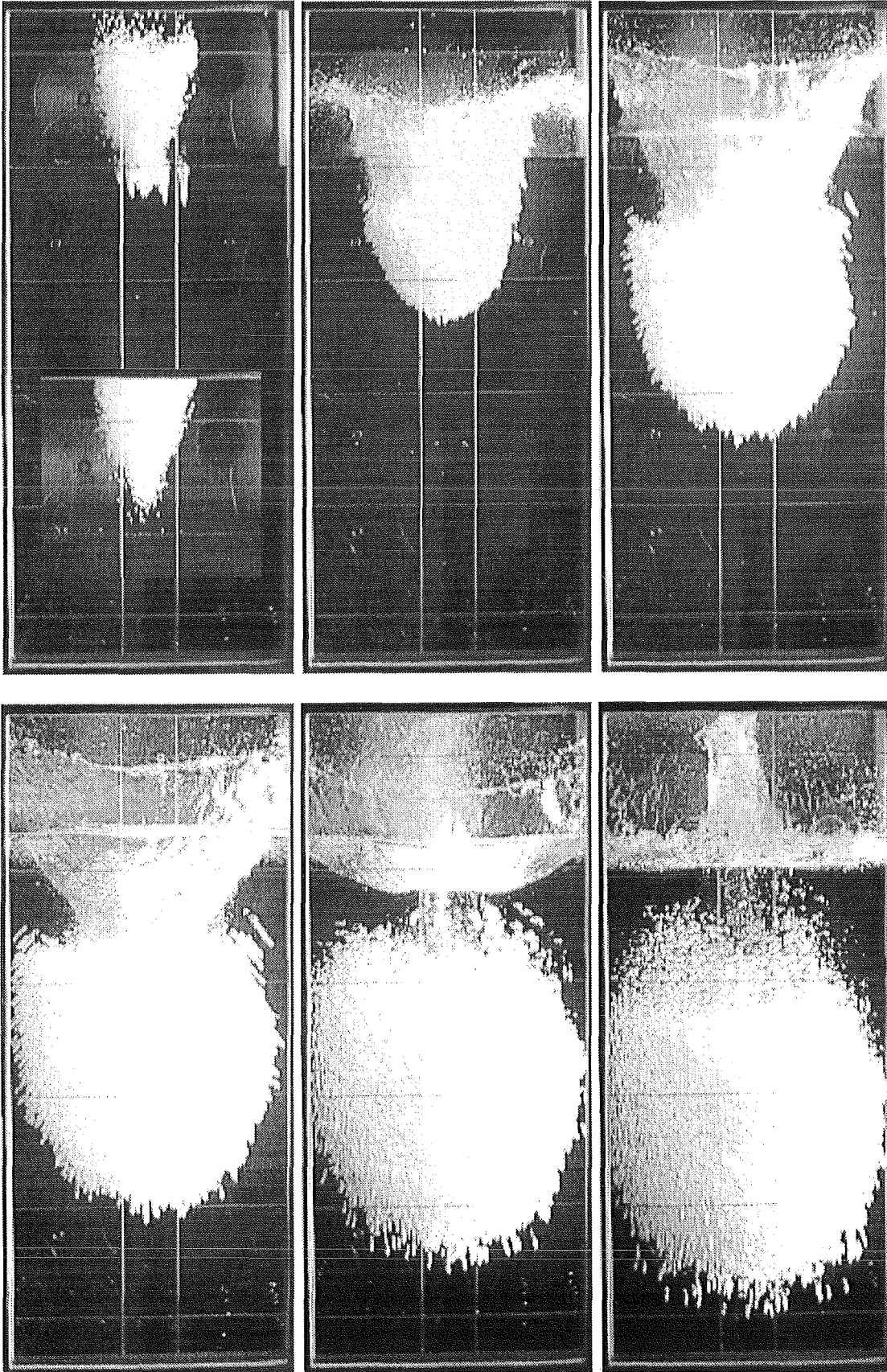
Fig. 4.6 **Q09**, Video west, $\Delta t = 80$ ms
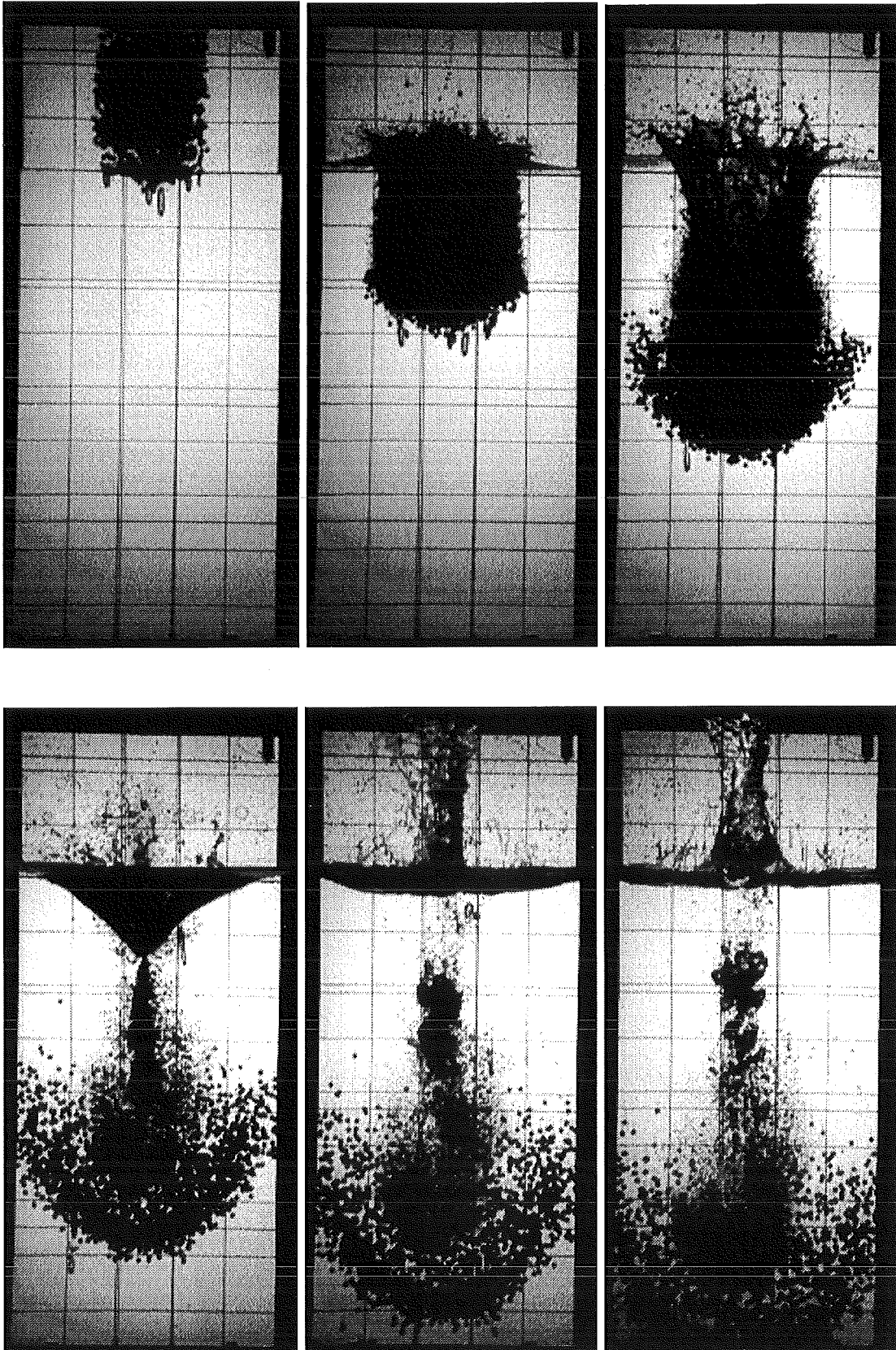
Fig. 4.7 **Q06**, Video north, $\Delta t = 80$ ms
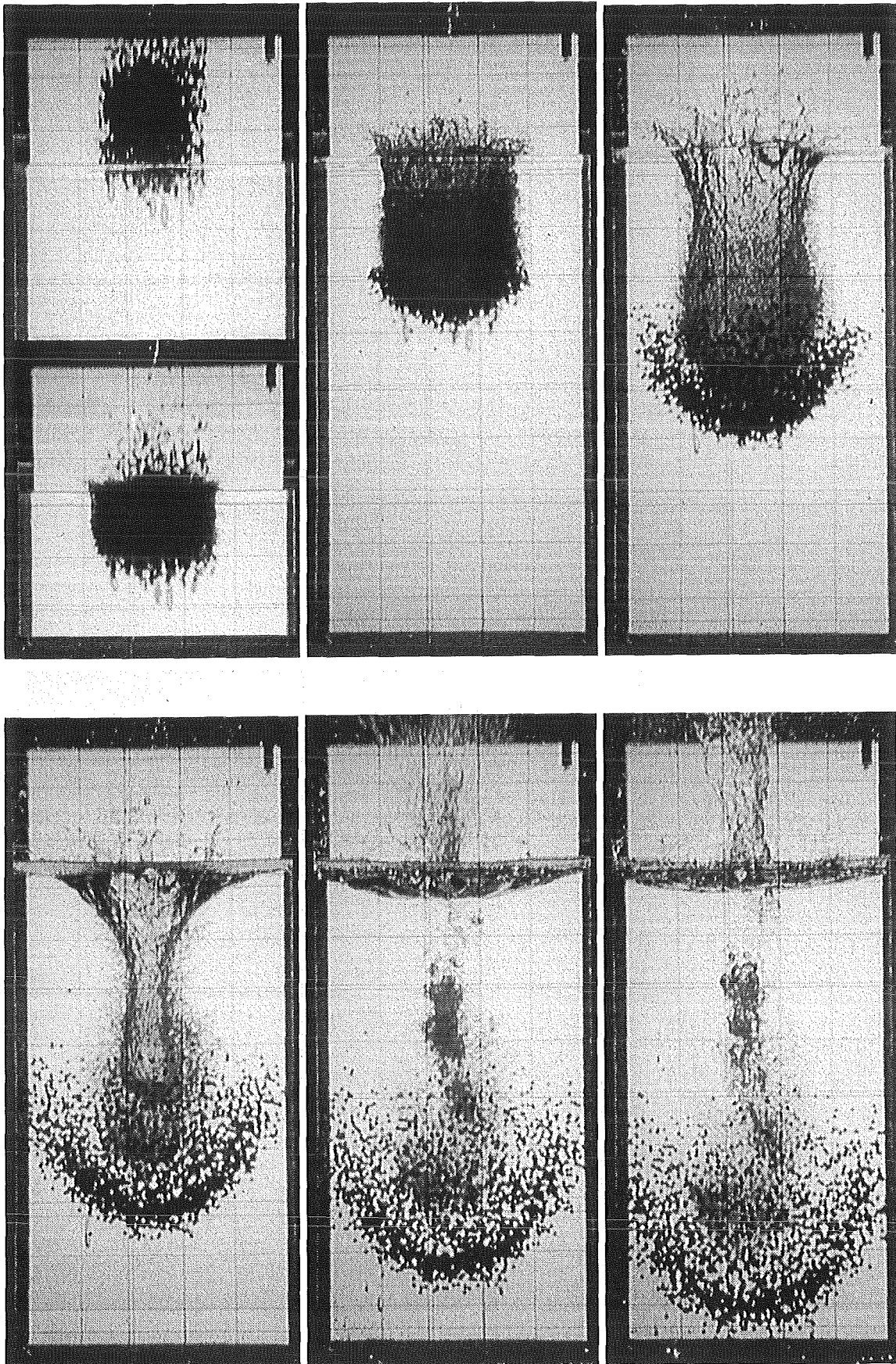
Fig. 4.8 **Q06,** PS, North
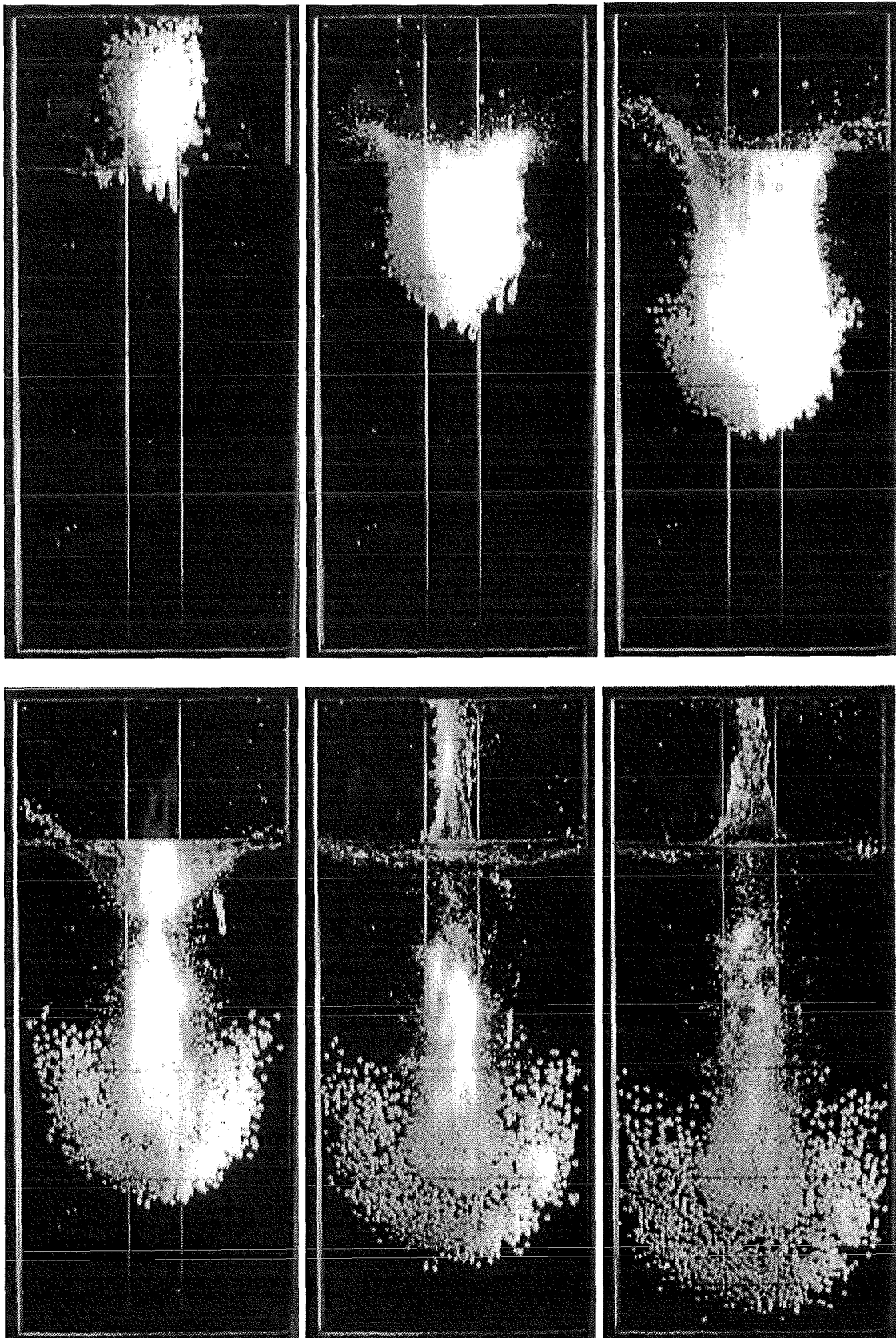
Fig. 4.9 **Q06,** Video west, $\Delta t = 80$ ms
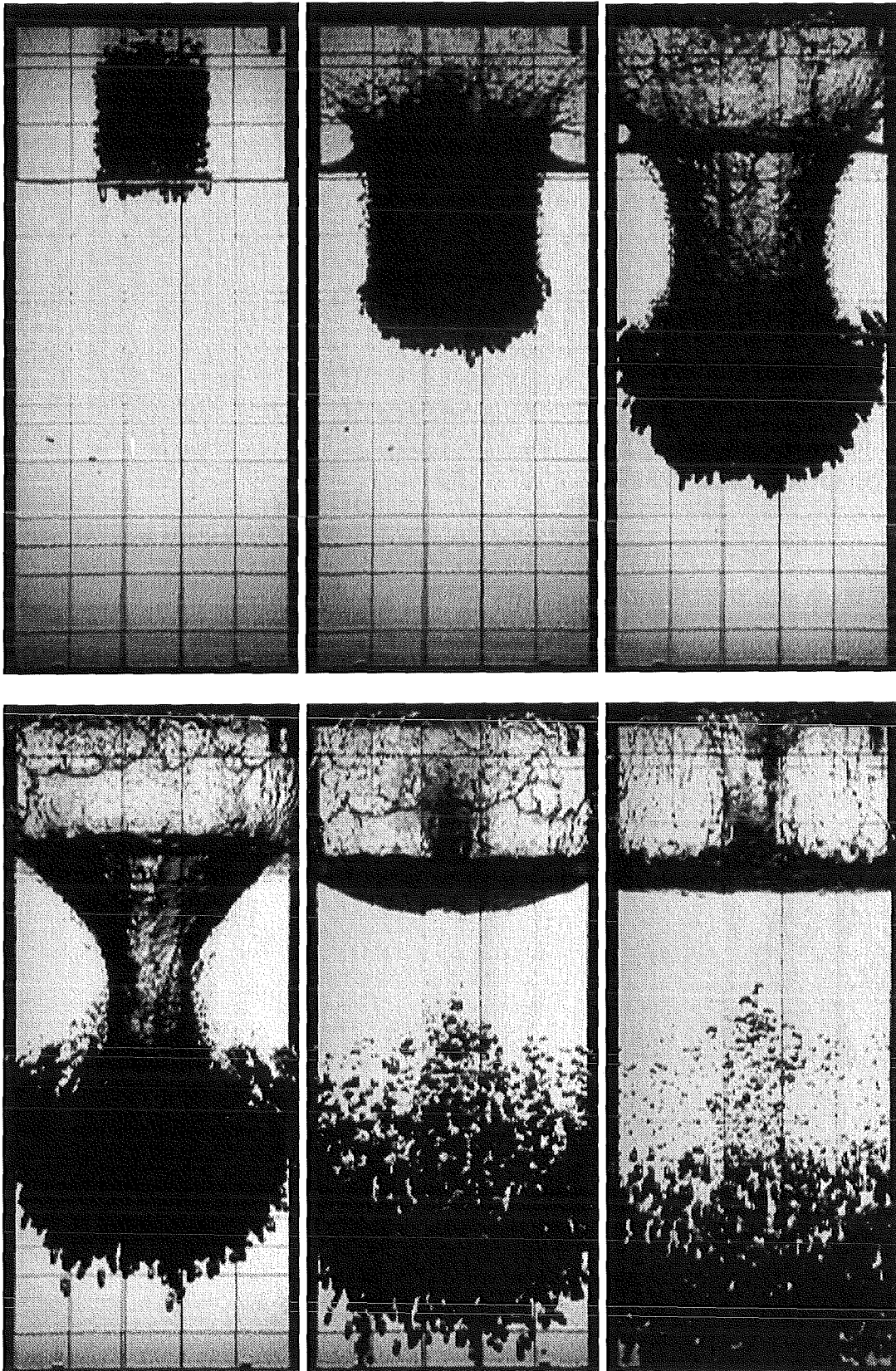
Fig. 4.10 **Q07**, Video north, $\Delta t = 80$ ms
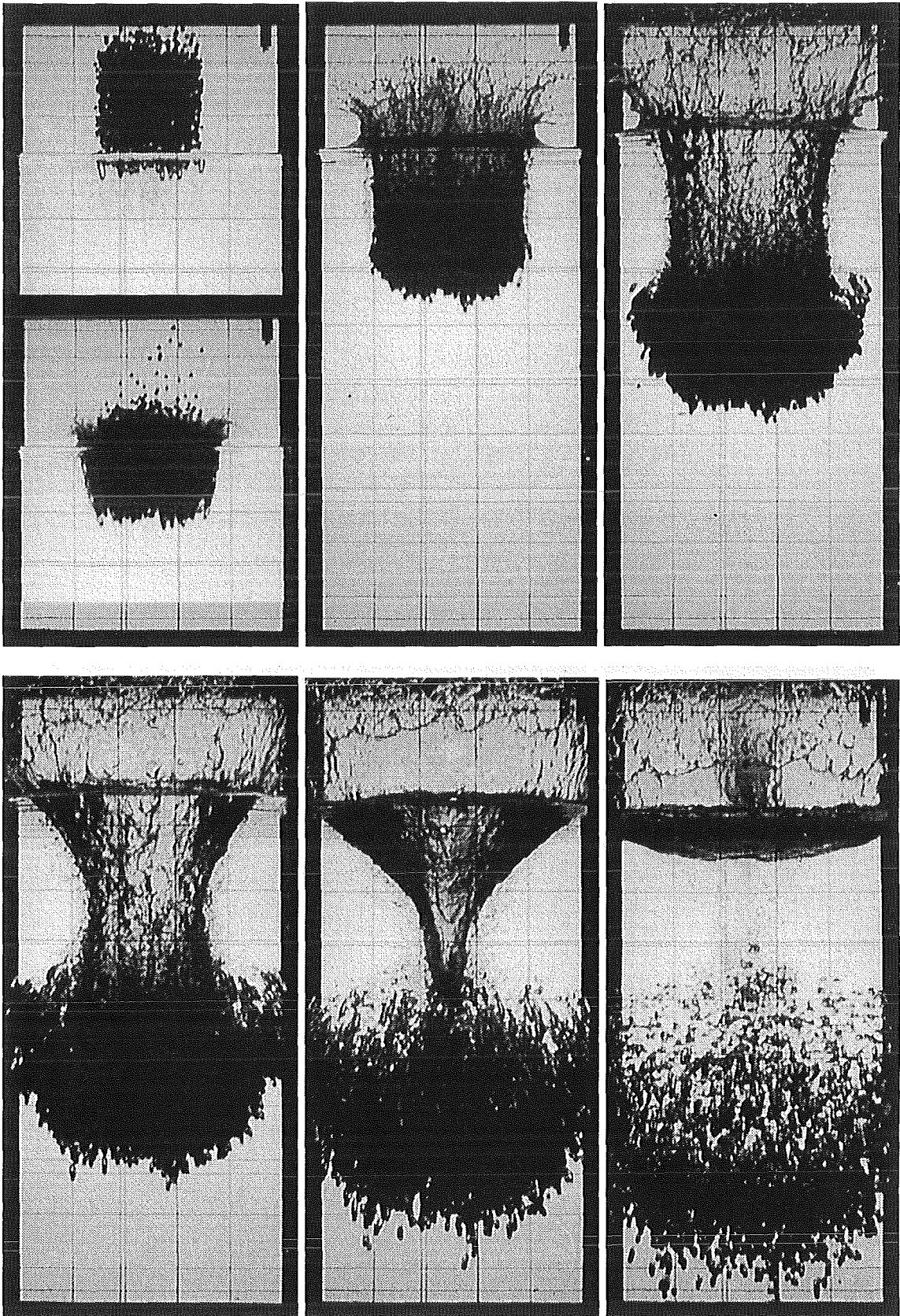
Fig. 4.11 **Q07,** PS, north
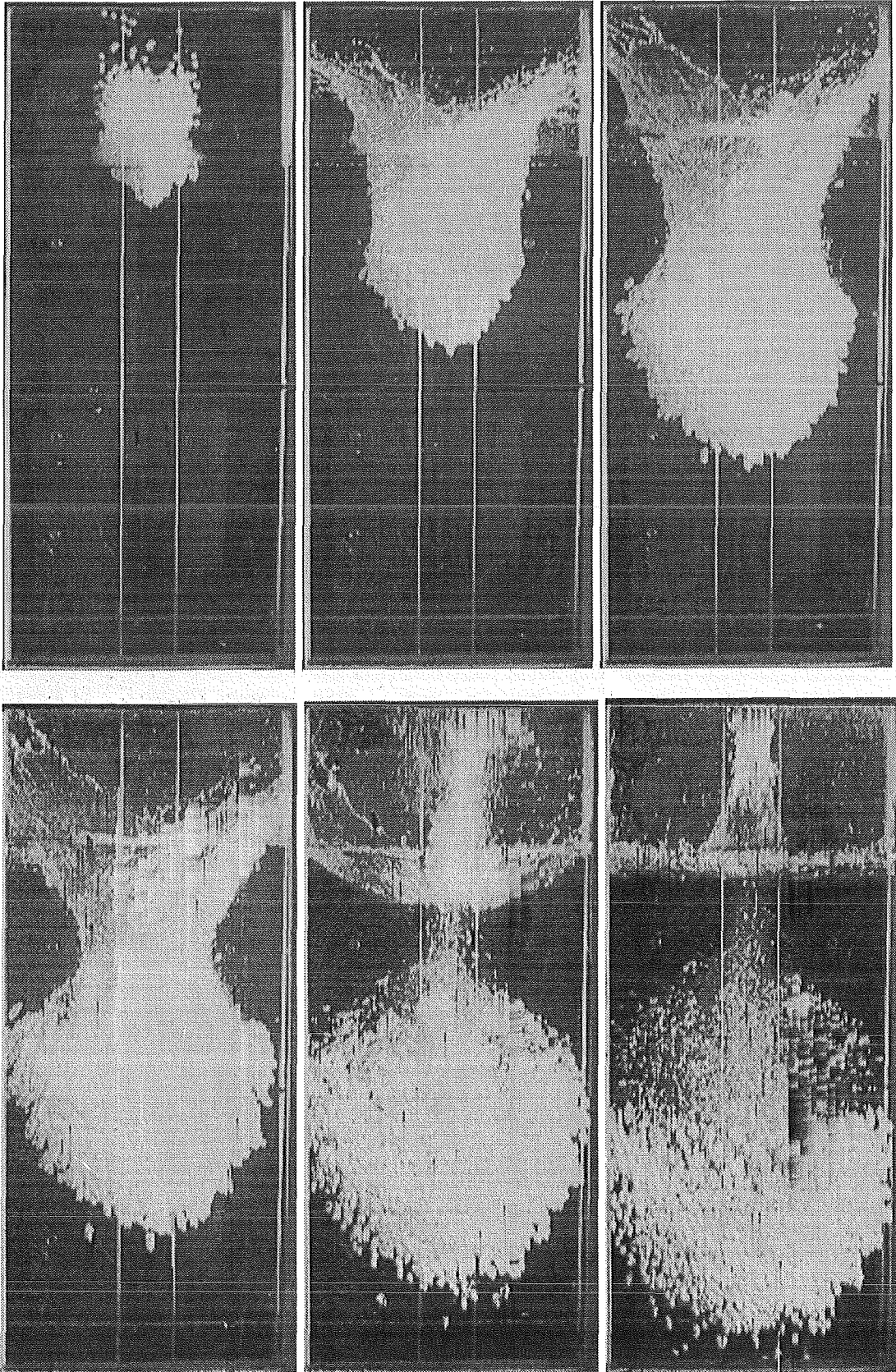
Fig. 4.12 Q07, Video west, $\Delta t = 80$ ms
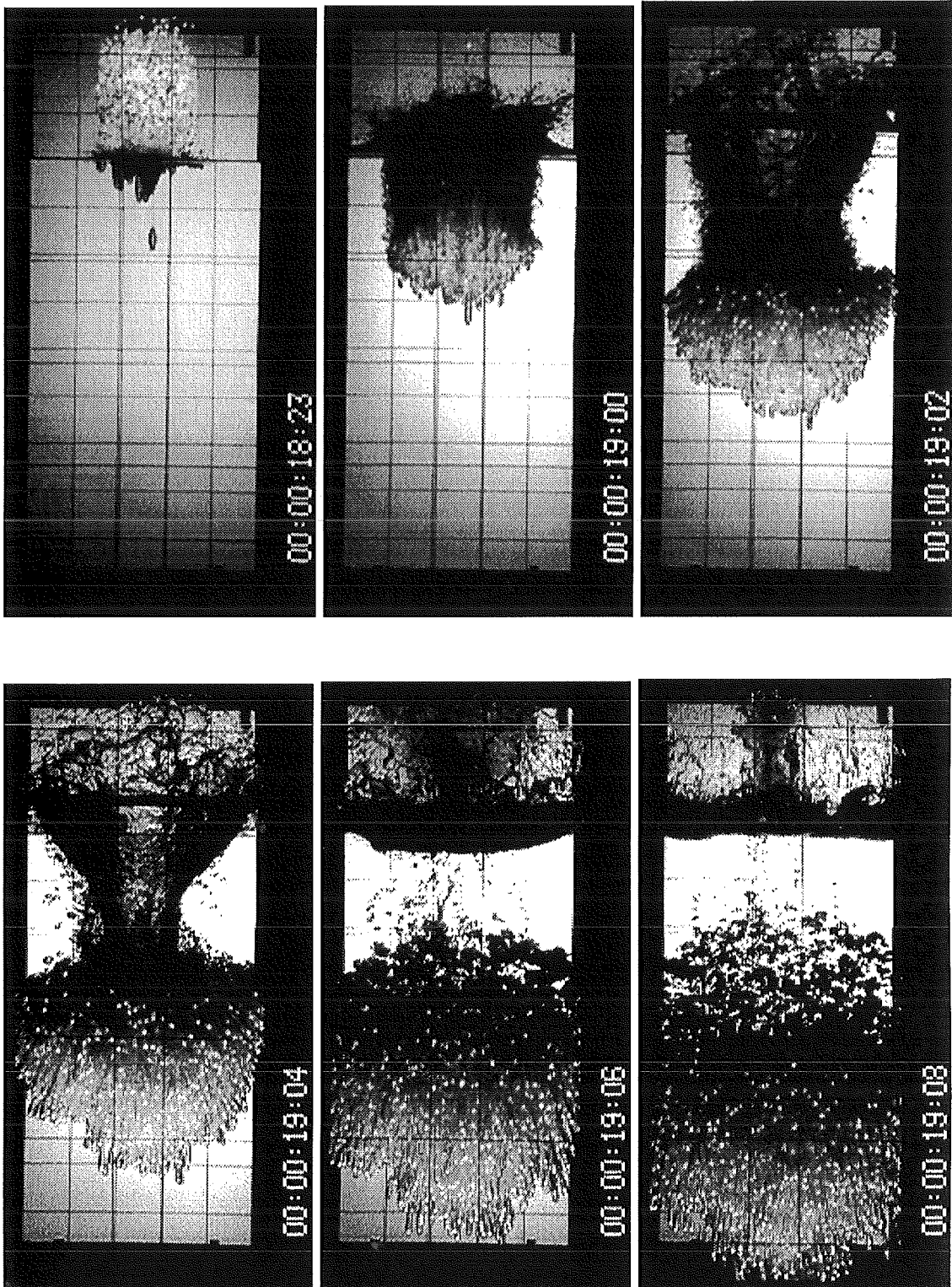
Fig. 4.13 **Q10,** Video (color), north, $\Delta t = 80$ ms
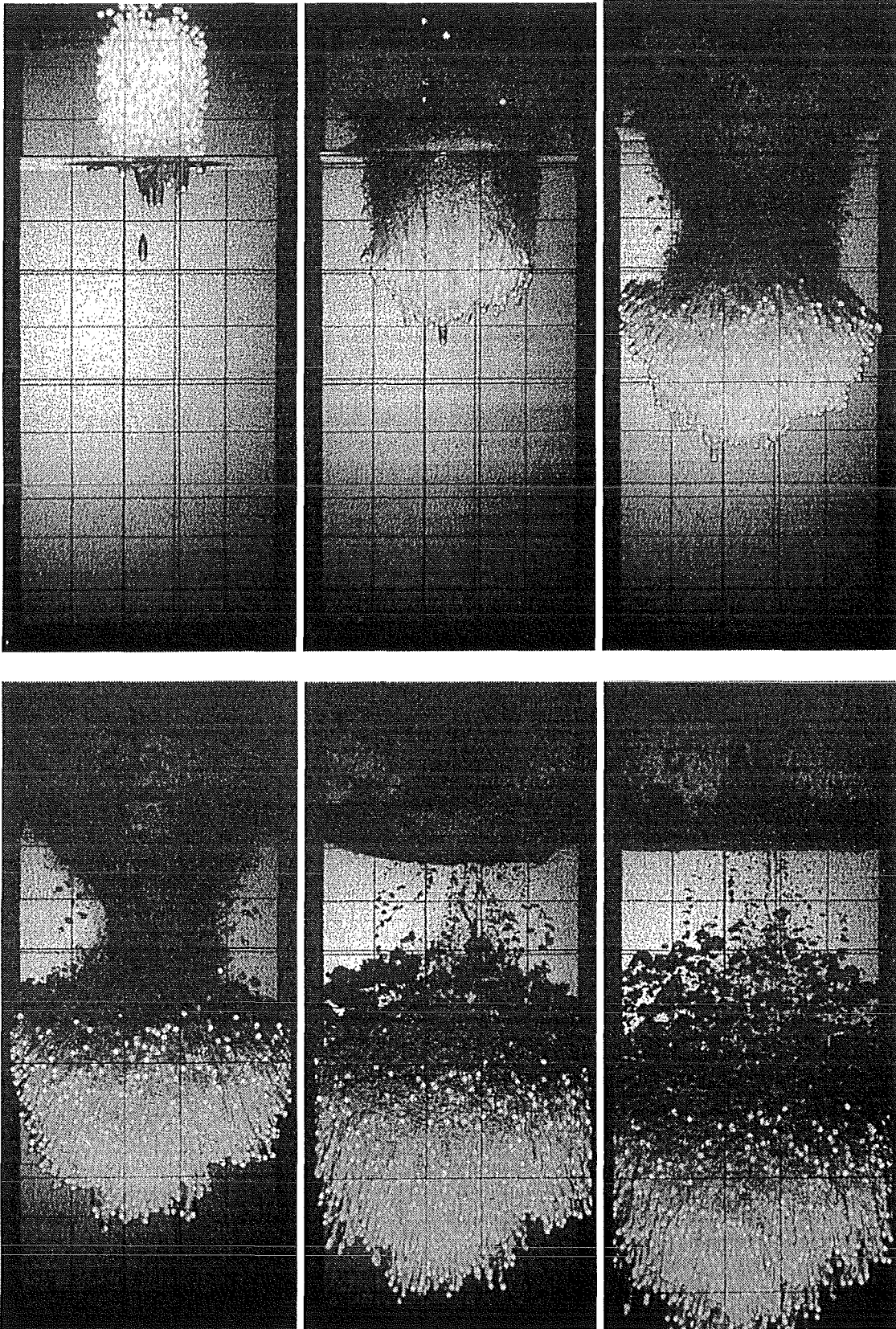
Fig. 4.14 **Q10**, PS (color), north
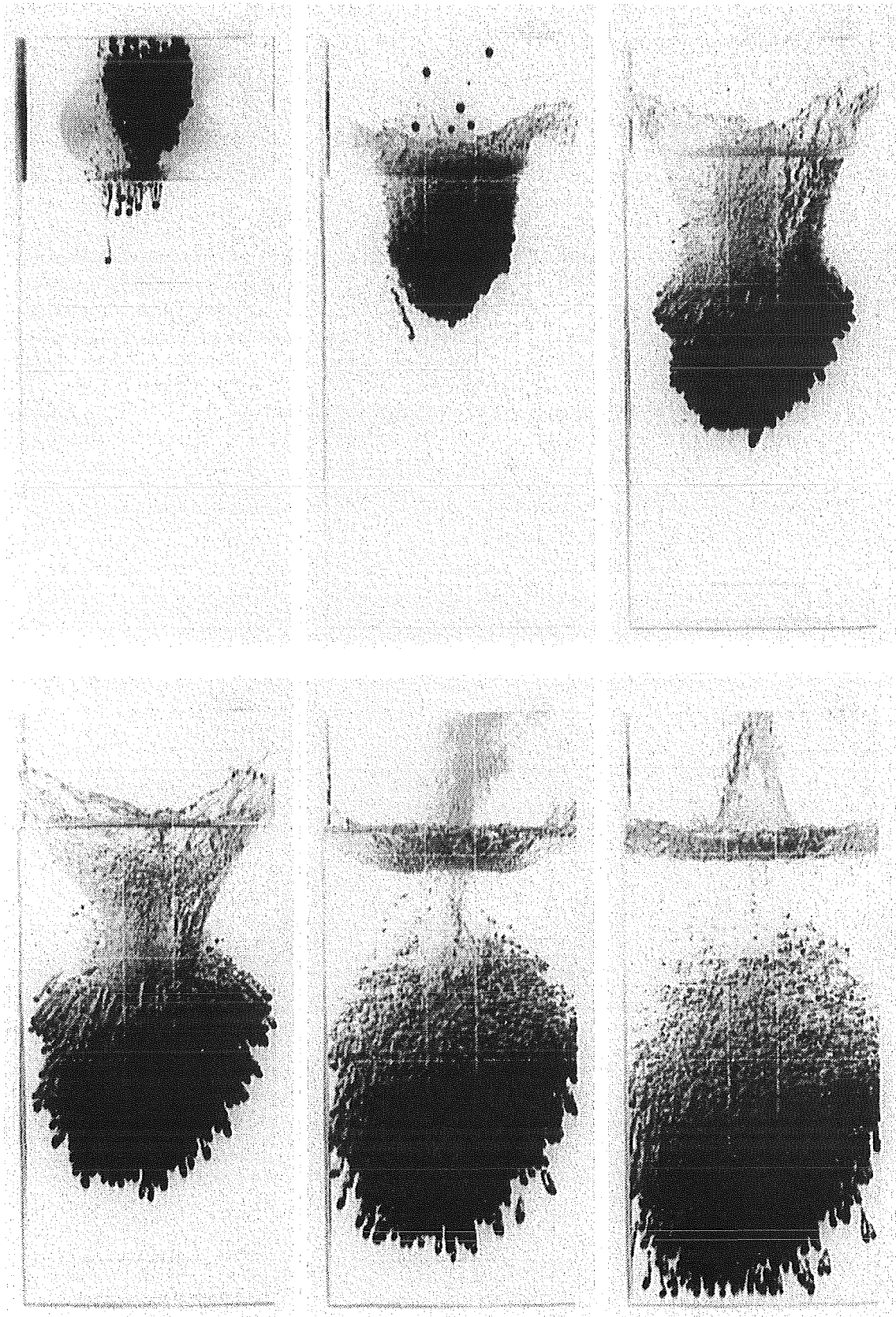
Fig. 4.15 **Q10**, LO (negativ from color), west
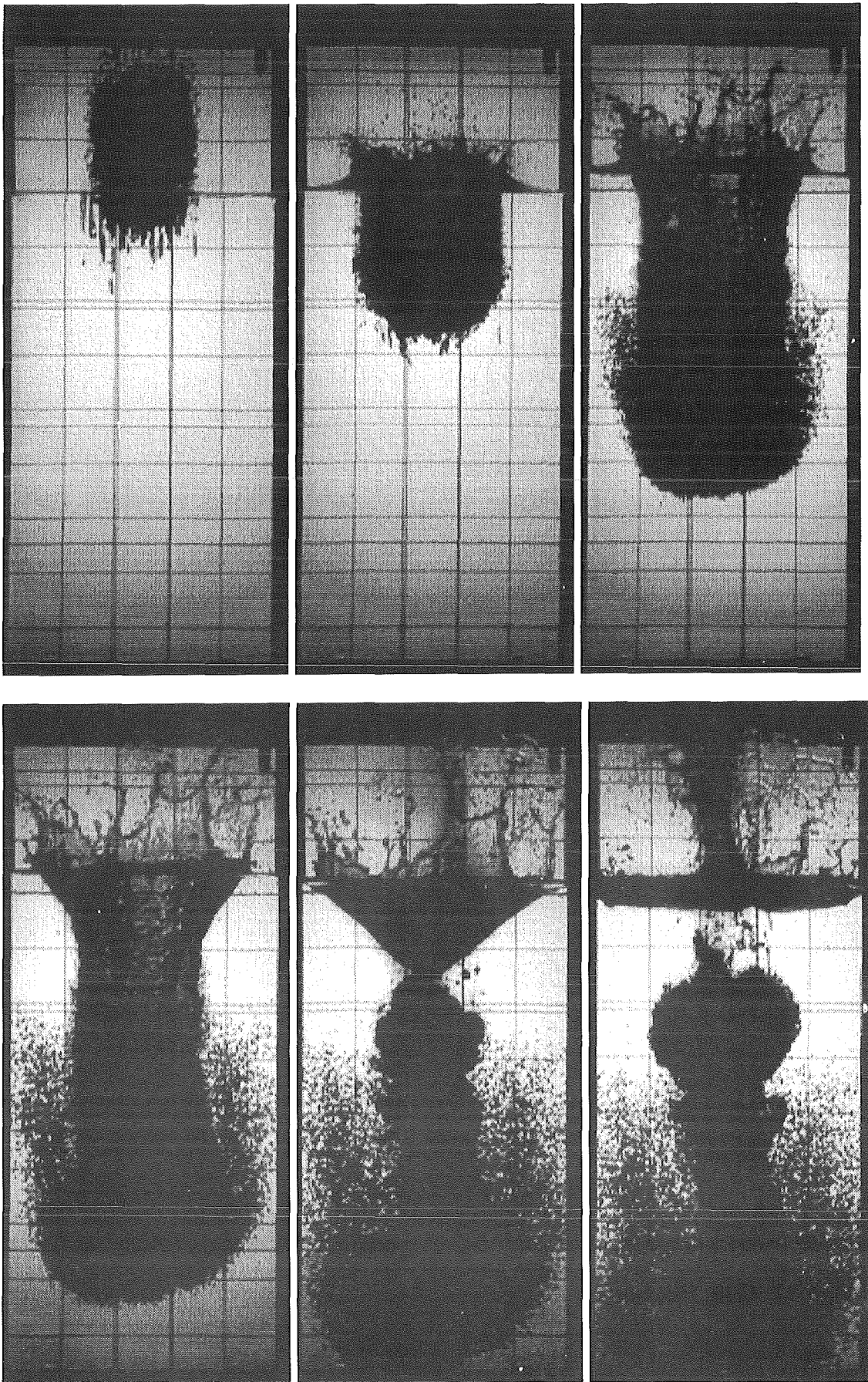
Fig. 4.16 **Q08**, Video north, $\Delta t = 60$ ms
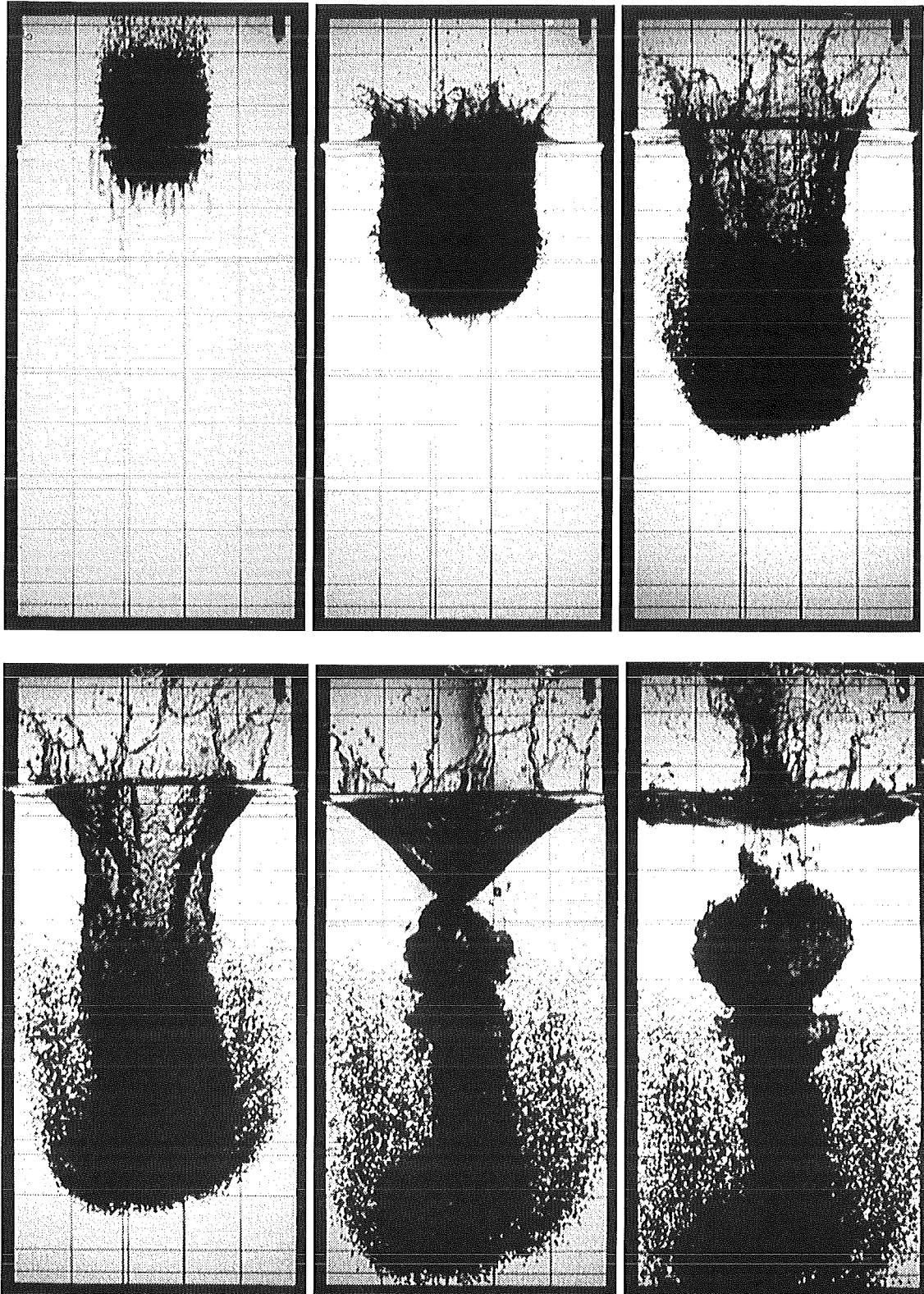
Fig. 4.17 **Q08**, PS, north
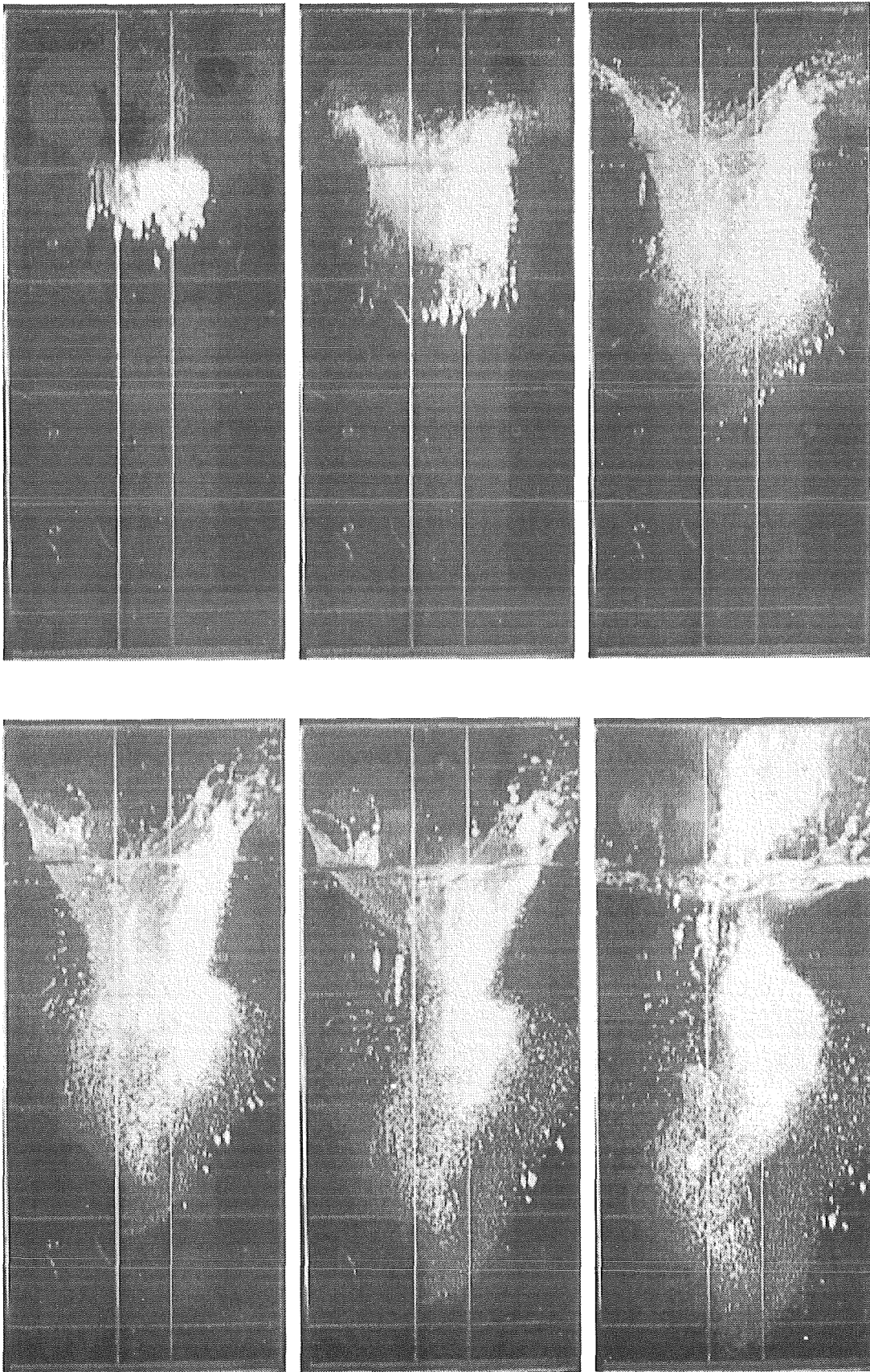
Fig. 4.18 **Q08**, video, west, $\Delta t = 60$ ms
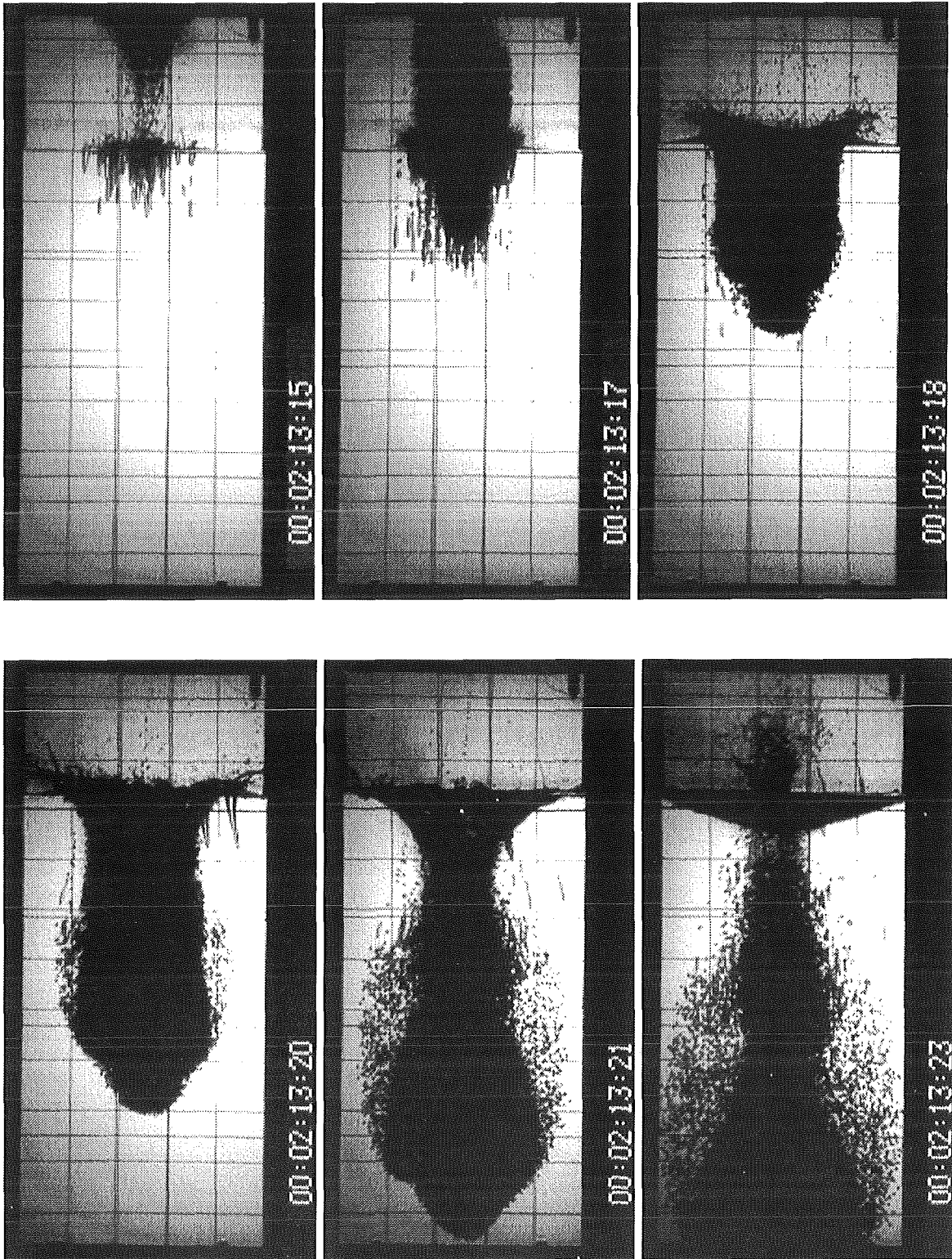
Fig. 4.19 **Q03,** Video, north, $\Delta t = 60$ ms
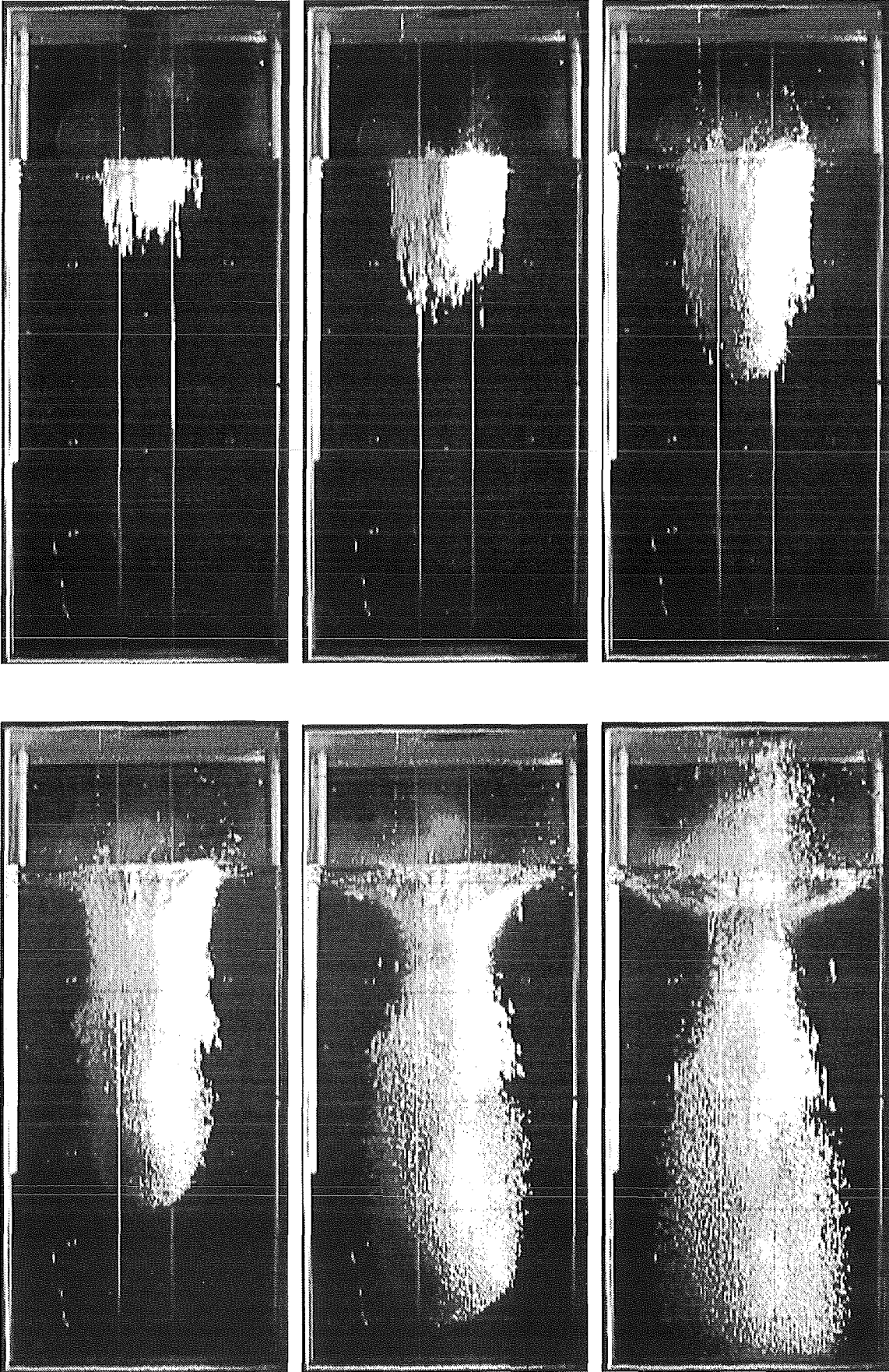
Fig. 4.20 **Q03**, Video, west, $\Delta t = 60$ ms
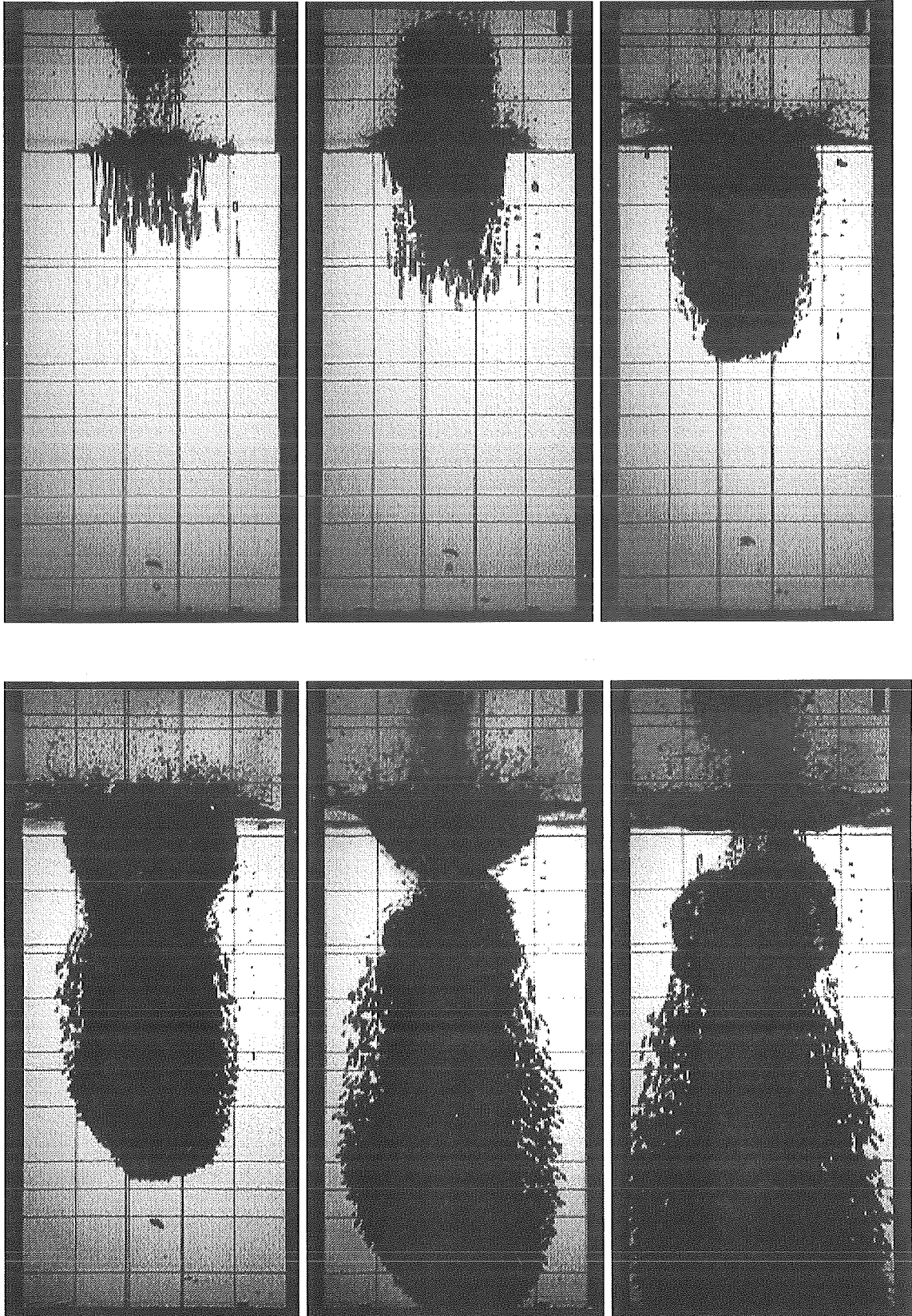
Fig. 4.21 **Q04**, Video, north, $\Delta t = 60$ ms
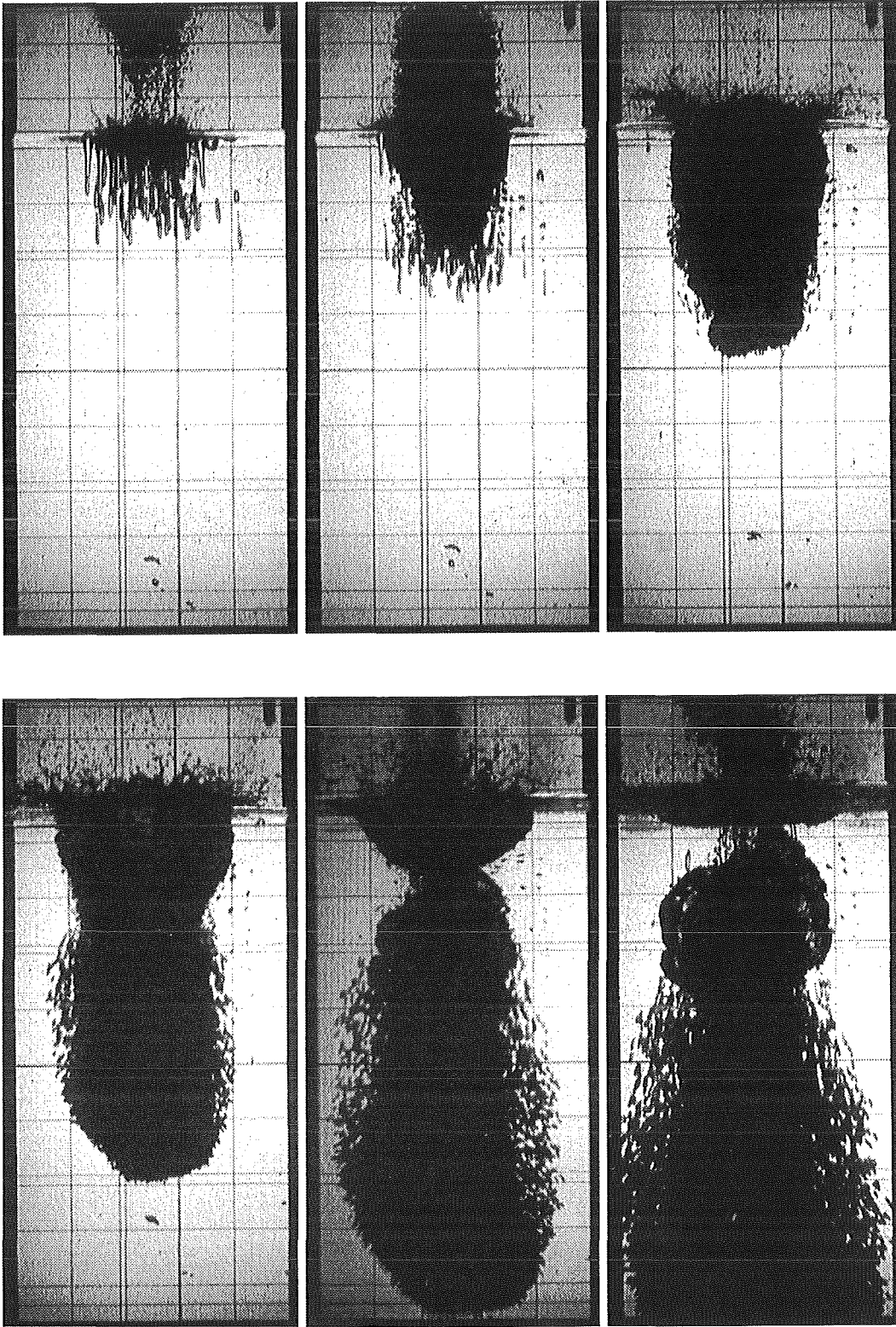
Fig. 4.22 **Q-04**, PS, north, $\Delta t = 60$ ms
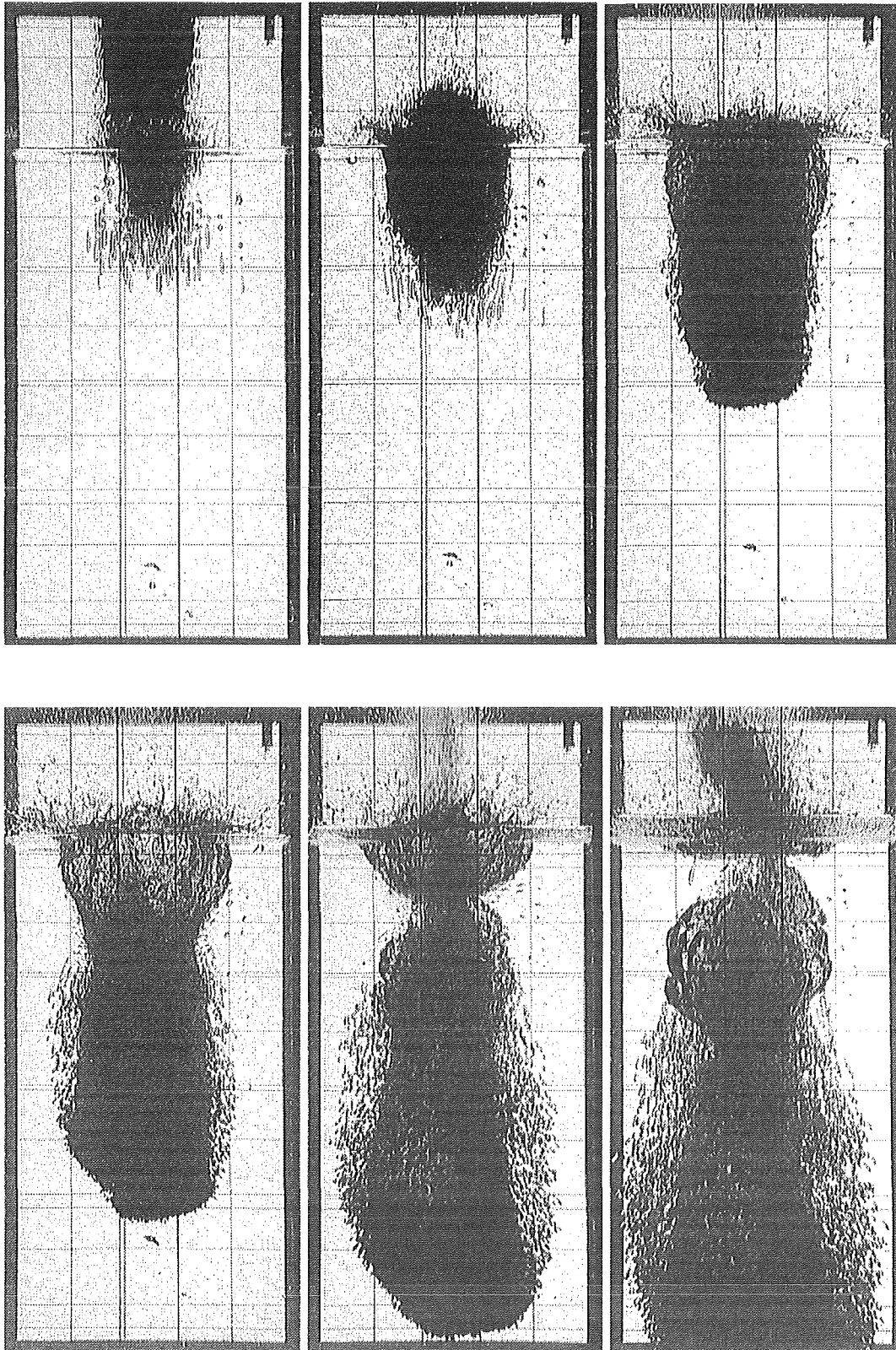
Fig. 2.23 **Q-04**, LO (negativ), north
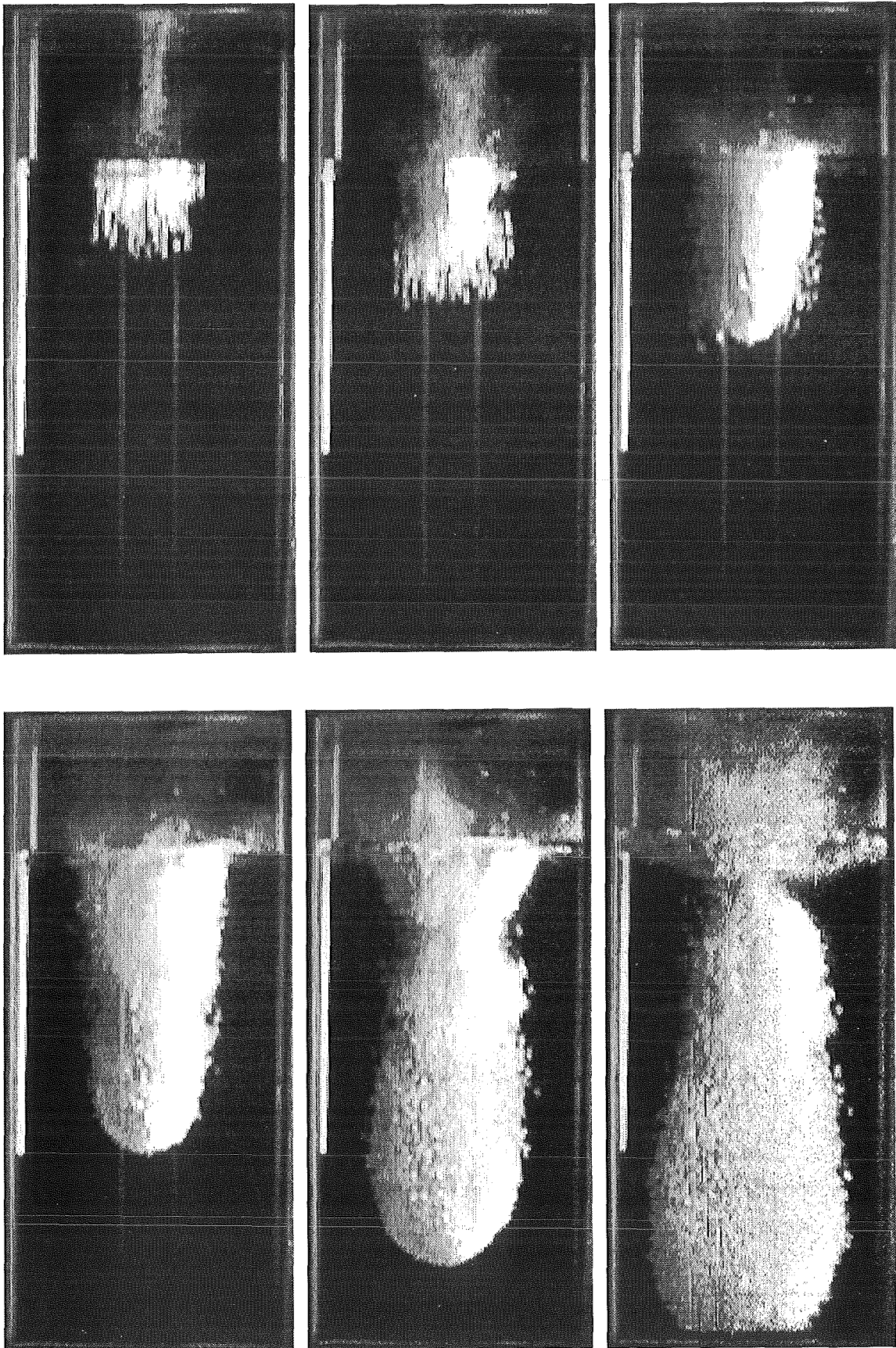
Fig. 4.24 **Q04**, Video, west, $\Delta t = 60$ ms
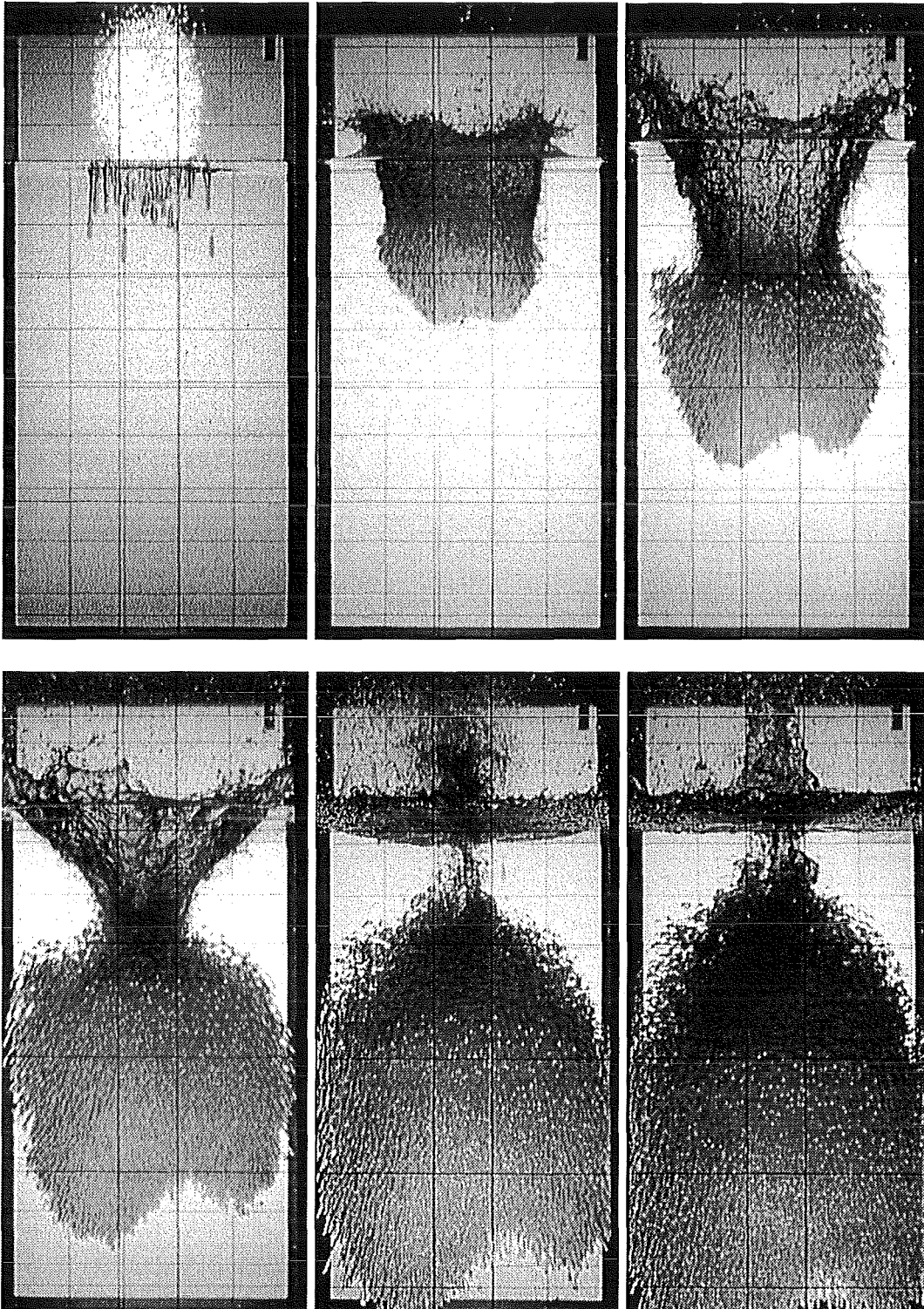
Fig. 4.25 **Q11**, PS (color), north , $\Delta t = 80$ ms
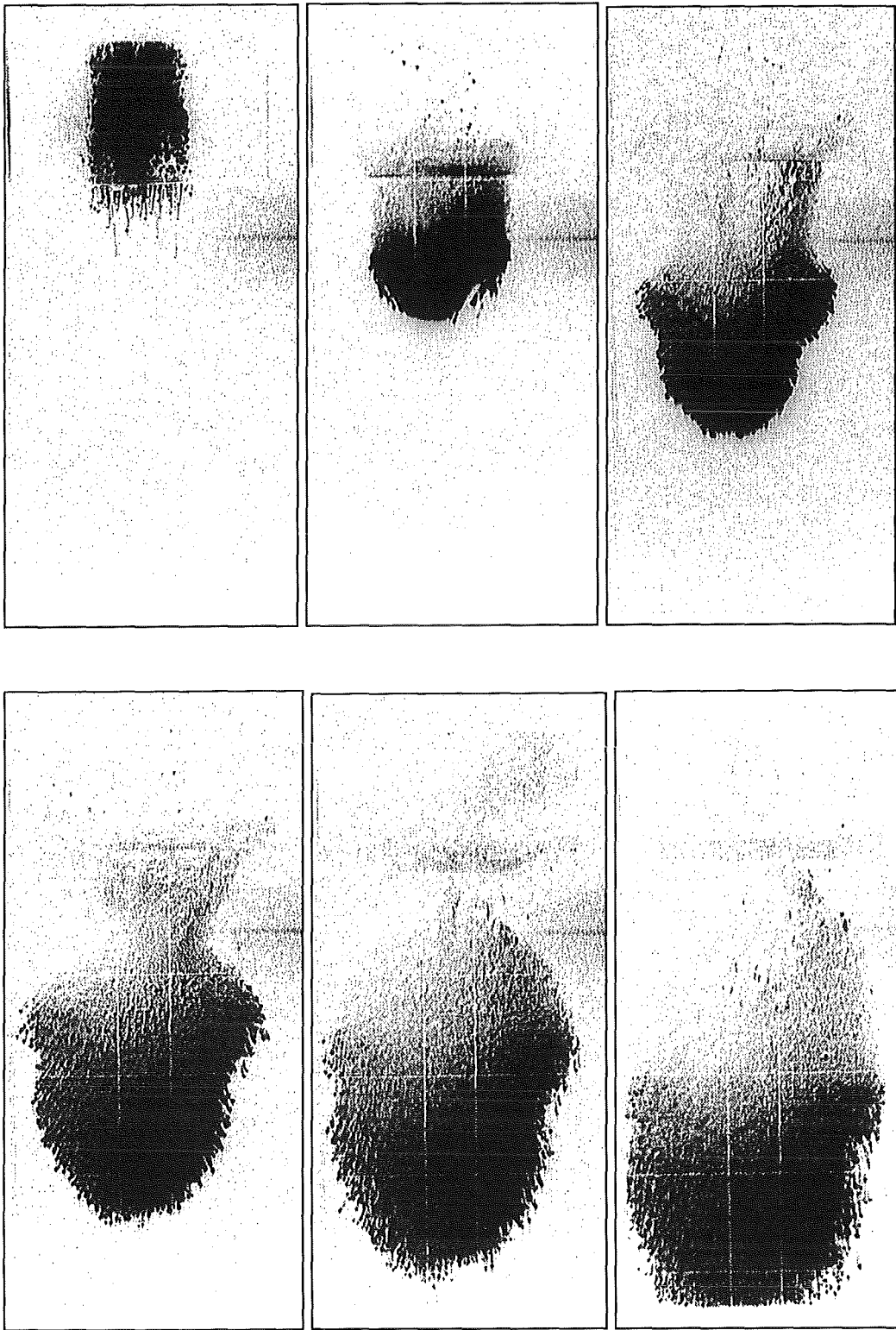
Fig.4.26 **Q11**, LO (negativ from color), west, Δt = 80 ms
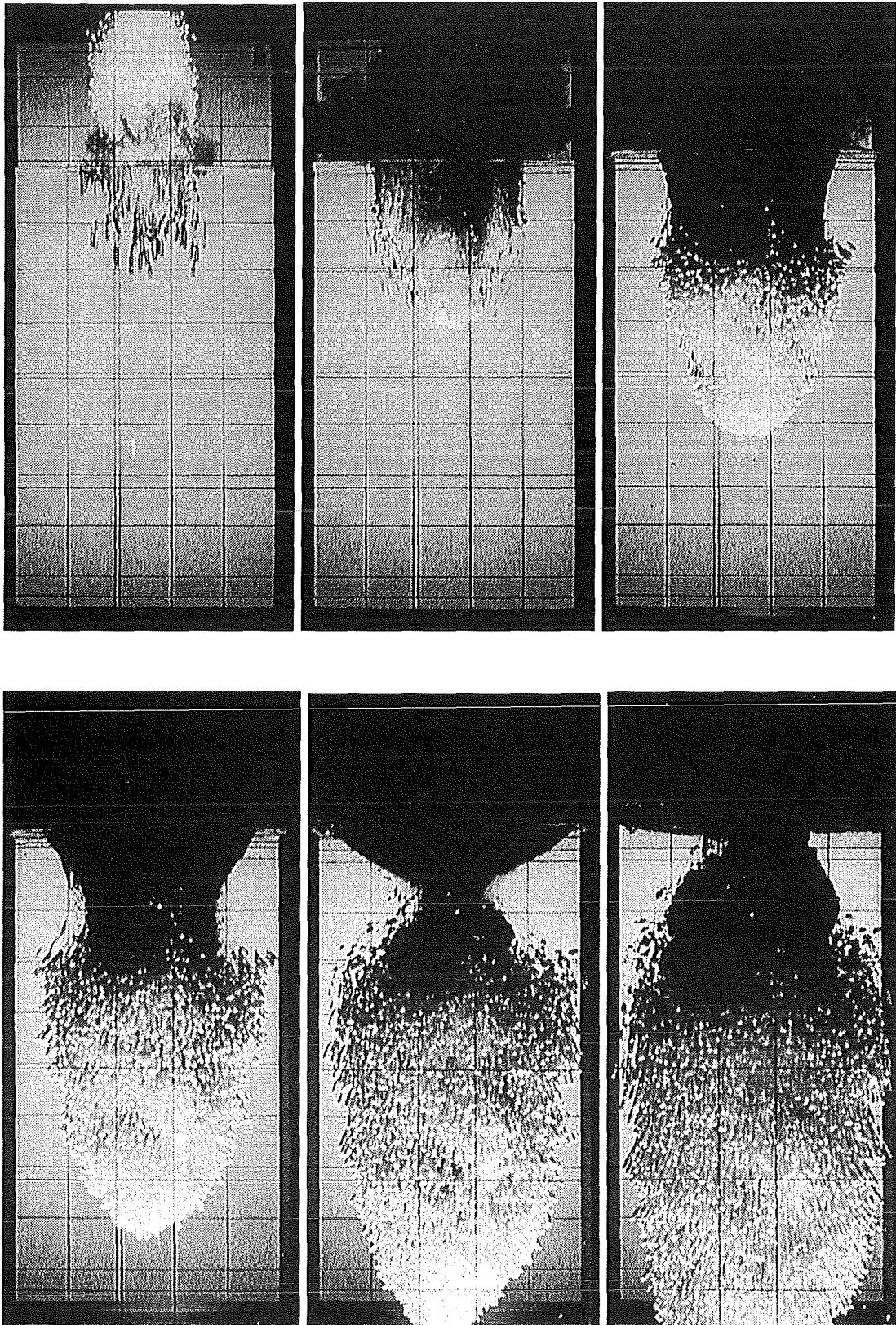
Fig. 4.27.1   **Q12** , PS (color), north, $\Delta t = 56$ ms
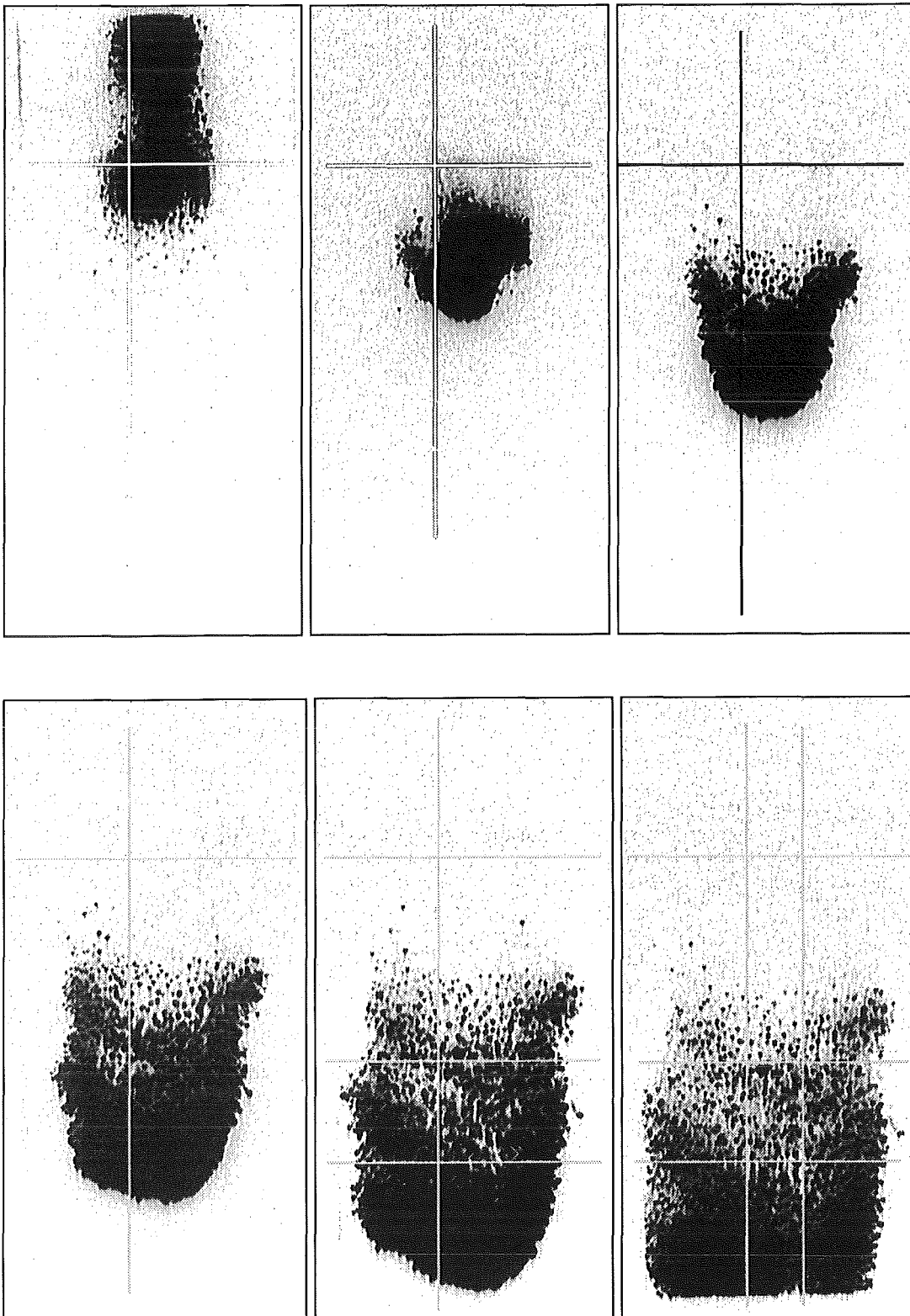
Fig.4.27.2   **Q12**, LO (negativ from color), west, Δt = 56 ms
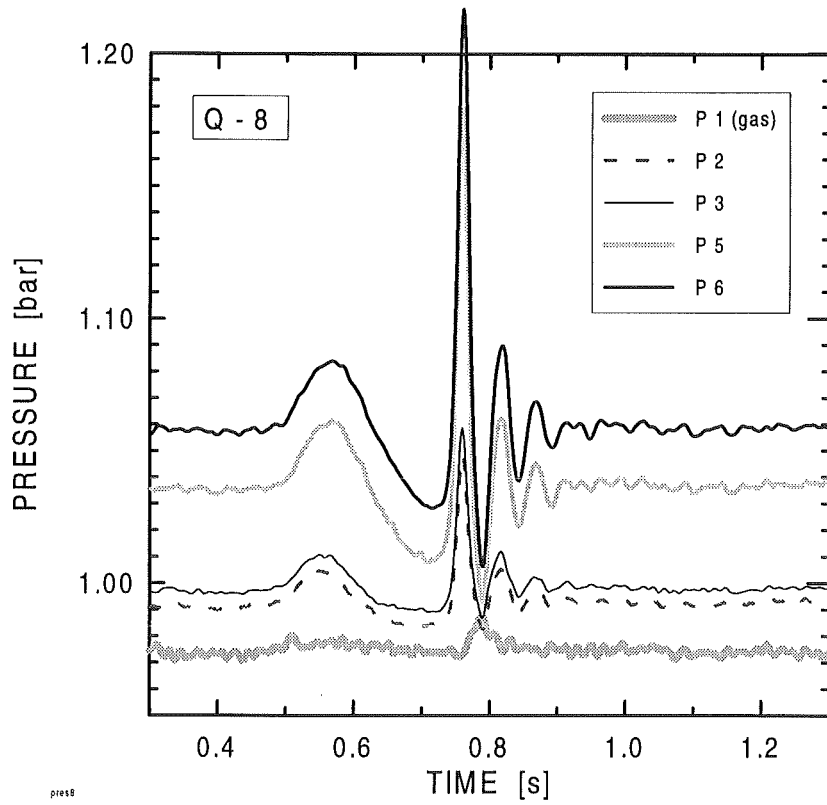
Fig. 4.28 Pressure with cold molybdenum spheres of 4.2 mm diameter
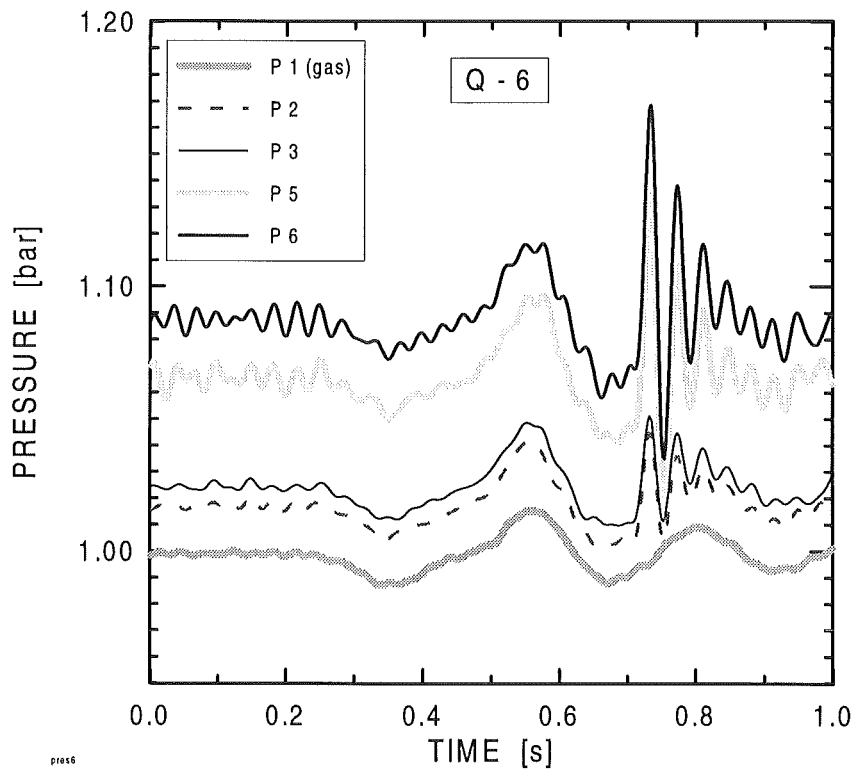
Fig. 4.29 Pressure with cold zirconia spheres of 10 mm diameter
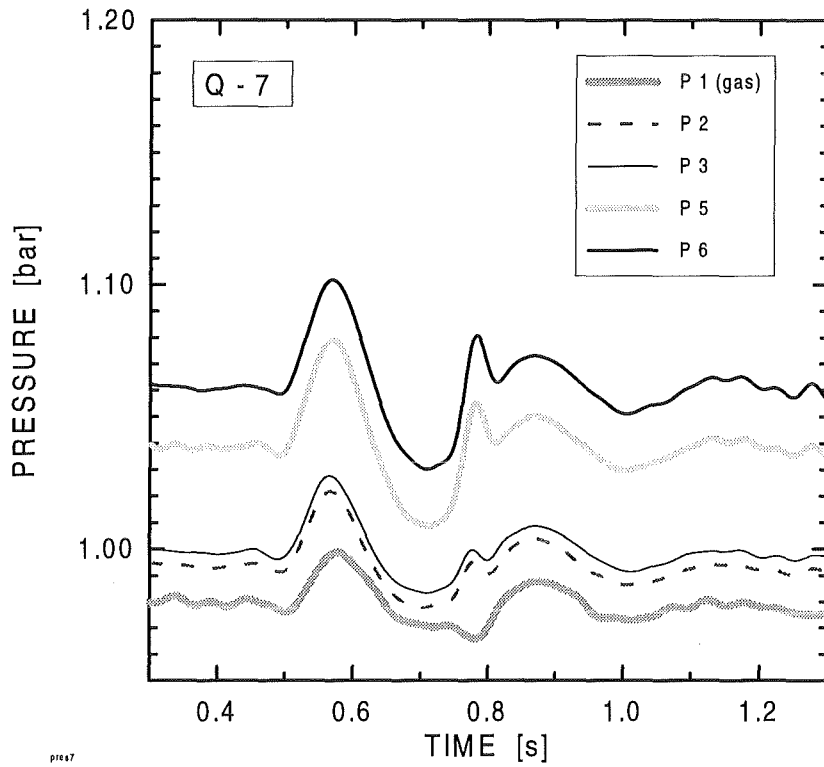
Fig. 4.30 Pressure with hot zirconia spheres of 10 mm diameter, 1300 K
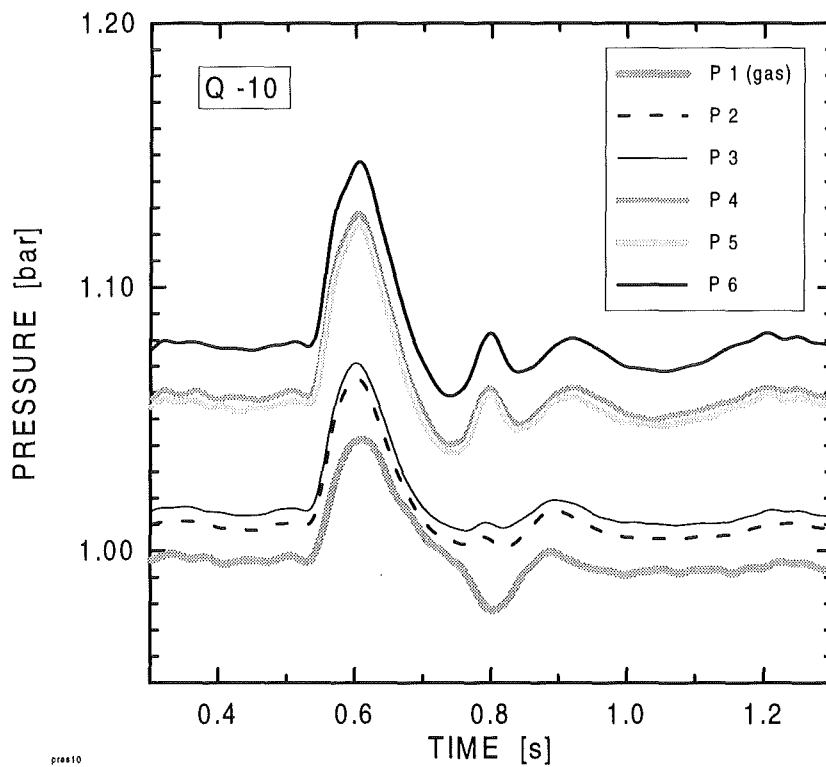
Fig. 4.31 Pressure with hot zirconia spheres of 10 mm diameter, 1800 K
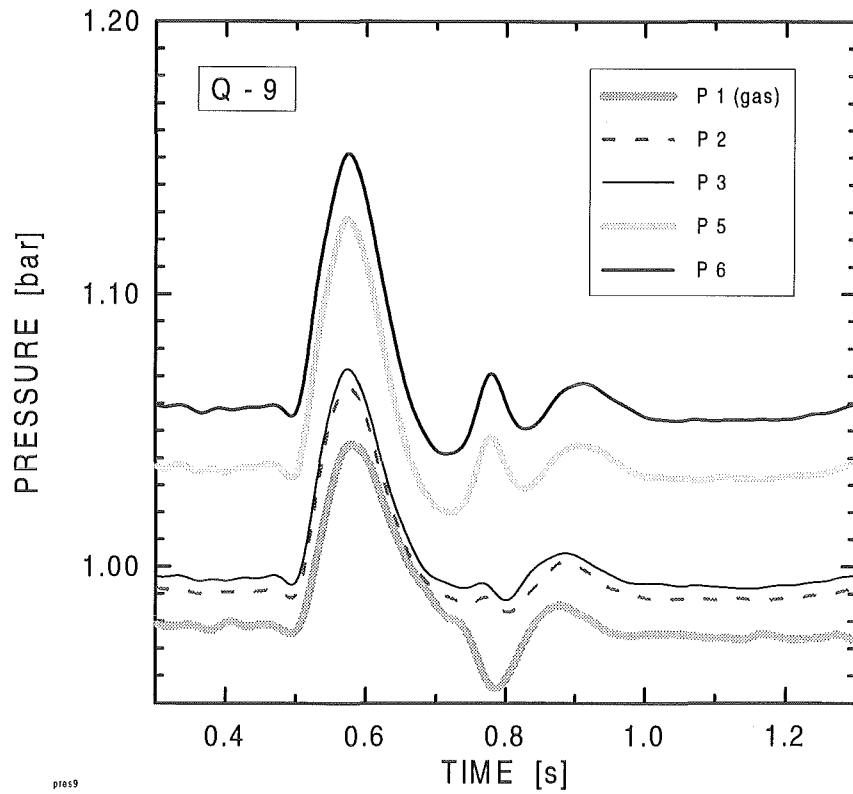
Fig. 4.32 Pressure with hot zirconia spheres of 5 mm diameter, 1300 K
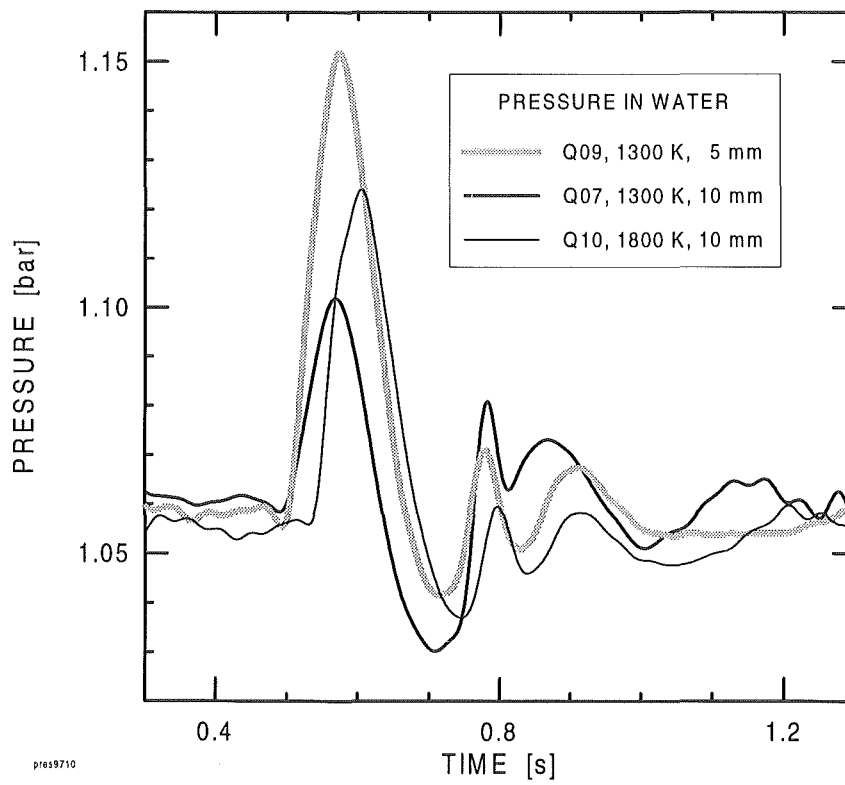
Fig. 4.33 Comparison of pressure with hot zirconia spheres
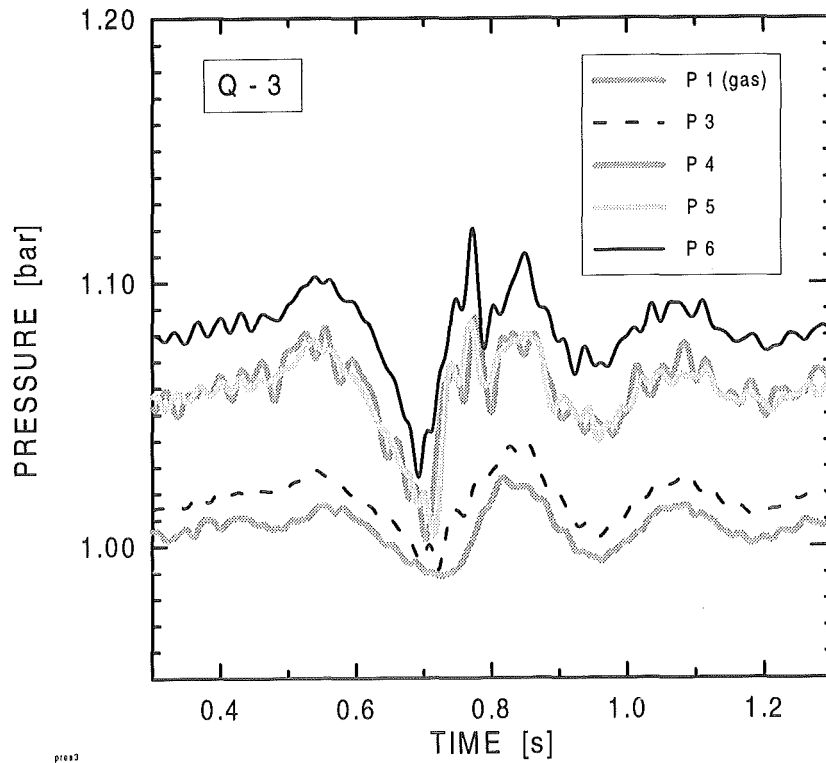
Fig. 4.34 Pressure with hot molybdenum spheres of 4.2 mm diameter, 900 K
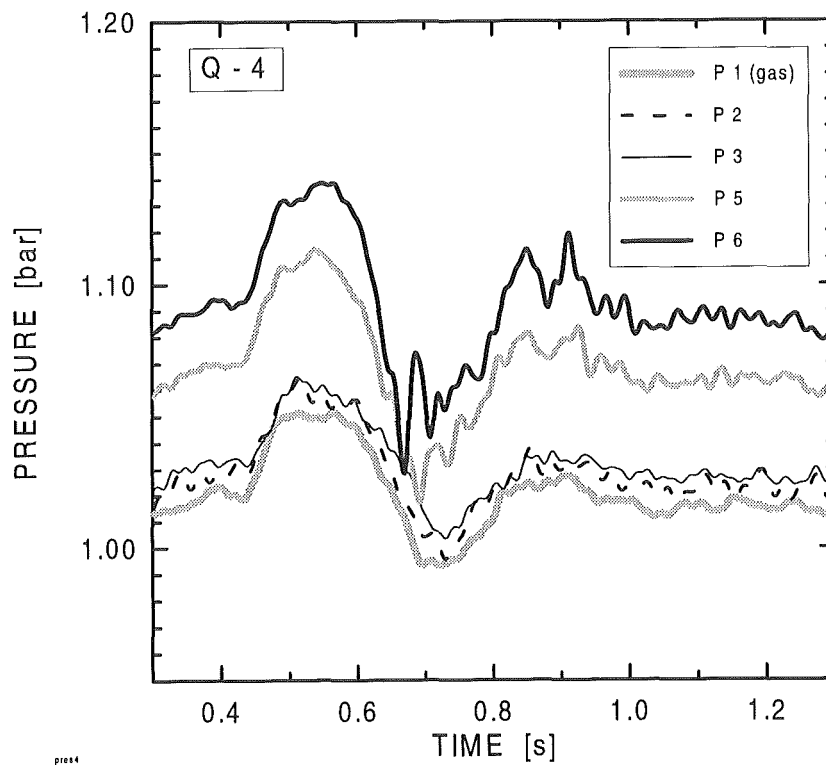
Fig. 4.35 Pressure with hot molybdenum spheres of 4.2 mm diameter, 1300 K
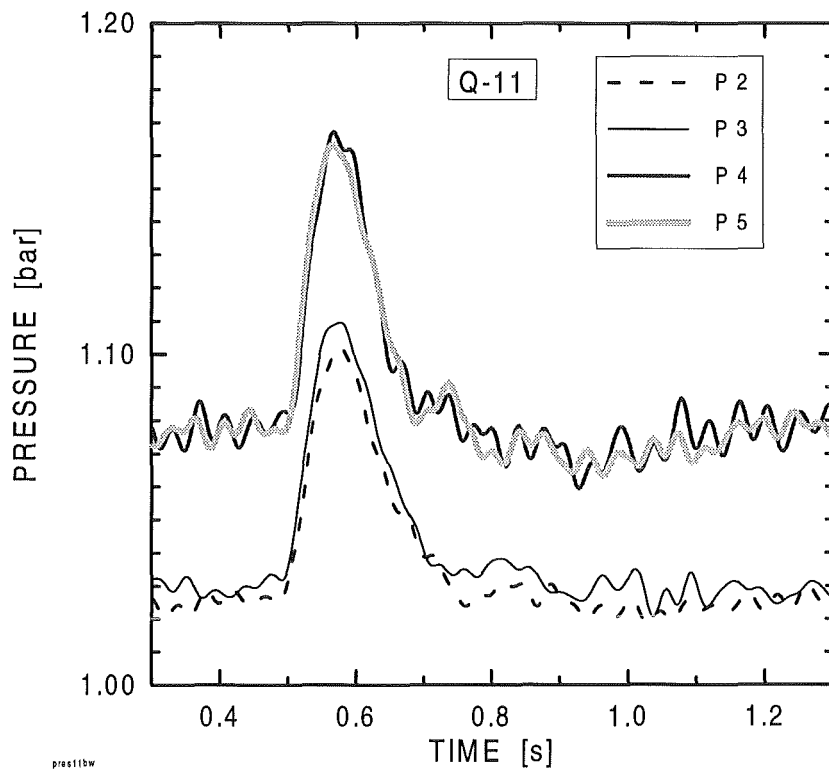
Fig. 4.36 Pressure with hot molybdenum spheres of 4.2 mm diameter, 1800 K
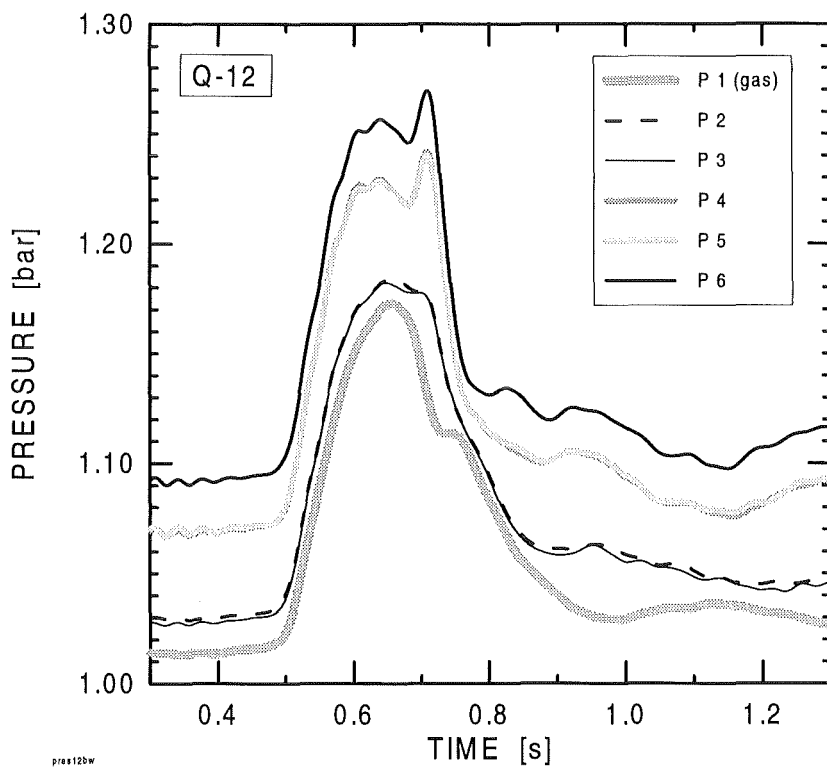
Fig. 4.37 Pressure with hot molybdenum spheres of 4.2 mm diameter, 2300 K
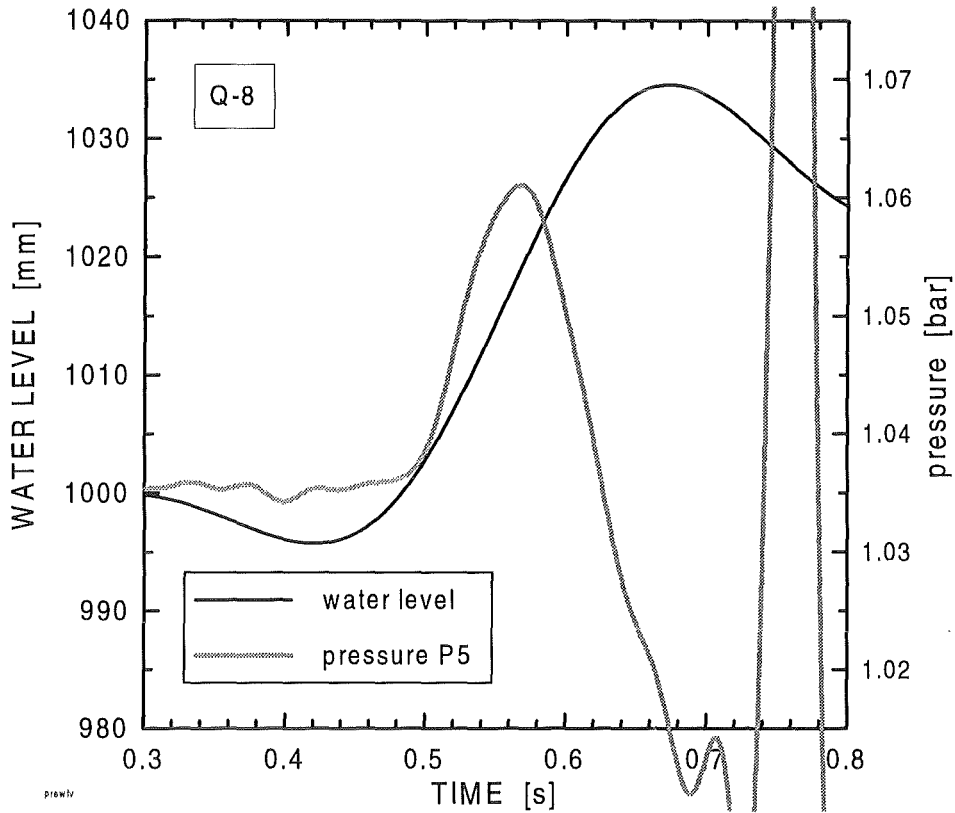
Fig. 4.38 Comparison of pressure and water level rise with cold spheres
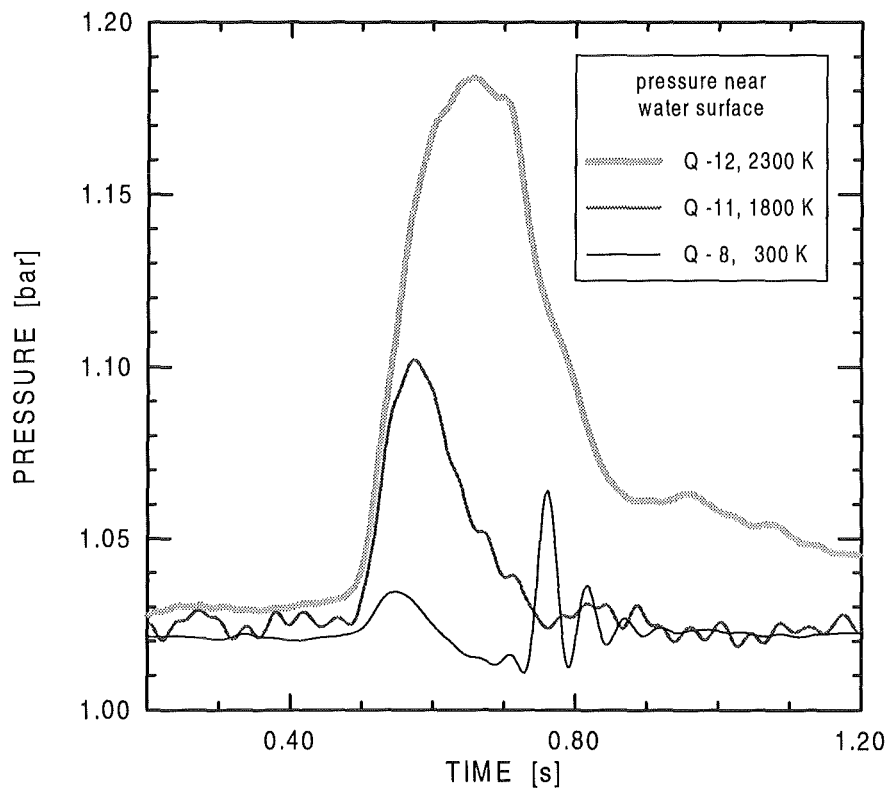
Fig. 4.39 Pressure in three experiments with molybdenum spheres
at different temperatures
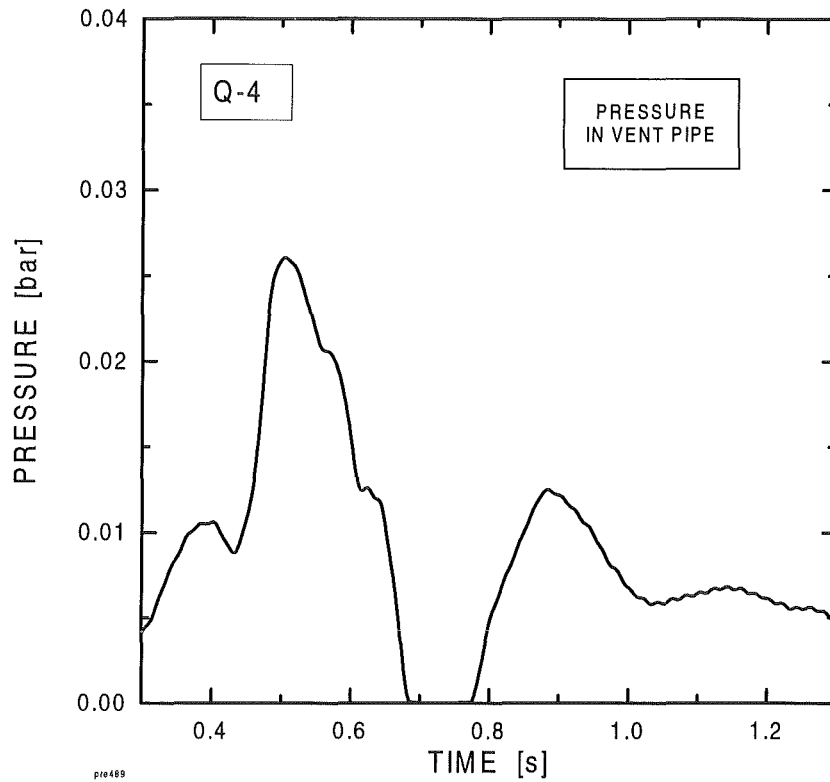
Fig. 4.40 Gauge pressure in vent pipe upstream of vortex meter
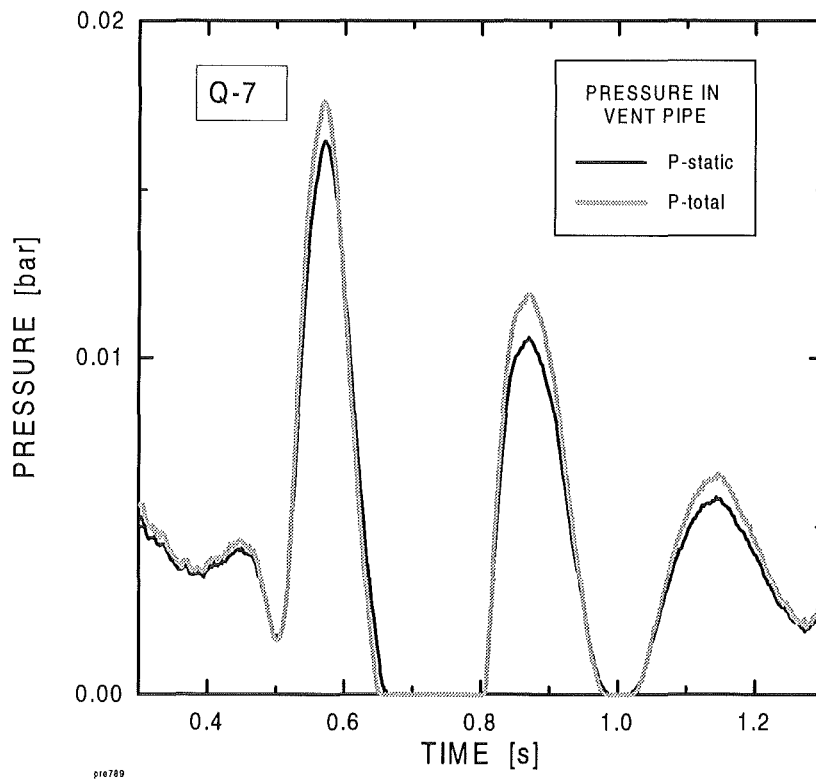
Fig. 4.41 Gauge pressure in vent pipe upstream of vortex meter
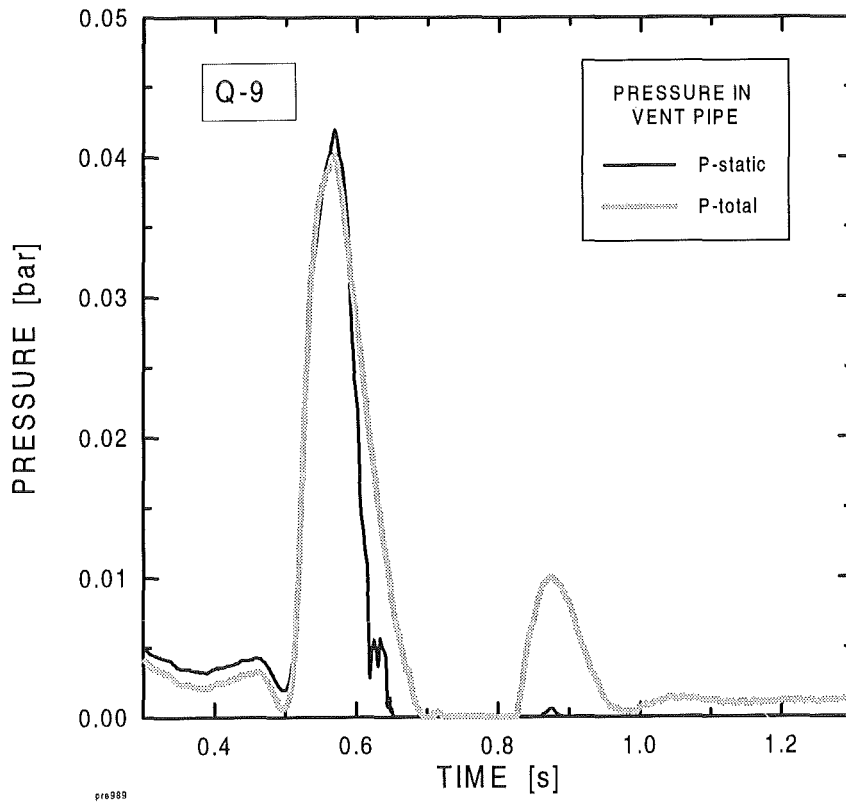
Fig. 4.42 Gauge pressure in vent pipe upstream of vortex meter
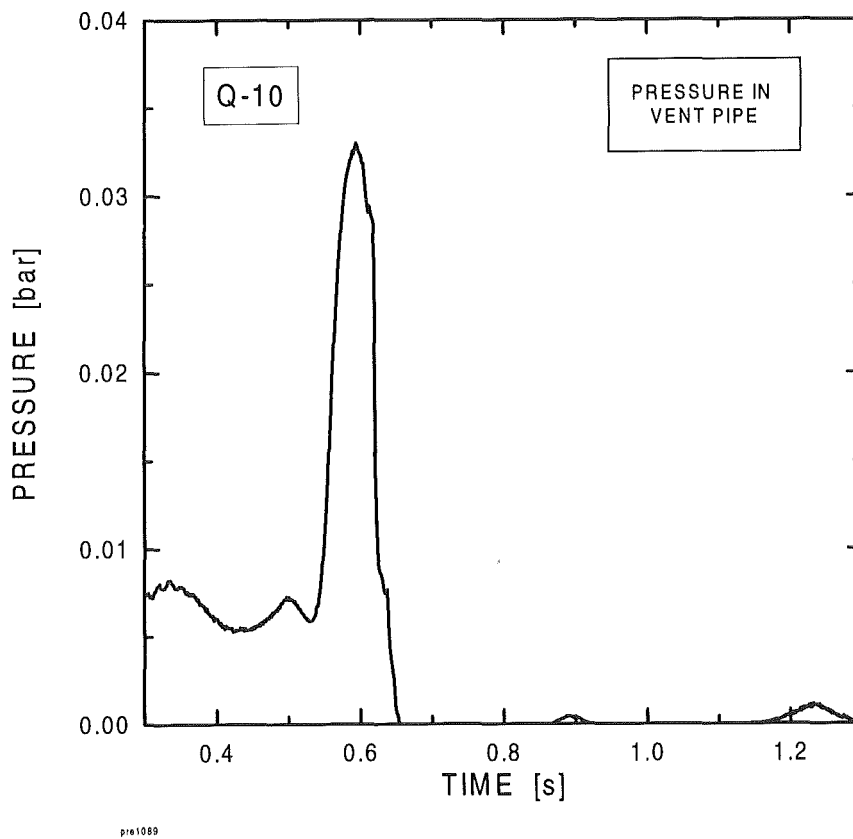
Fig. 4.43 Gauge pressure in vent pipe upstream of vortex meter
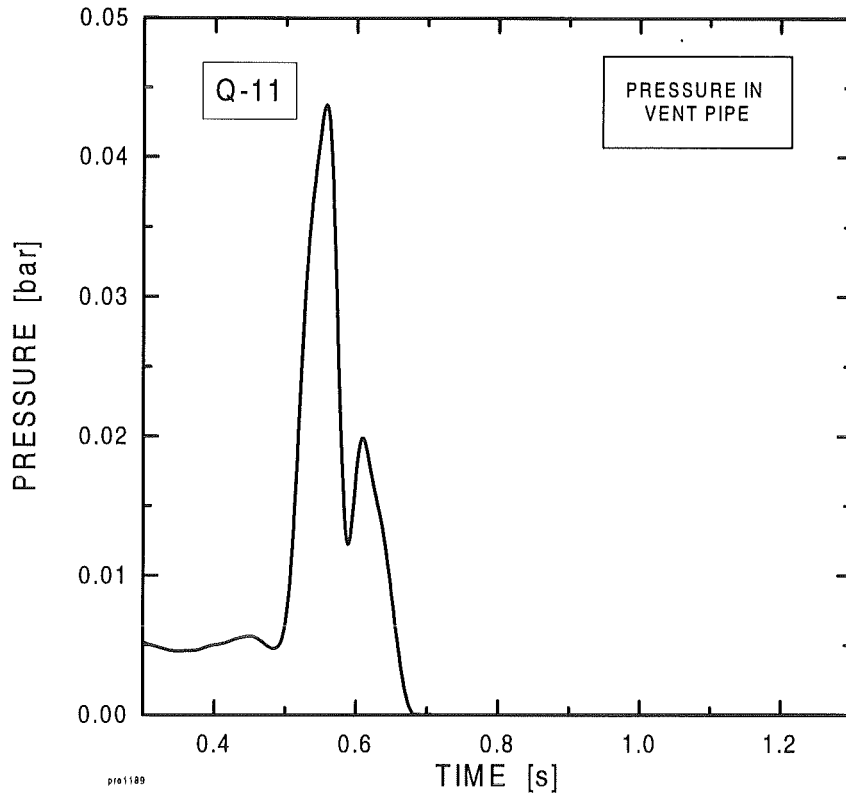
Fig. 4.44 Gauge pressure in vent pipe upstream of vortex meter
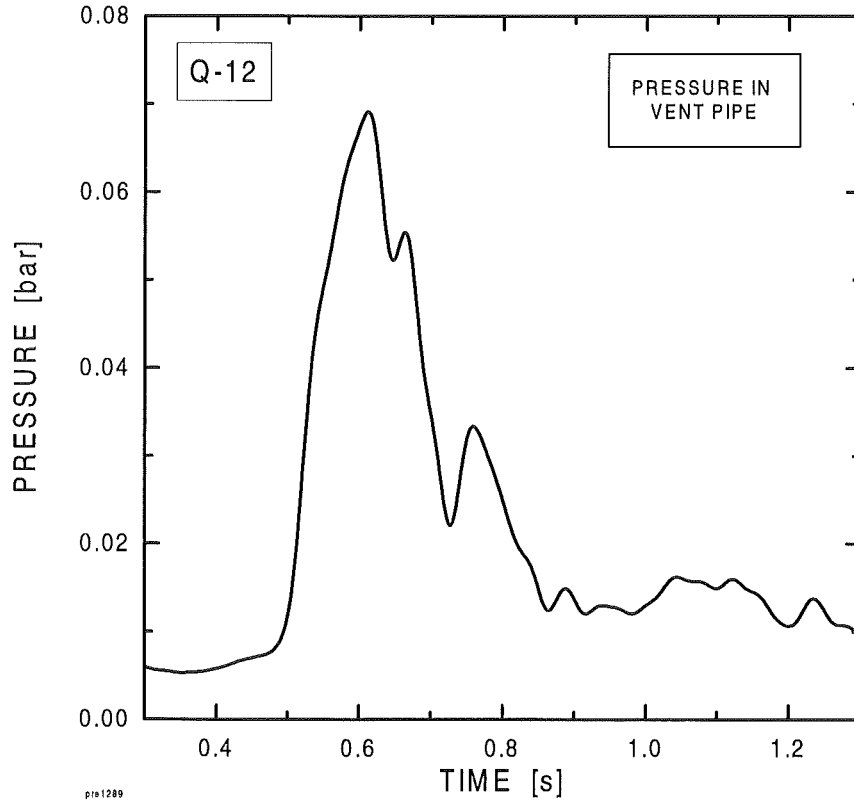
Fig. 4.45 Gauge pressure in vent pipe upstream of vortex meter
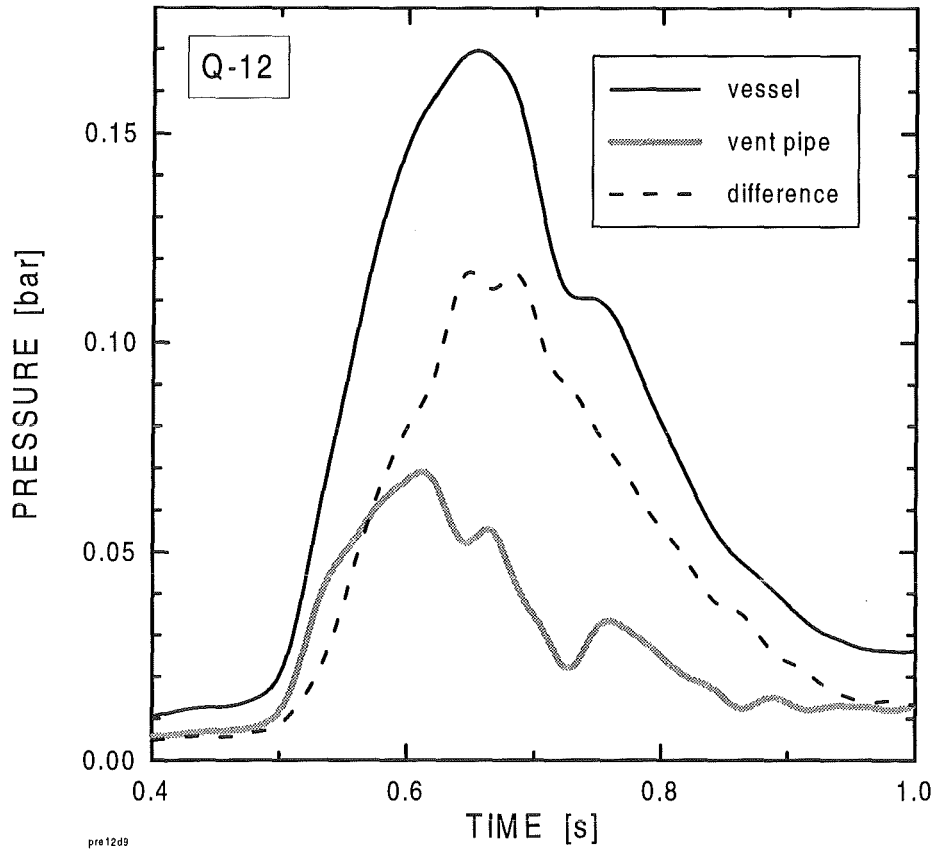
Fig. 4.46 Pressure in vessel, vent pipe and differential pressure
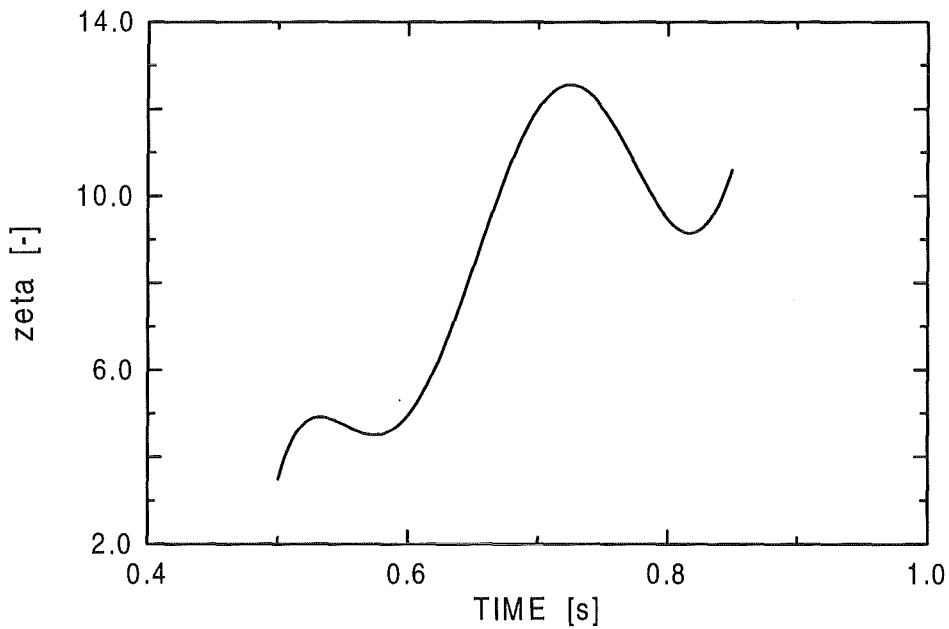
Fig.4.47 Pressure loss coefficient ζ in transient flow for the first part of the vent pipe
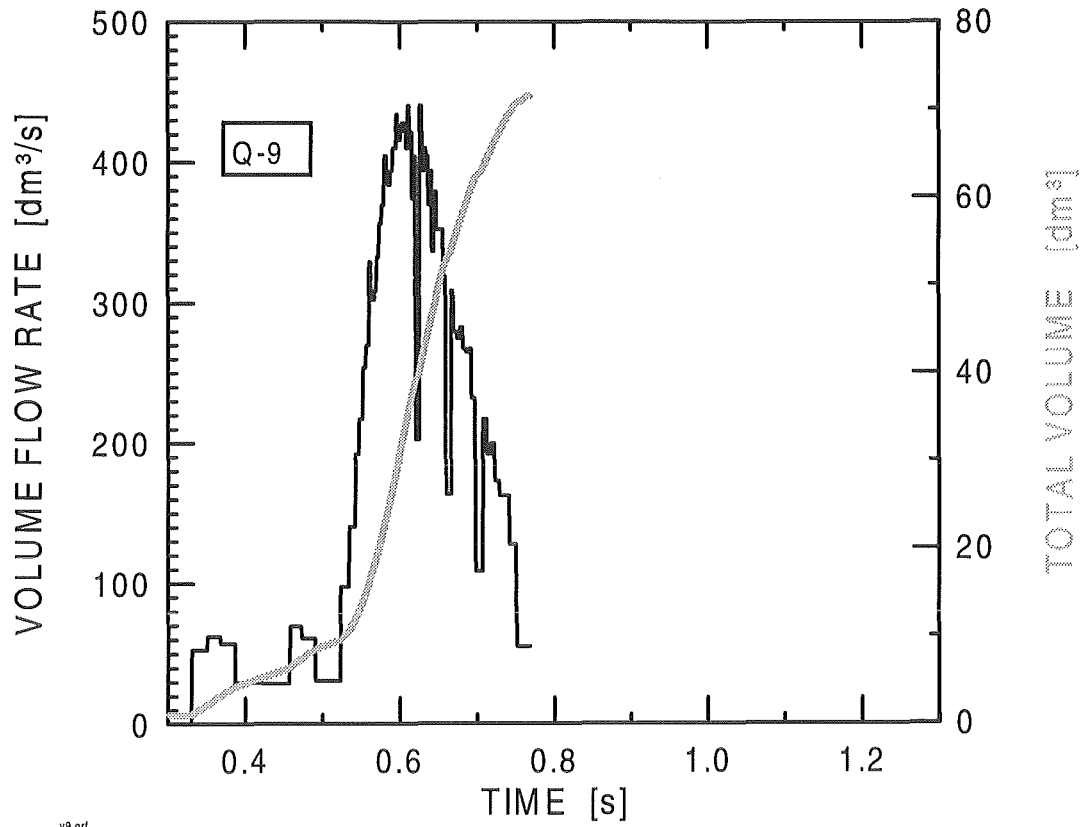
Fig. 4.48 Steam rate with zirconia spheres of 5 mm diameter, 1300 K
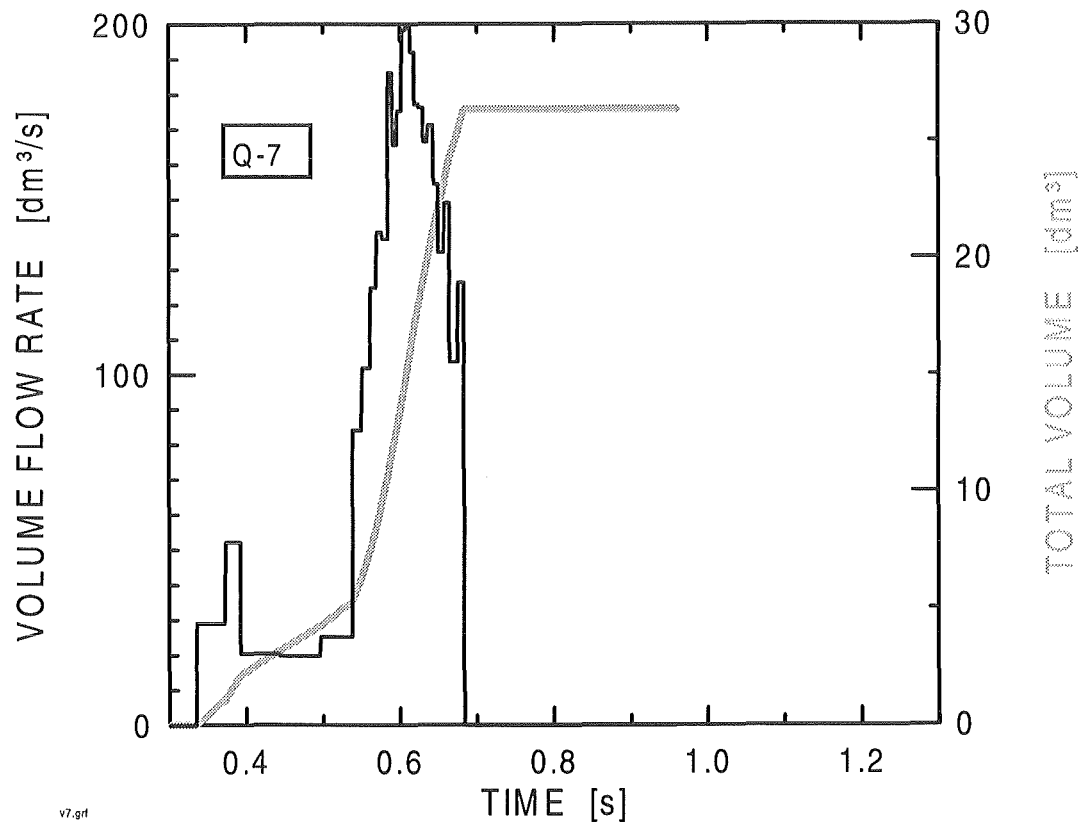
Fig. 4.49 Steam rate with zirconia spheres of 10 mm diameter, 1300 K
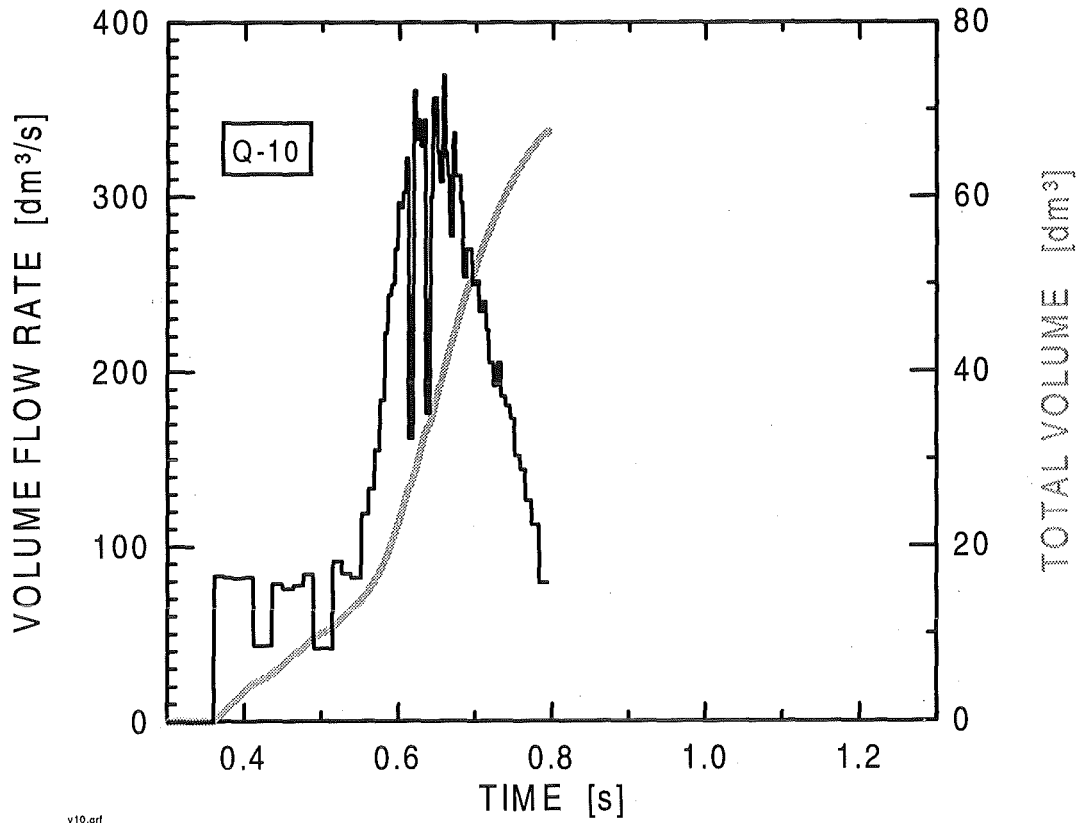
Fig. 4.50 Steam rate with zirconia spheres of 10 mm diameter, 1800 K
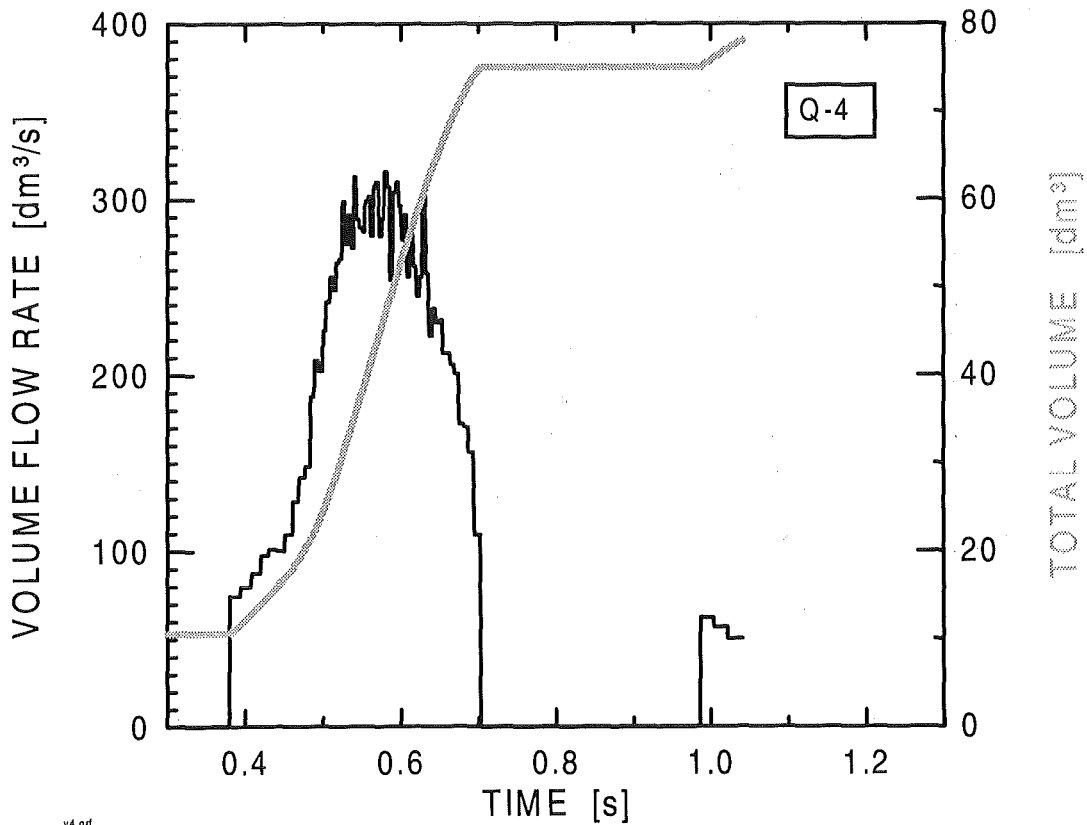
Fig. 4.51 Steam rate with molybdenum spheres of 4.2 mm diameter, 1300 K
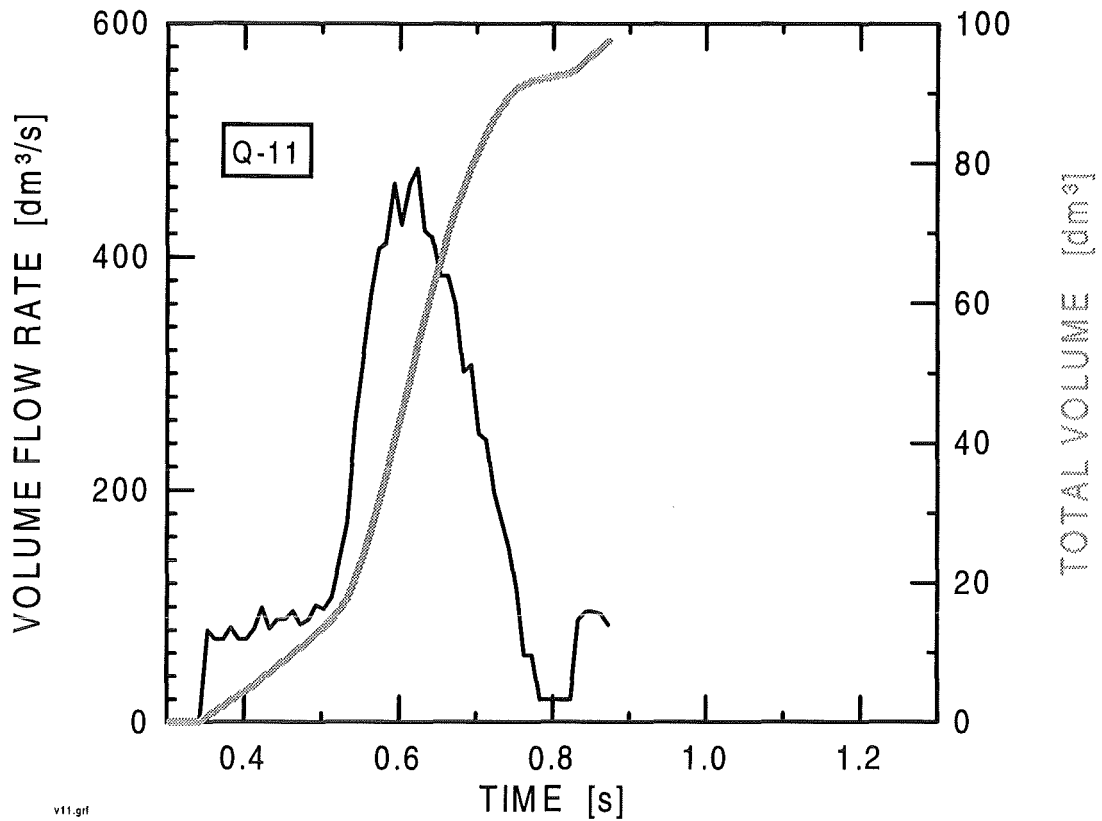
Fig. 4.52 Steam rate with molybdenum spheres of 4.2 mm diameter, 1800 K
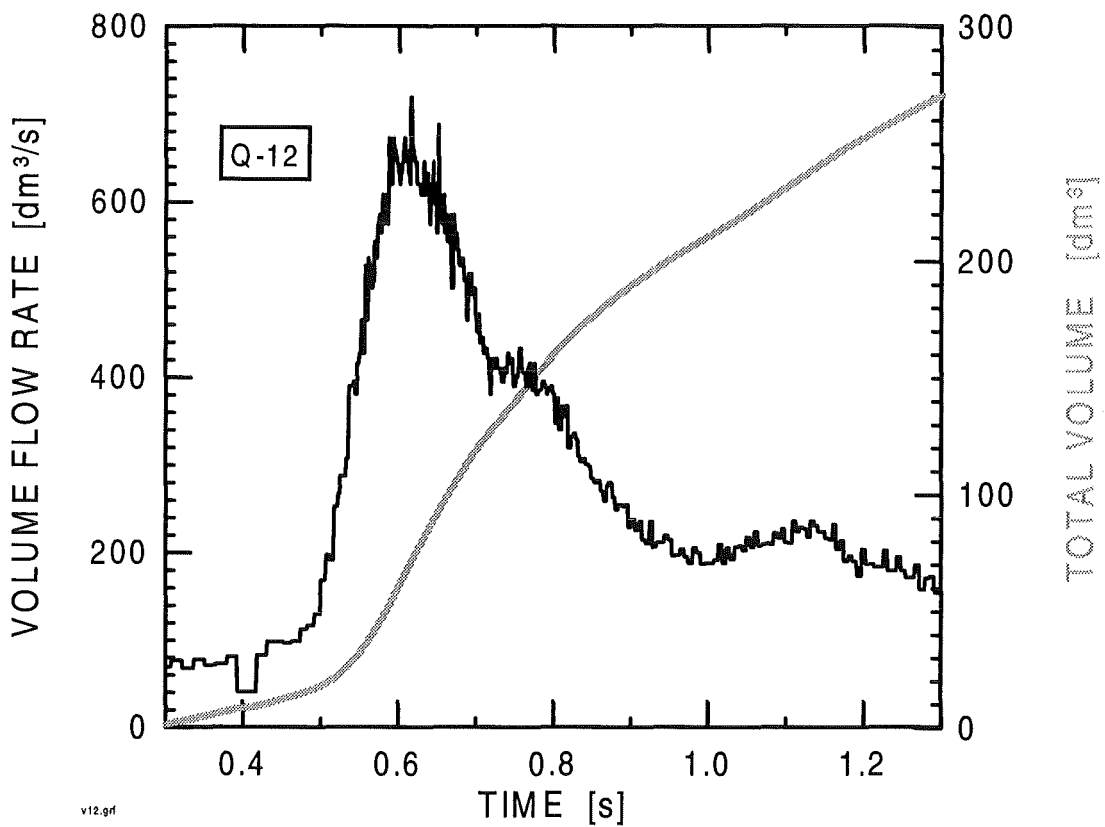
Fig. 4.53 Steam rate with molybdenum spheres of 4.2 mm diameter, 2300 K
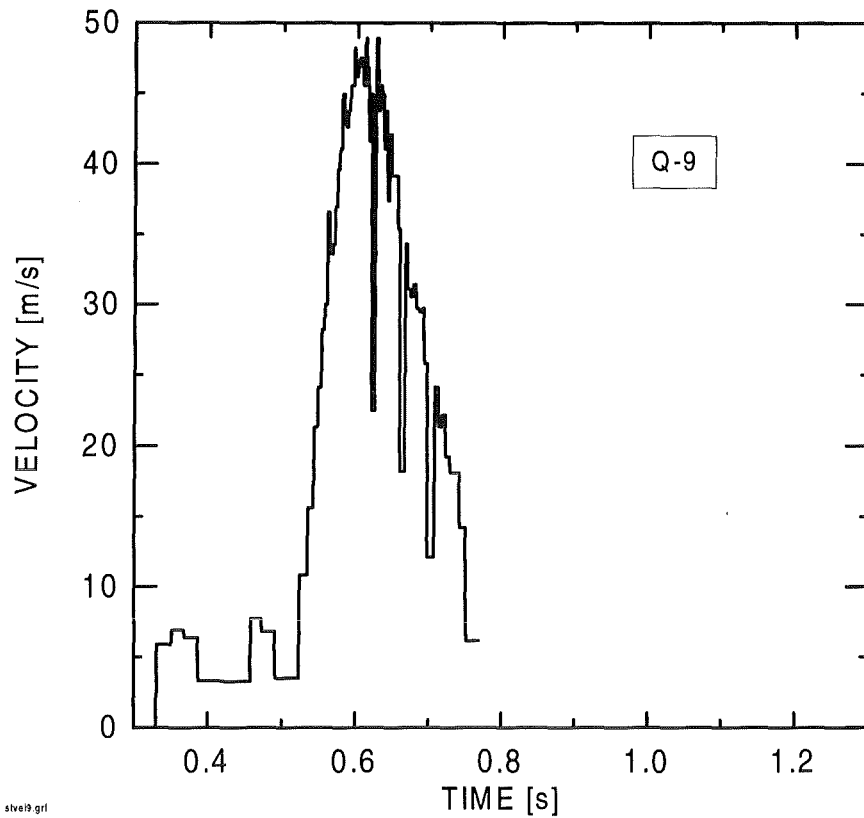
Fig. 4.54 Steam velocity with zirconia spheres of 4.2 mm diameter, 1300 K
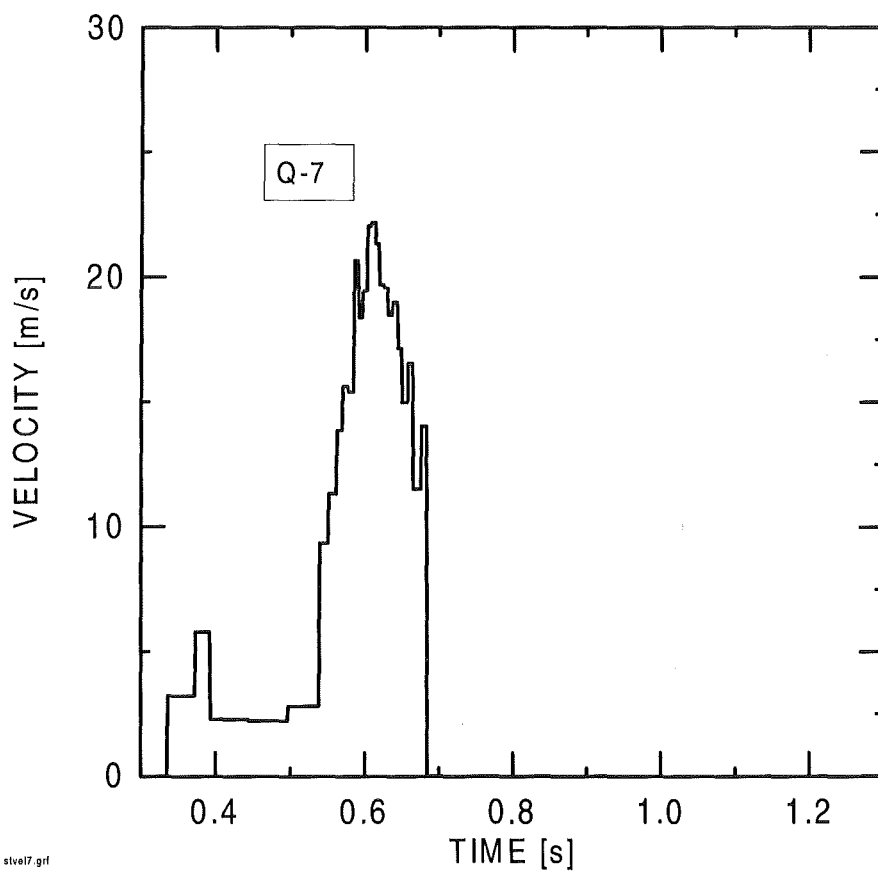
Fig. 4.55 Steam velocity with zirconia spheres of 10 mm diameter, 1300 K
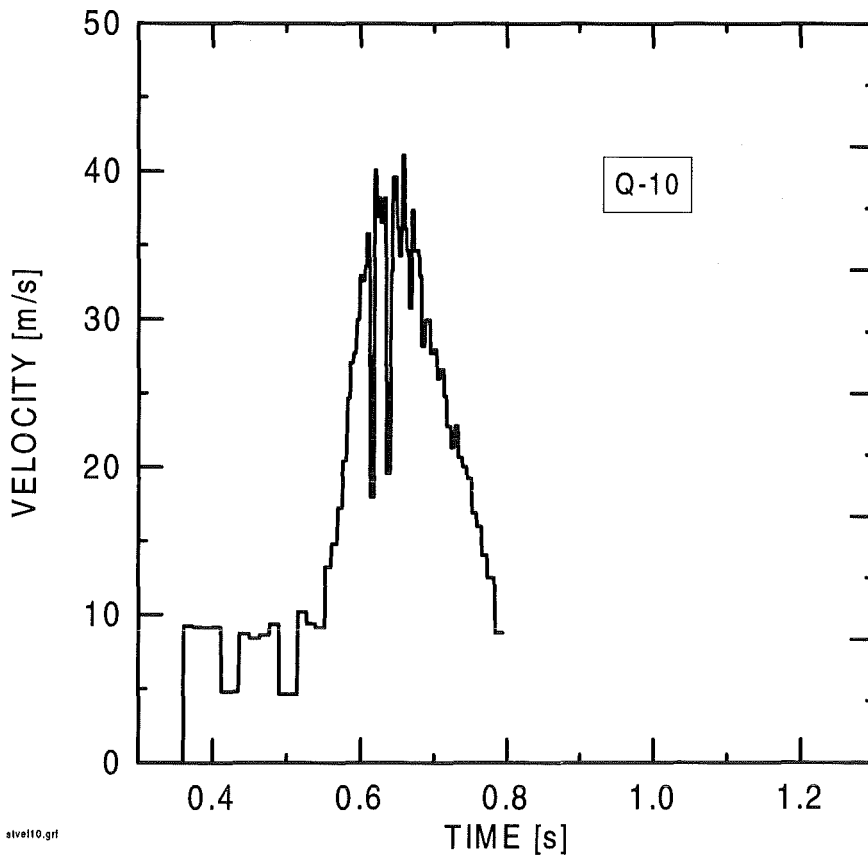
Fig. 4.56 Steam velocity with zirconia spheres of 10 mm diameter, 1800 K
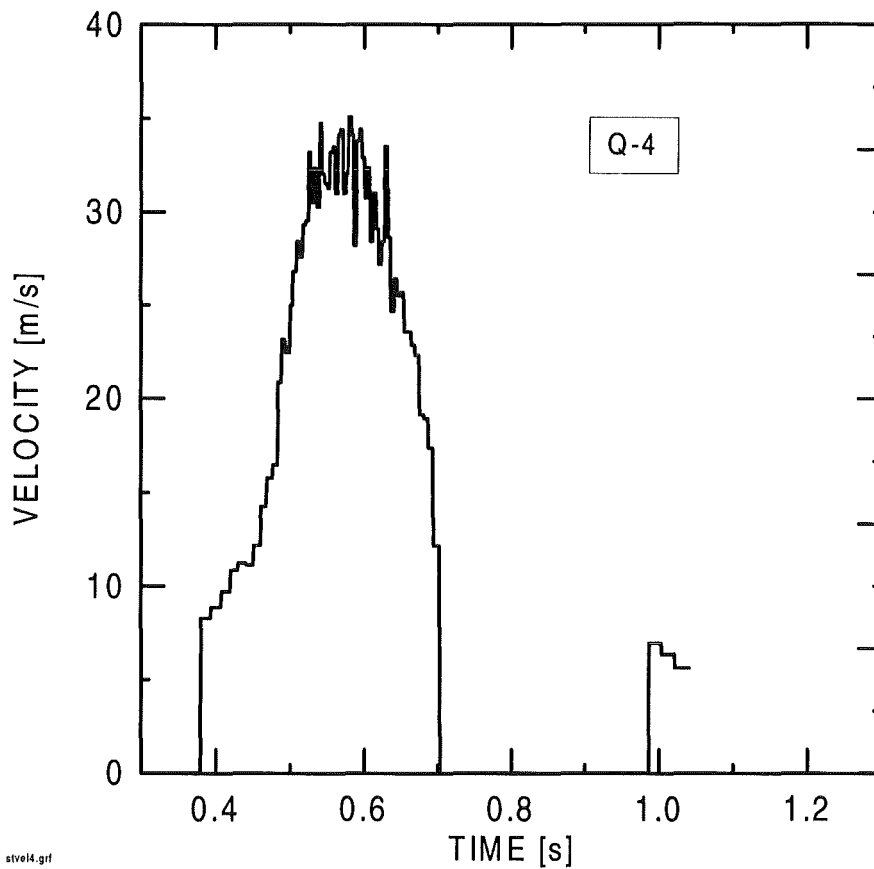
Fig. 4.57 Steam velocity with molybdenum spheres of 4.2 mm diameter, 1300 K
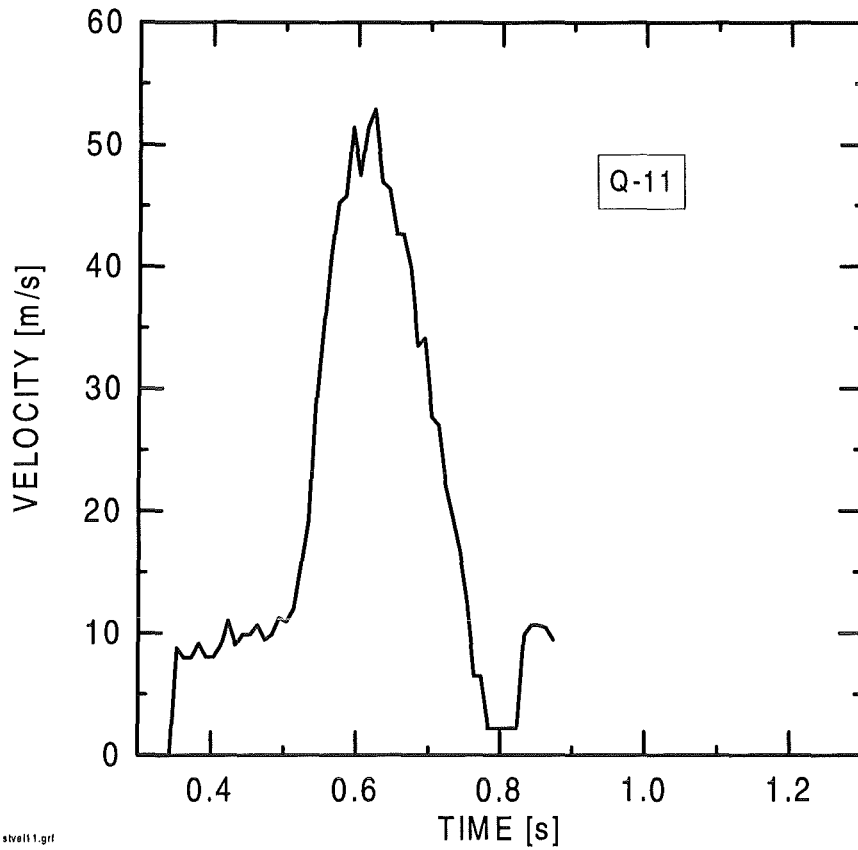
Fig. 4.58 Steam velocity with molybdenum spheres of 4.2 mm diameter, 1800 K
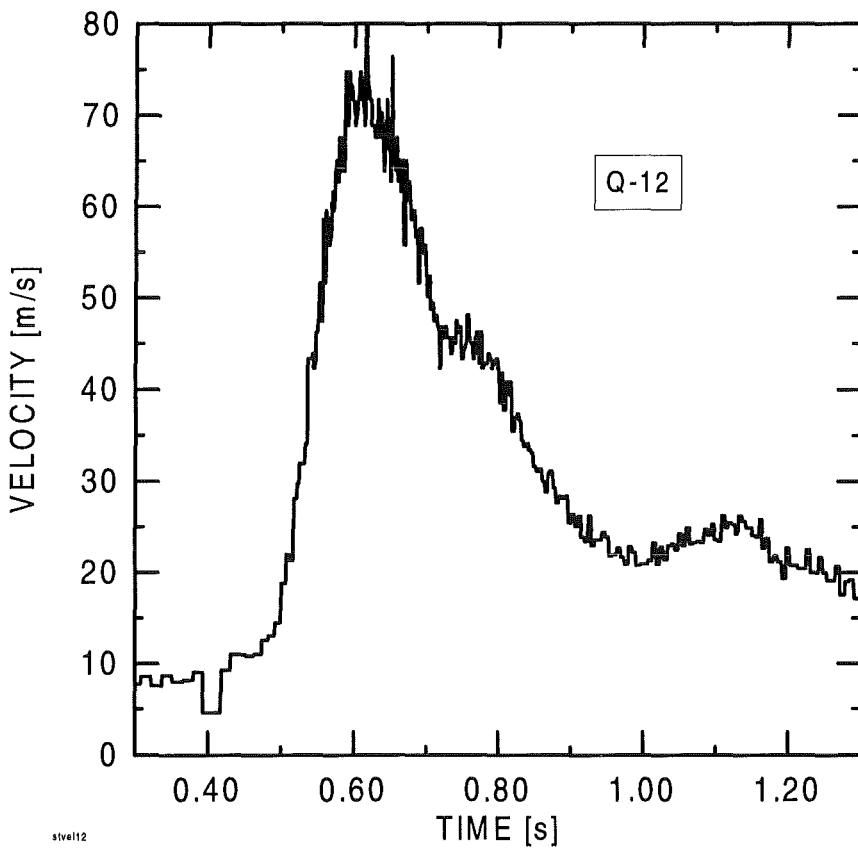
Fig. 4.59 Steam velocity with molybdenum spheres of 4.2 mm diameter, 2300 K
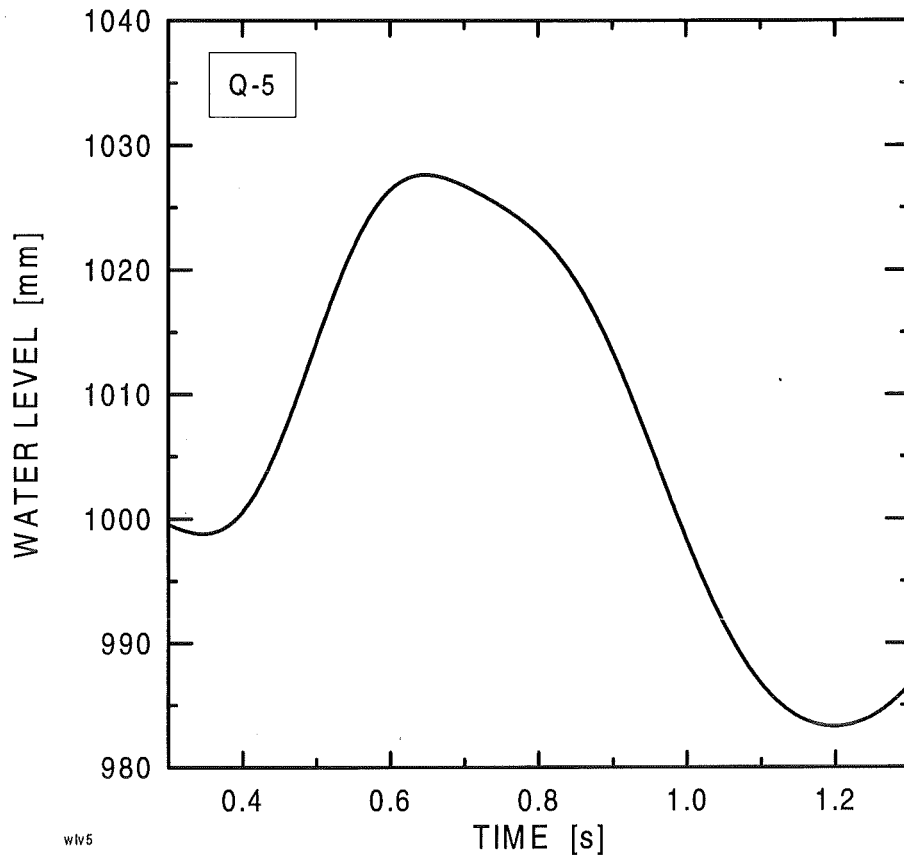
Fig. 4.60 Water level rise with zirconia spheres, ∅ 5 mm, cold
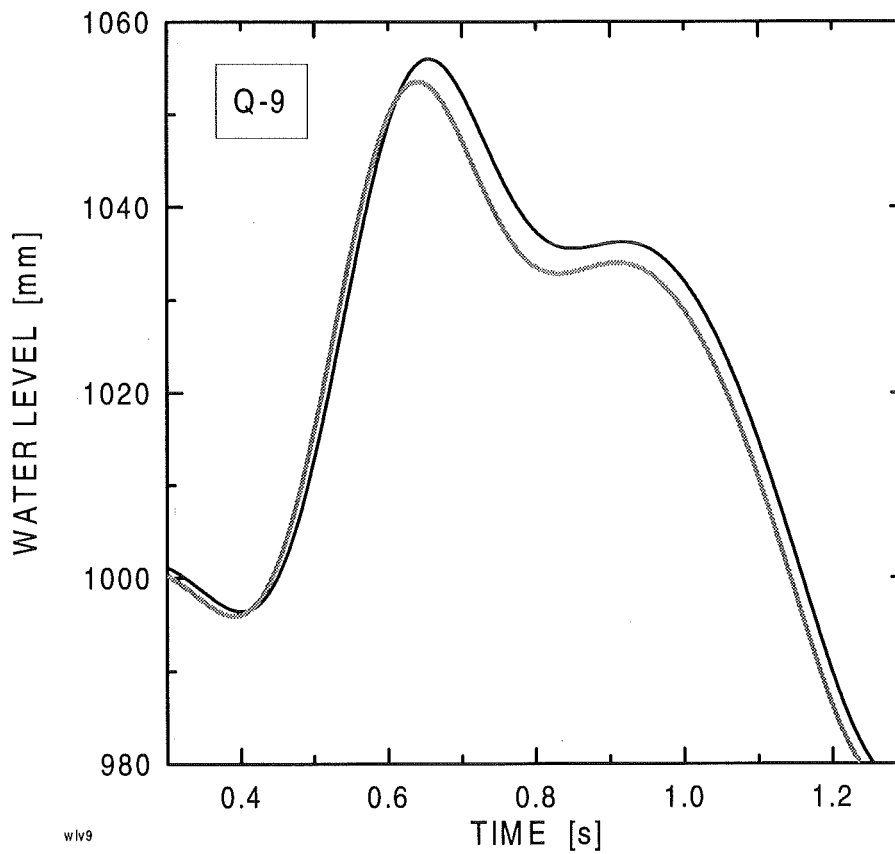
Fig. 4.61 Water level rise with zirconia spheres, ∅ 5 mm, 1300 K
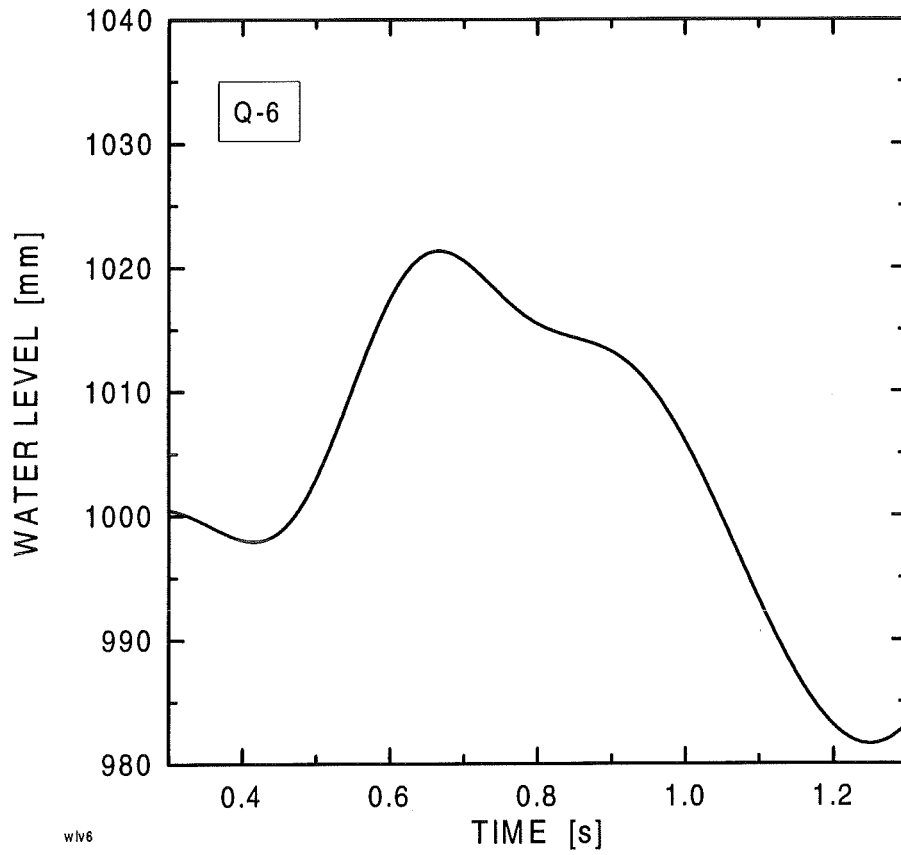
Fig. 4.62 Water level rise with zirconia spheres, Ø 10 mm, cold
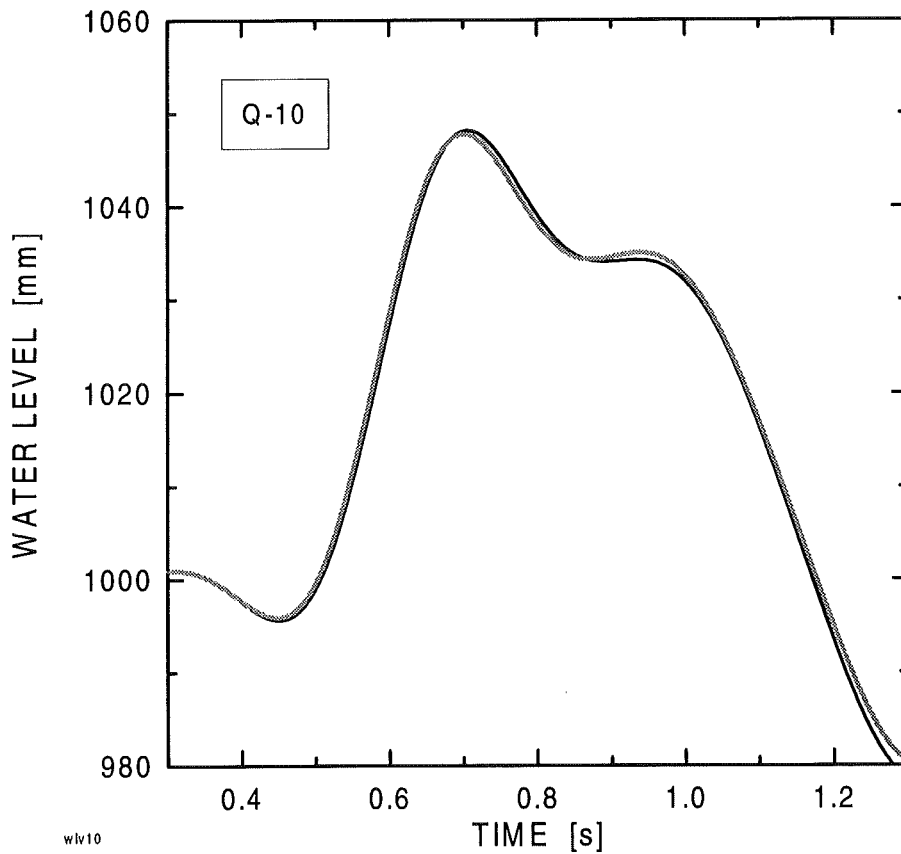
Fig. 4.63 Water level rise with zirconia spheres, Ø 10 mm, 1800 K
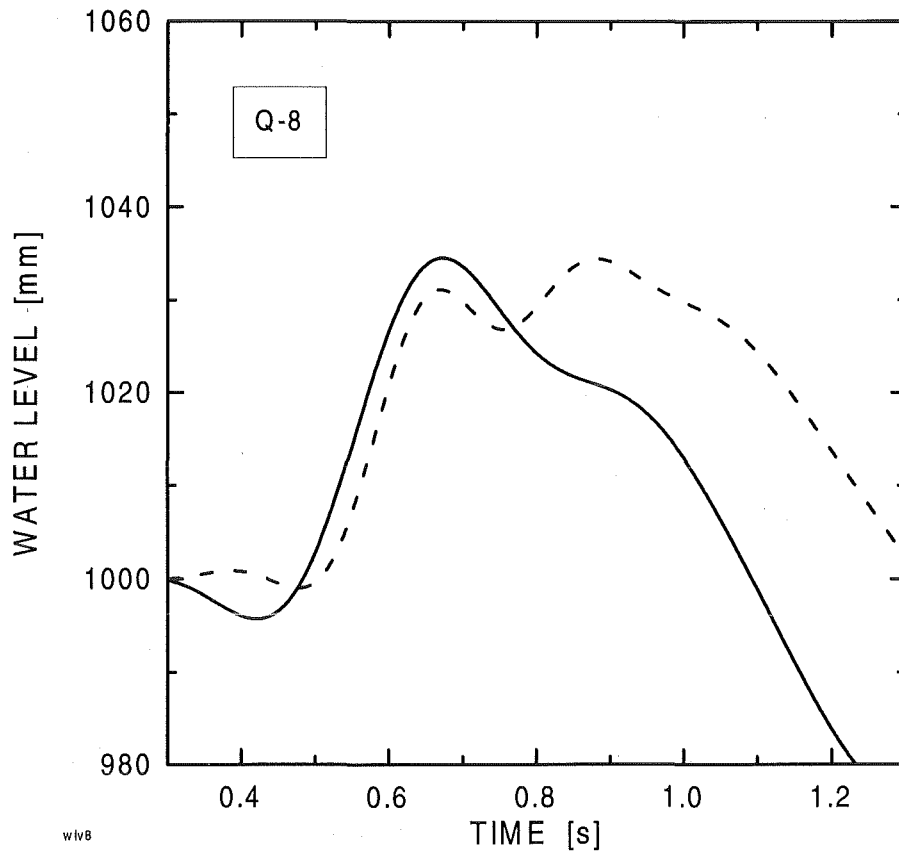
Fig. 4.64 Water level rise with molybdenum spheres, ∅ 4.2 mm, cold
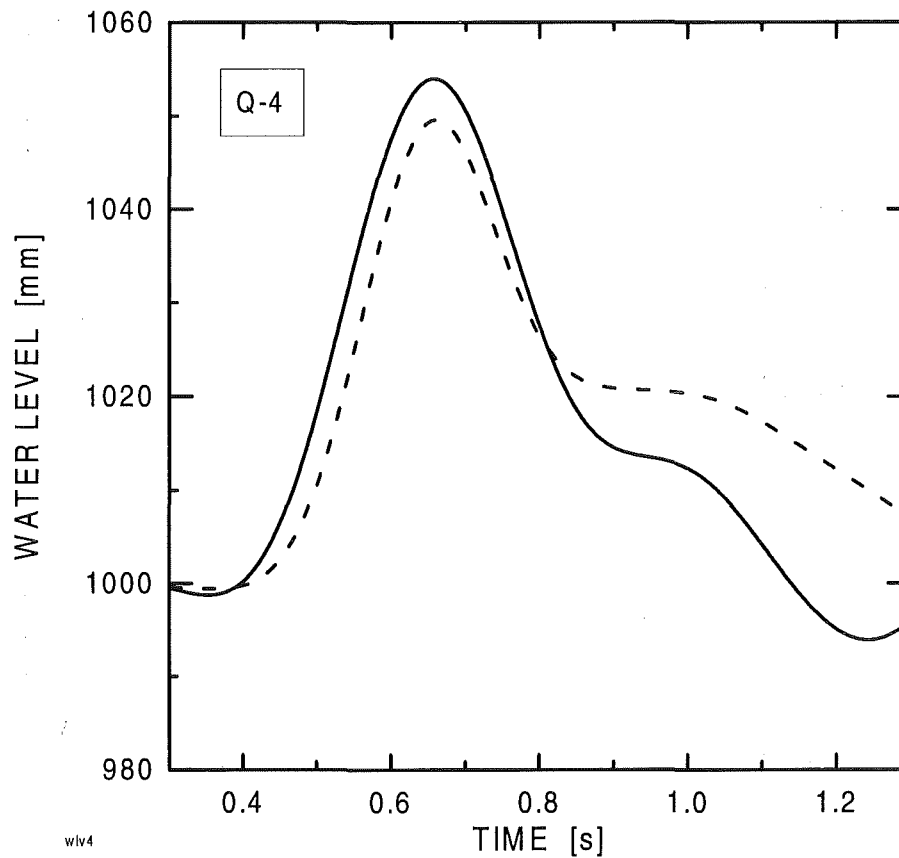
Fig. 4.65 Water level rise with molybdenum spheres, ∅ 4.2 mm, 1300 K
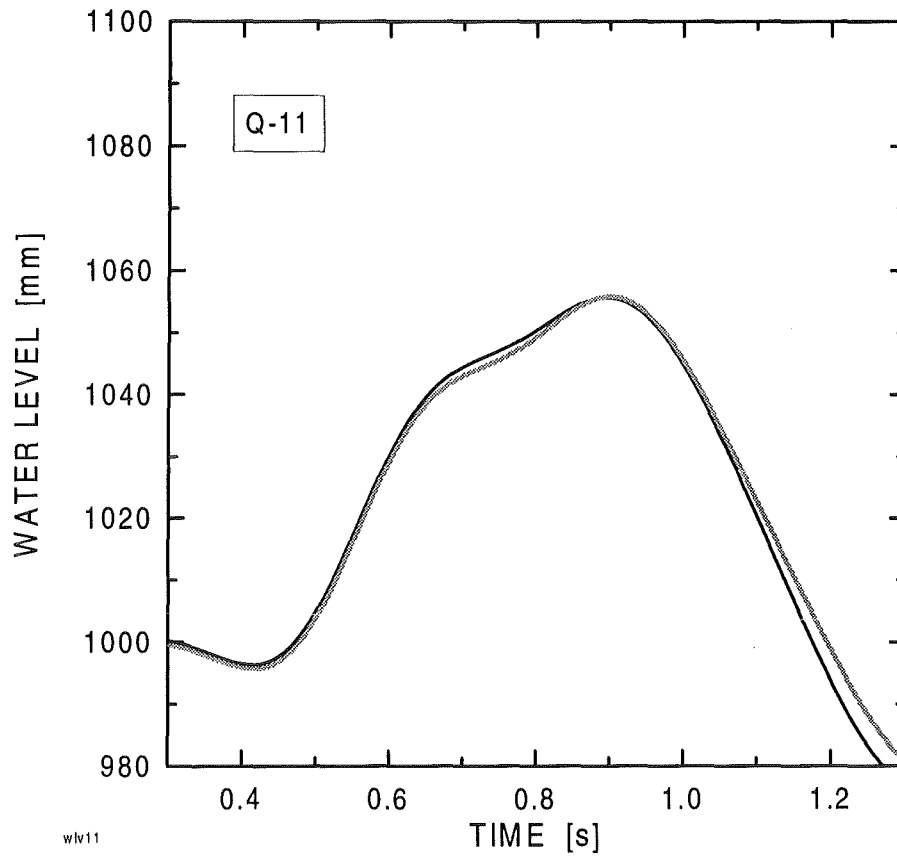
Fig. 4.66 Water level rise with molybdenum spheres, Ø 4.2 mm, 1800 K
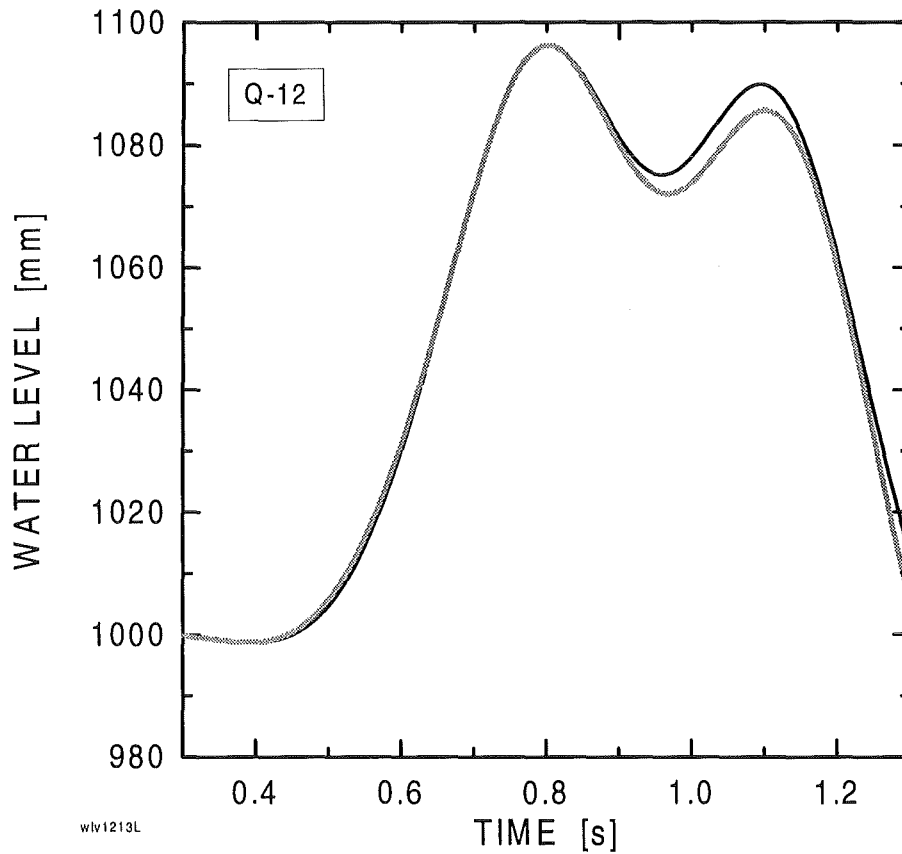
Fig. 4.67 Water level rise with molybdenum spheres, Ø 4.2 mm, 2300 K
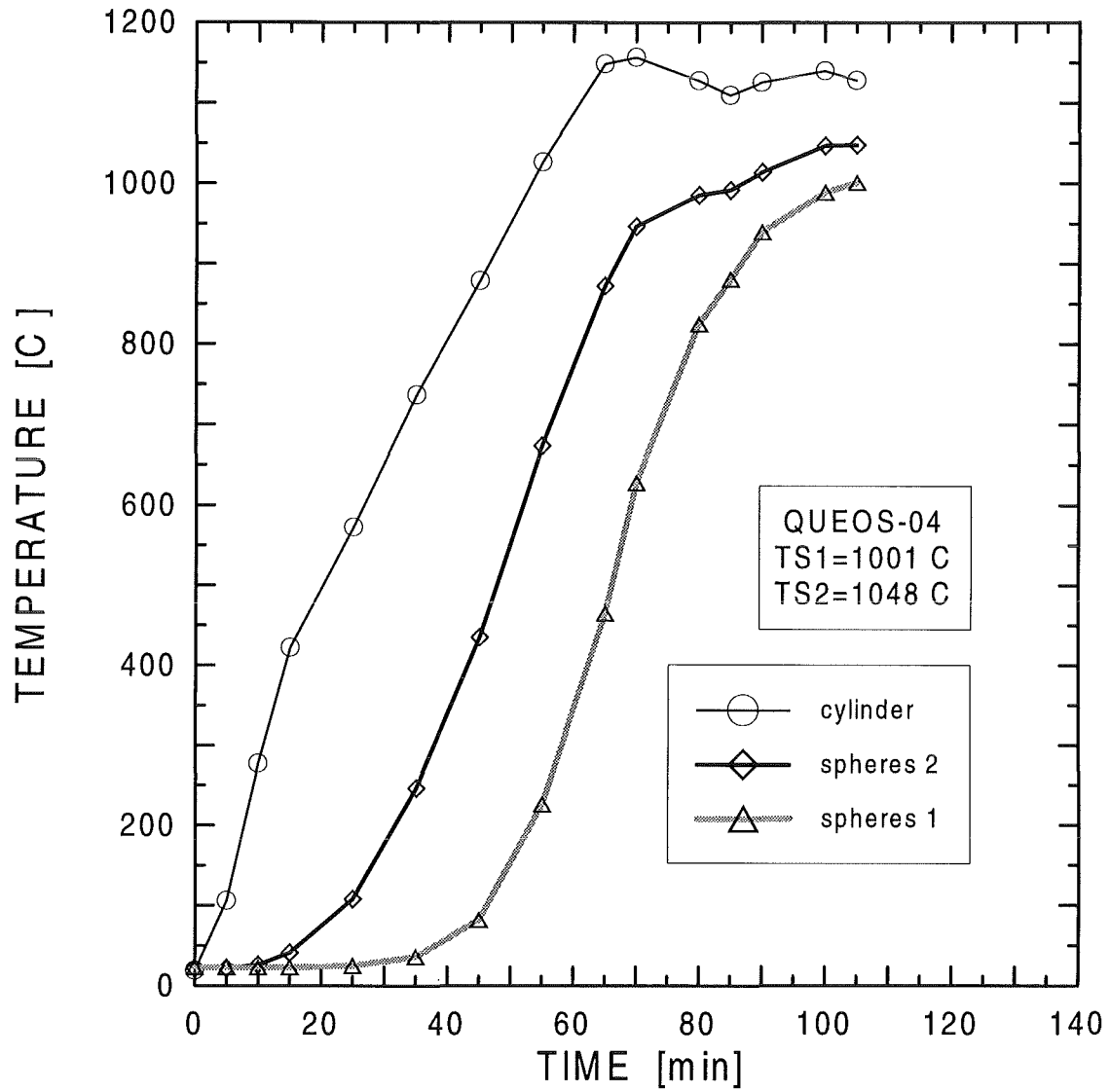
Fig. 4.68 Temperature in the furnace during the heating period with molybdenum spheres
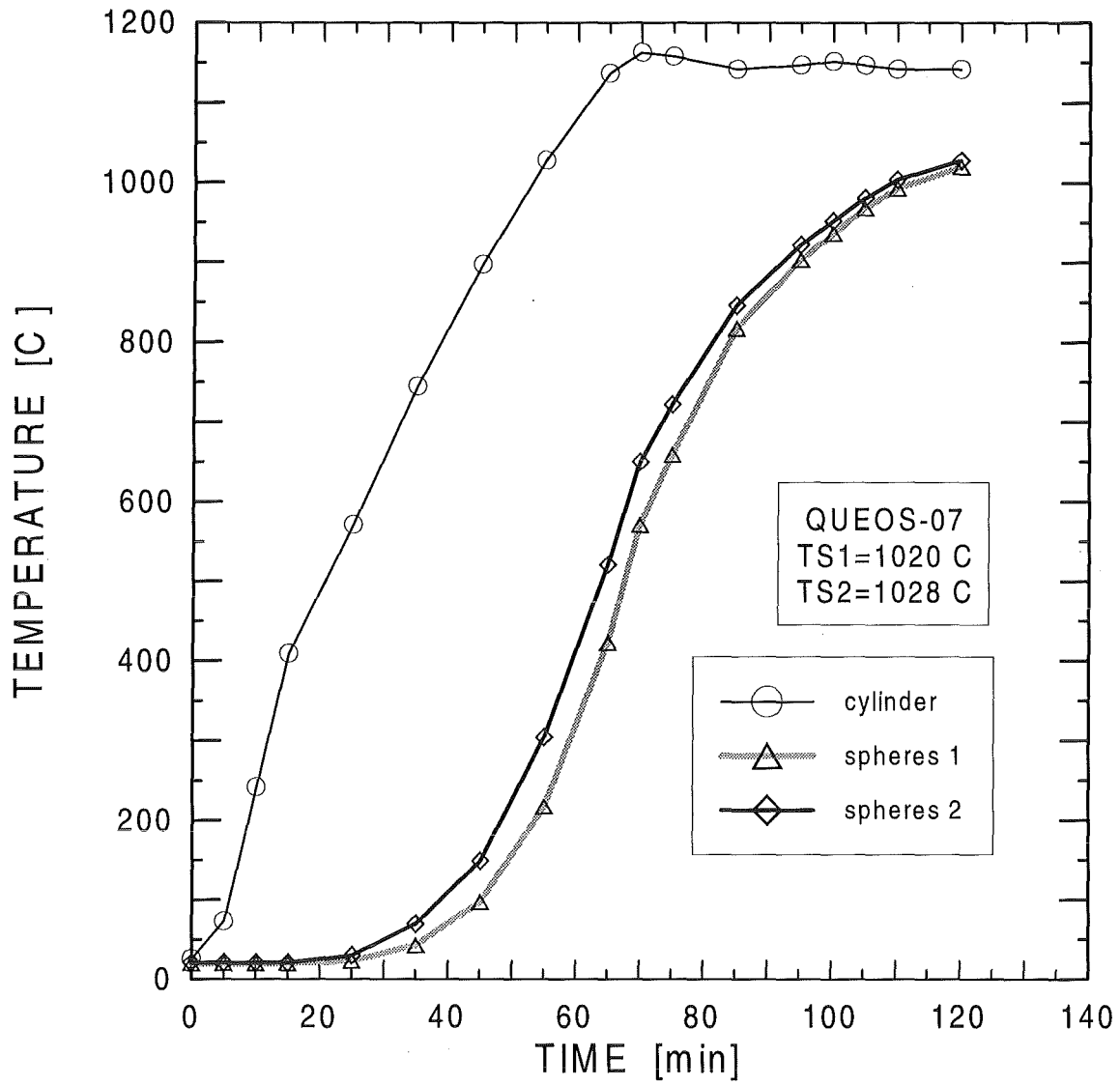
Fig. 4.69 Temperature in the furnace during the heating period with zirconia spheres
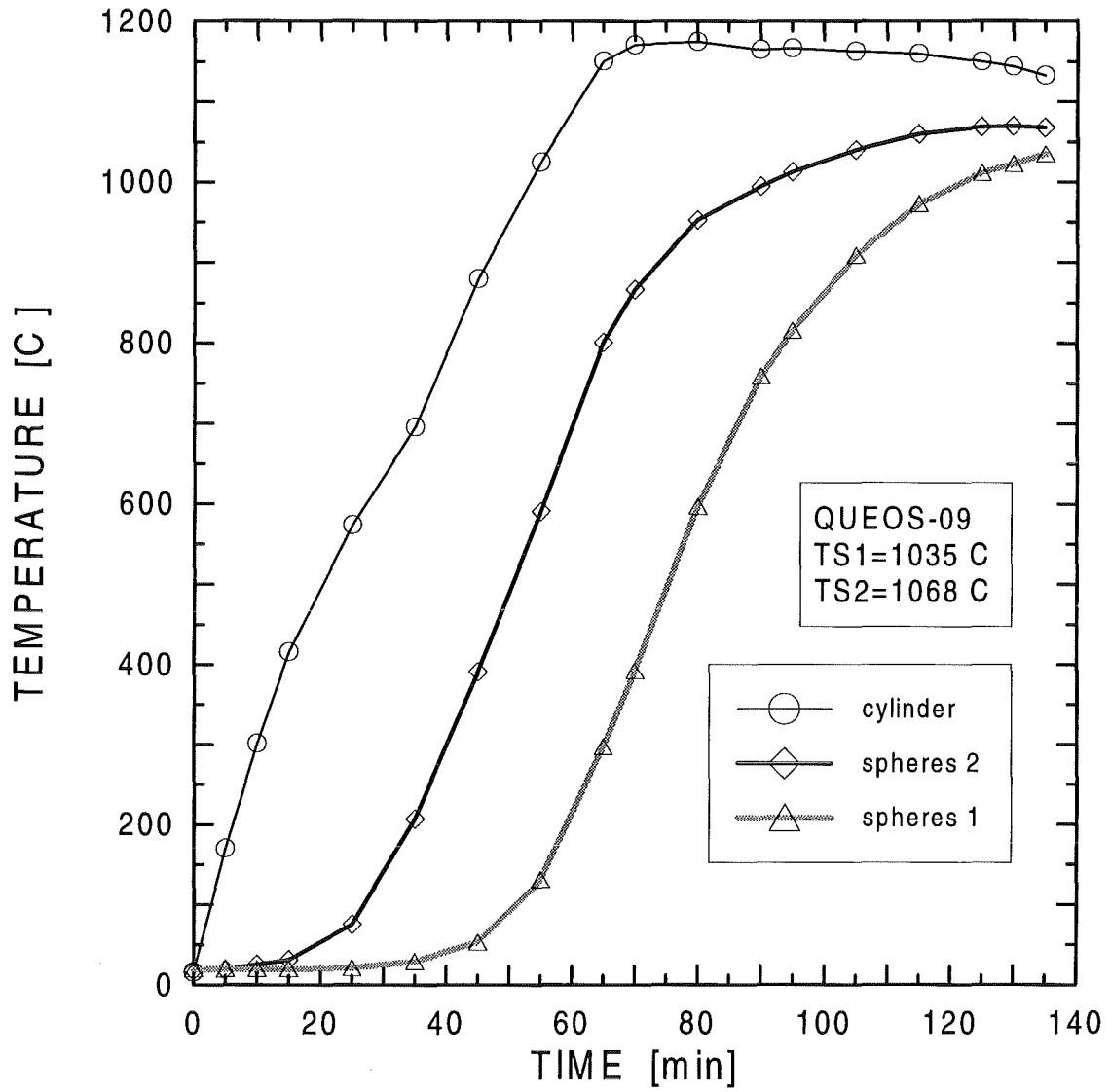
Fig. 4.70 Temperature in the furnace during the heating period with zirconia spheres
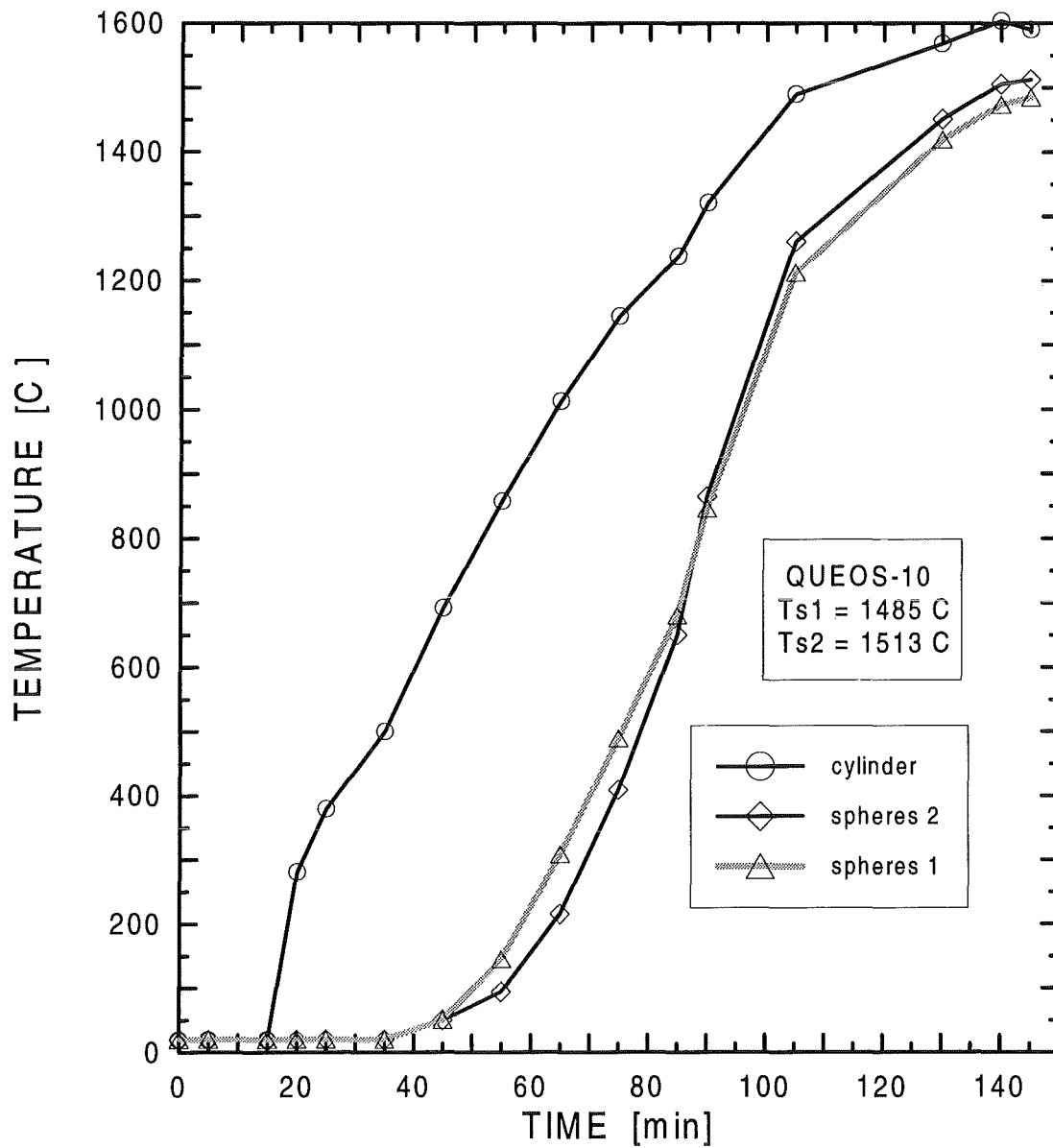
Fig. 4.71 Temperature in the furnace during the heating period with zirconia spheres
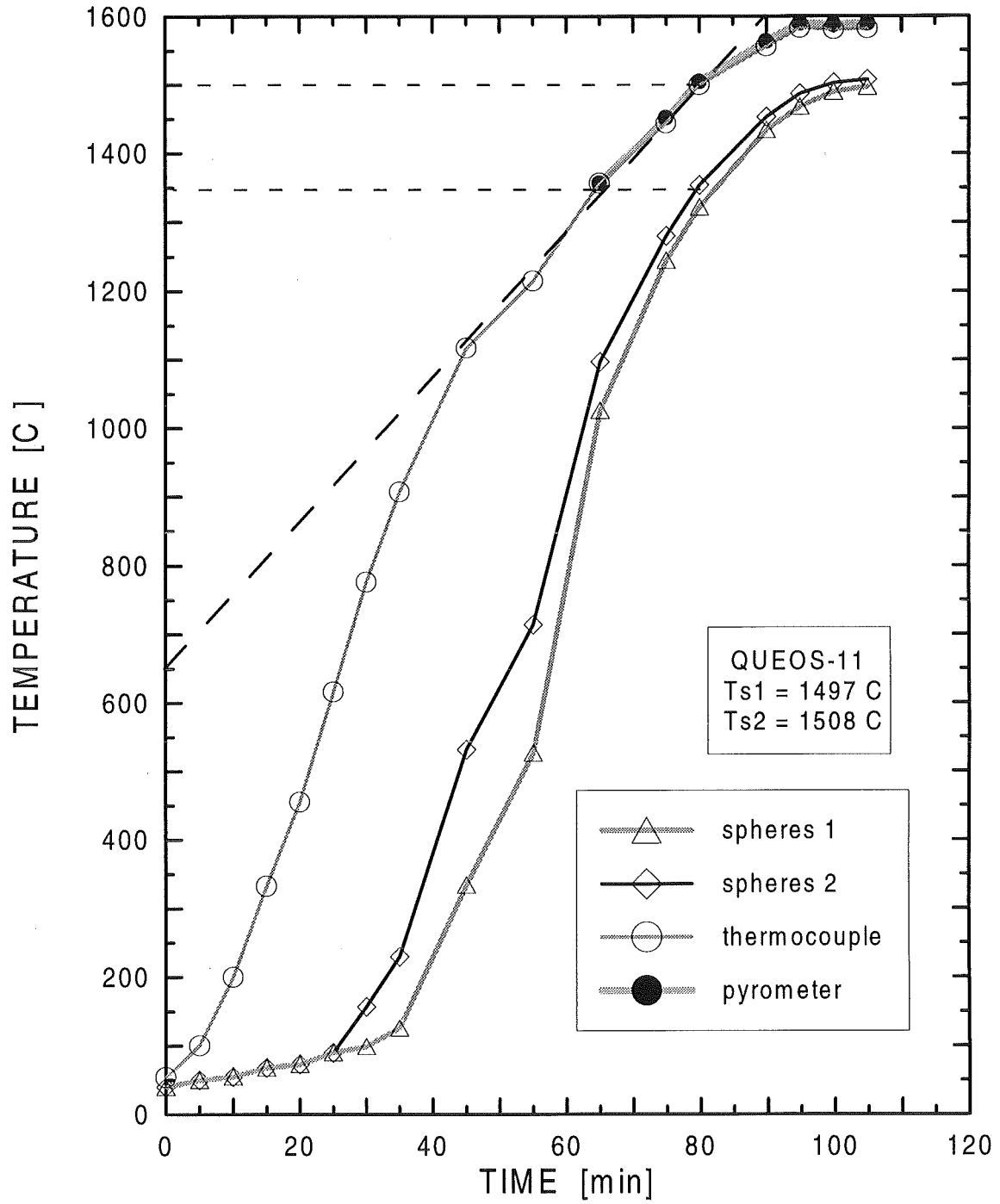
Fig. 4.72 Temperature in the furnace during the heating period with molybdenum spheres
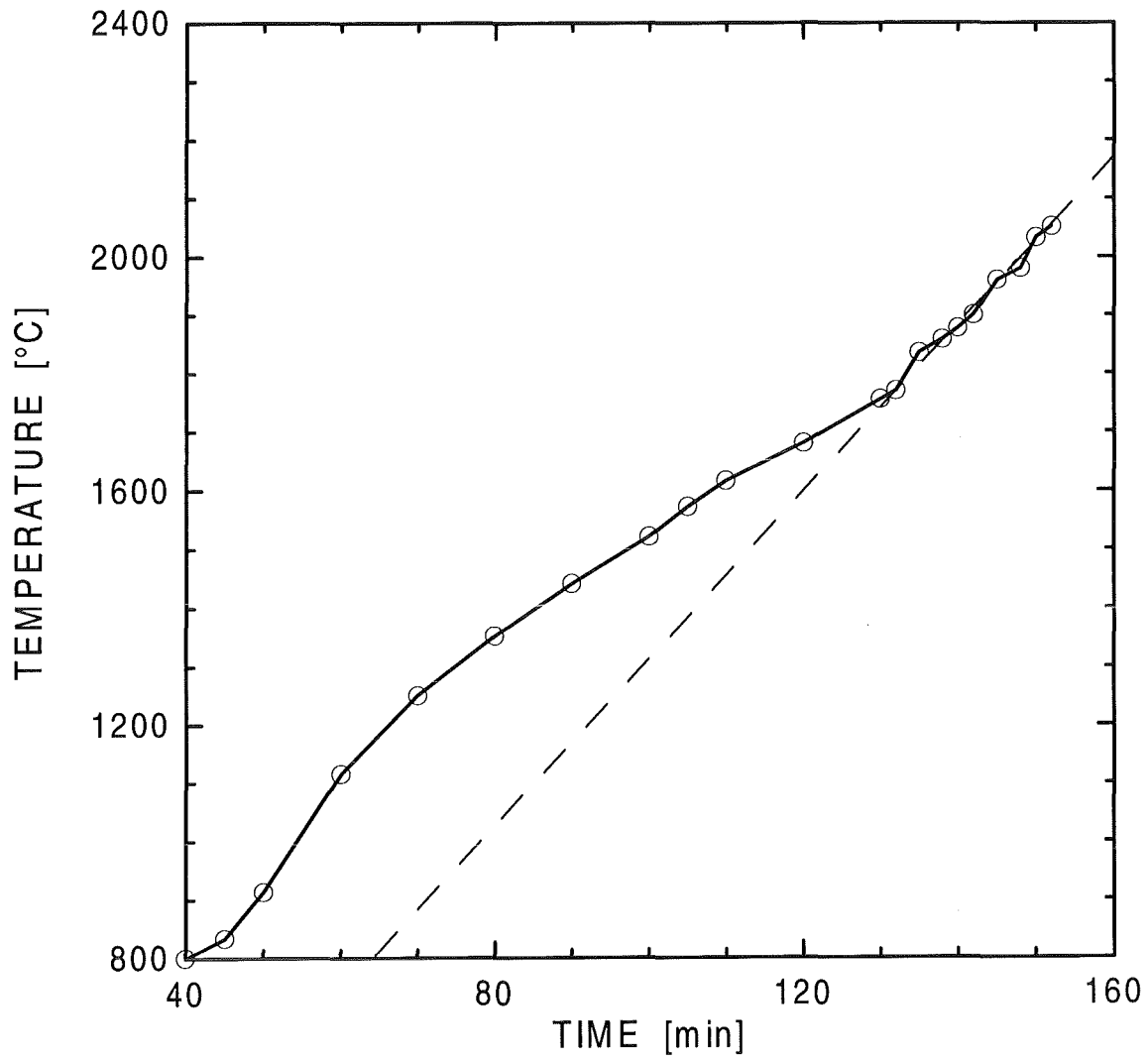
Fig. 4.73 Temperature in the furnace during the heating period with molybdenum spheres measured by pyrometer, Q12
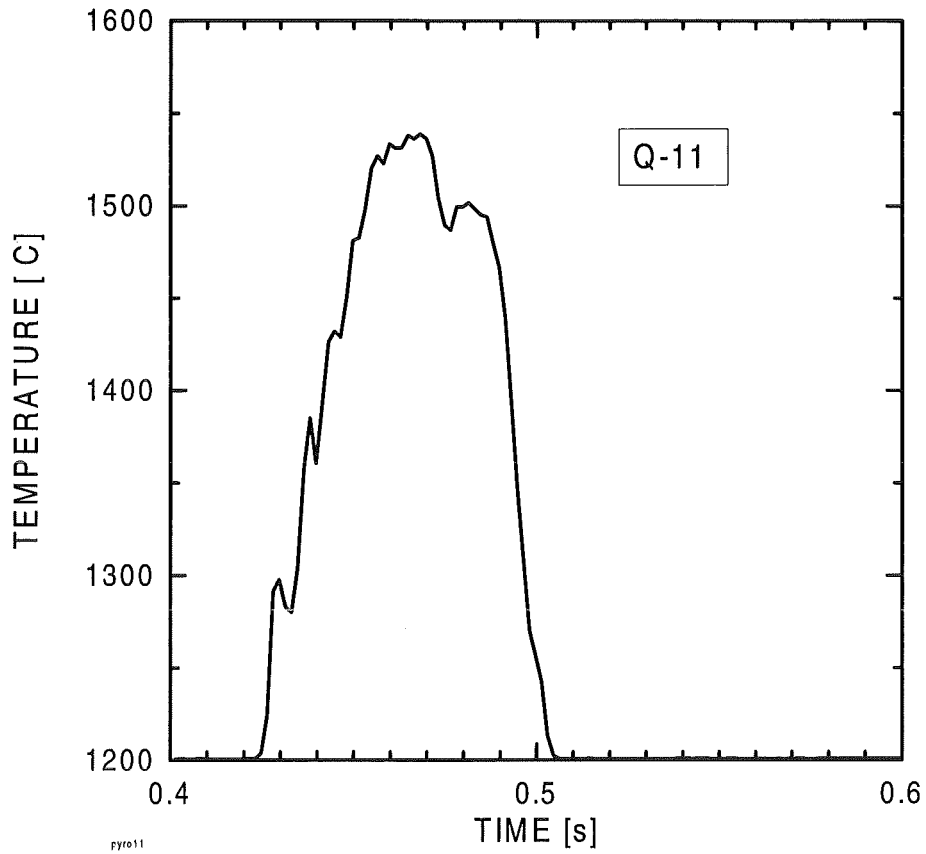
Fig. 4. 74 Pyrometer data of falling spheres 25 cm above water level, 1800 K
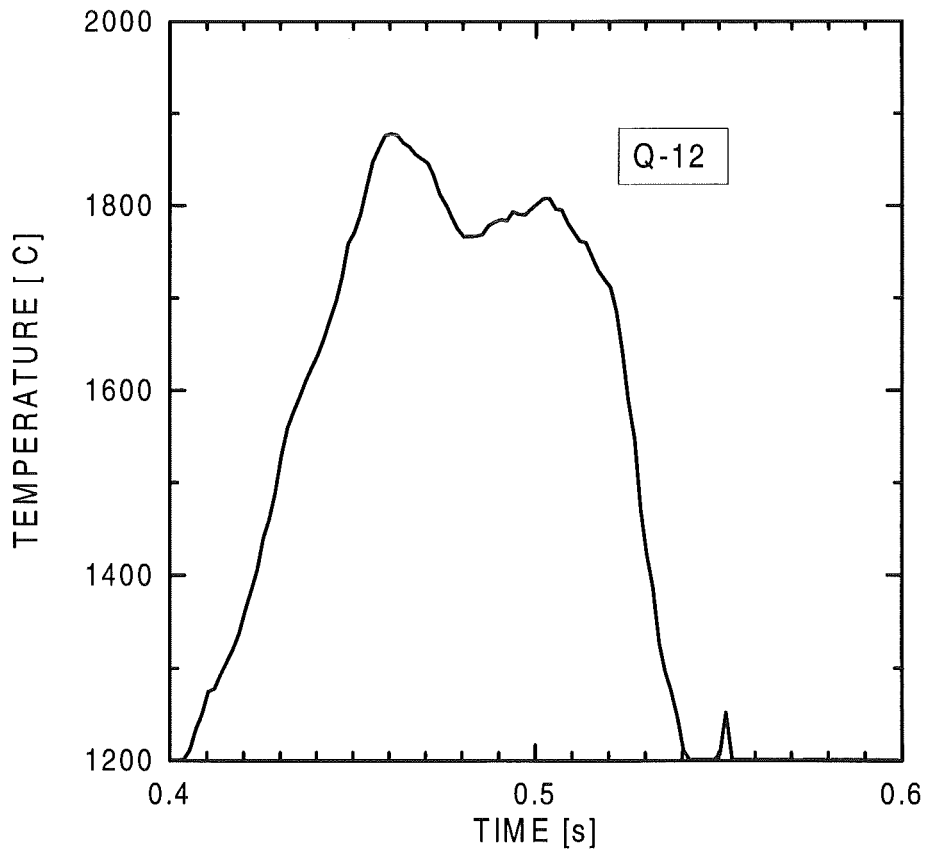
Fig. 4. 75 Pyrometer data of falling spheres 25 cm above water level, 2300 K
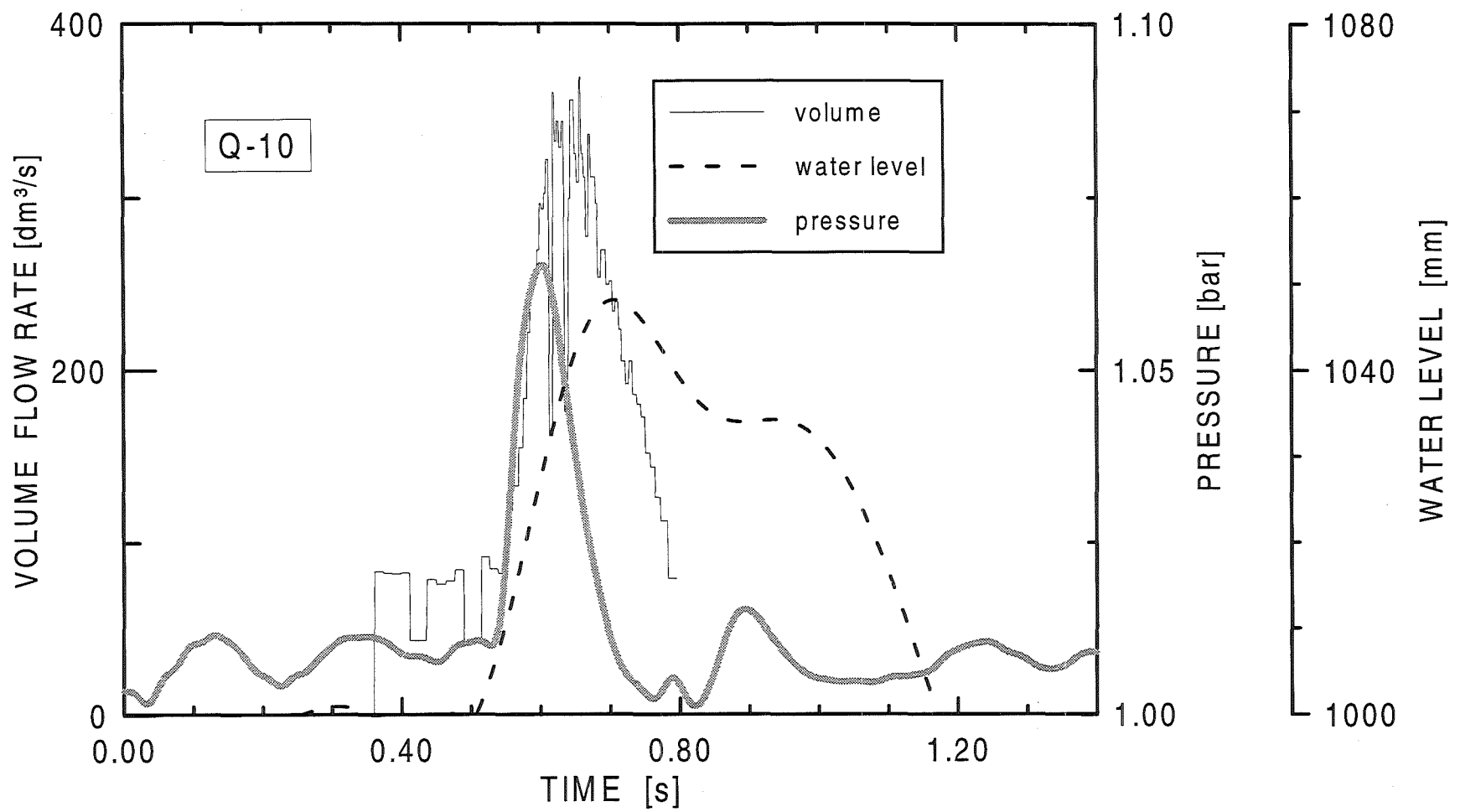
Fig. 4.76 Histories of volume flow rate, pressure above water and water level rise in Q10
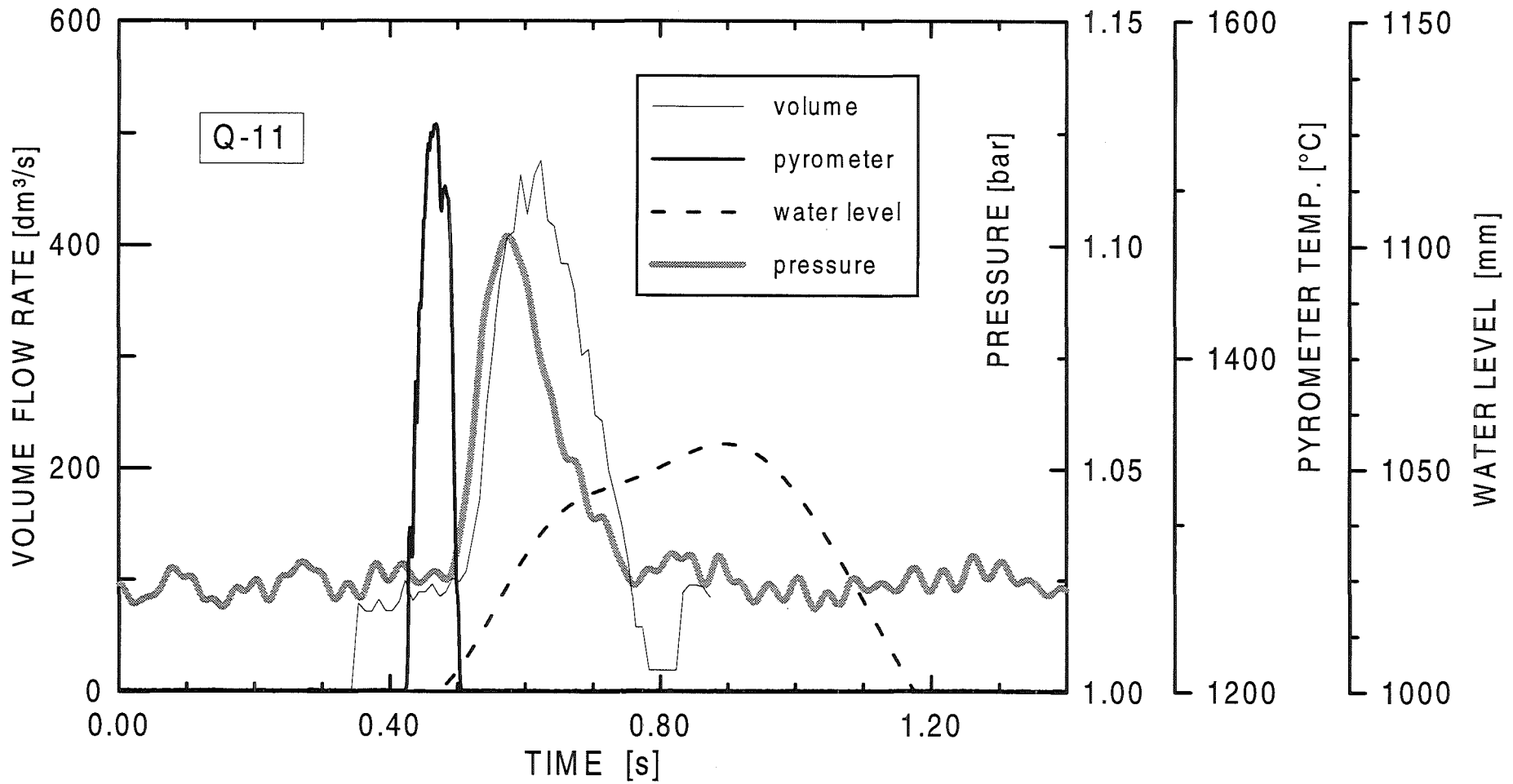
Fig. 4.77 Histories of volume flow rate, pressure above water, pyrometer signal and water level rise in Q11
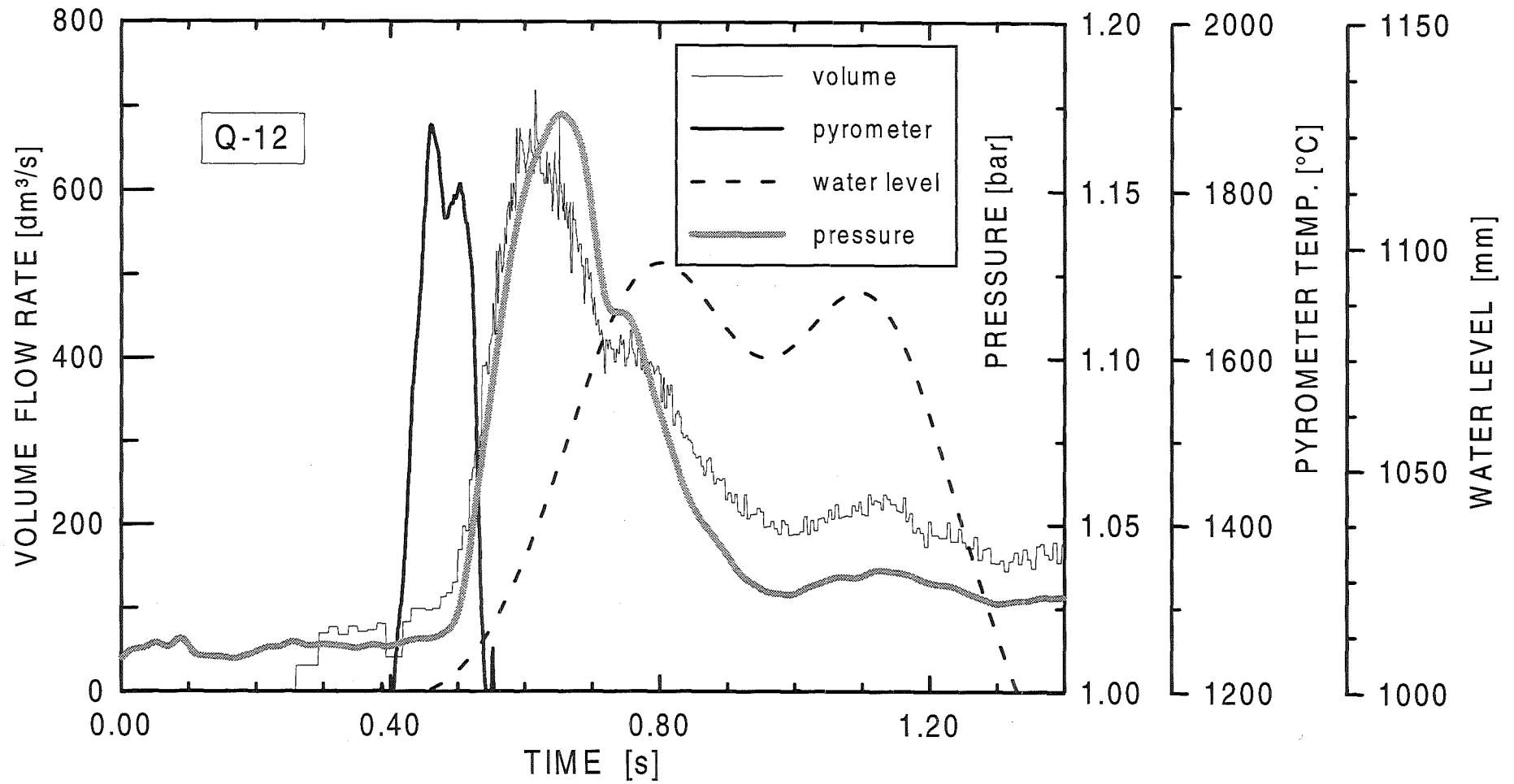
Fig. 4.78 Histories of volume flow rate, pressure above water, pyrometer signal and water level rise in Q12

QUEOS-01

DISTRIBUTION OF MASS ON GROUND [gr/dm²]

20 kg cold steel spheres d = 4.76 mm
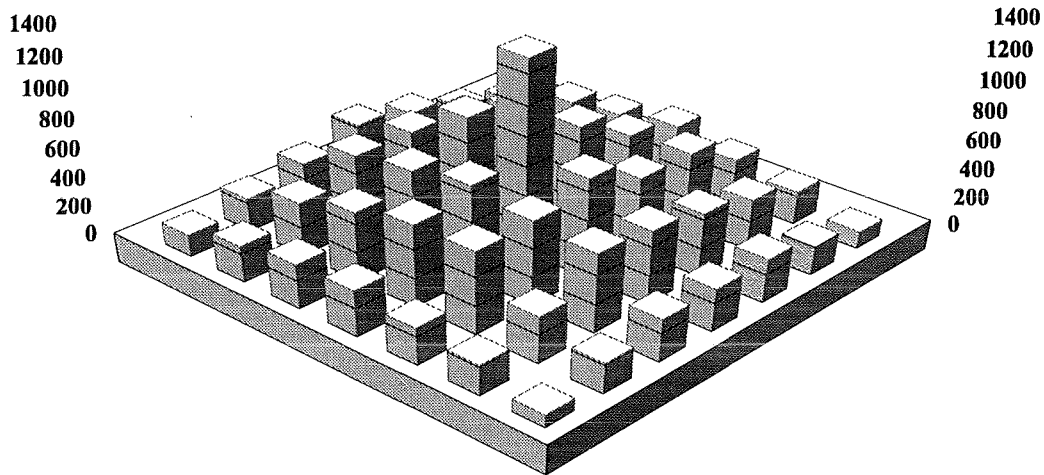
153.1	228.3	302.1	414.5	335.1	217.3	124.3
252	367.8	520	514.4	465	362.7	189
308.4	475	577.2	769	544.3	557	313.3
320	566	648	1298	701	477.7	378.5
259.3	570.1	584.3	686	513.1	509	293.4
211.8	323.4	545.8	505.5	438	348	229
87.2	213.4	294.7	295.5	301	201	115.5

Fig. 4.79 Distribution of the spheres on the vessel bottom, Q01

QUEOS-02

DISTRIBUTION OF MASS ON GROUND [gr/dm²]

10 kg cold steel spheres d = 4,76 mm
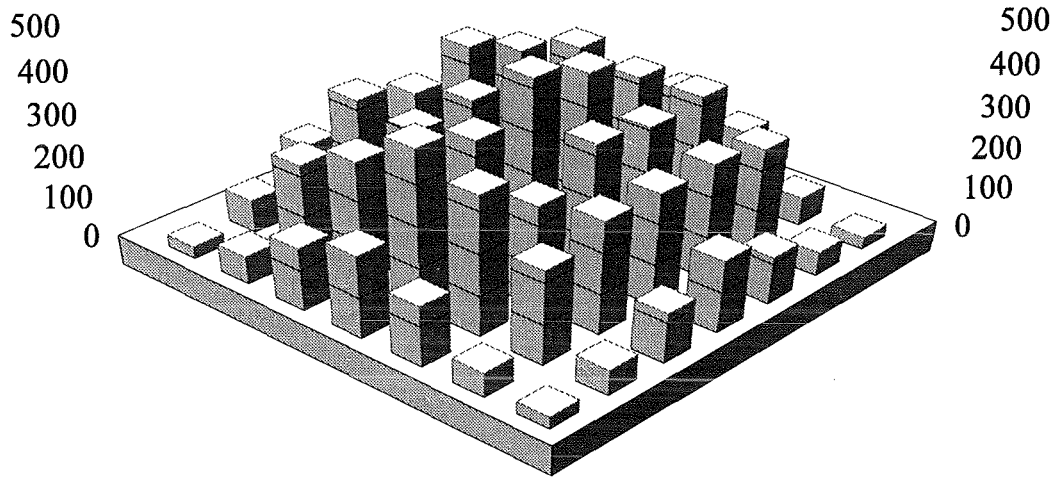
29.5	80	156.8	211.5	136.9	56.9	40.4
67.7	226.6	321.9	281.9	340.5	279.3	69.4
153.1	291.8	303	318.7	290.8	335.8	137
199.4	379.6	337.4	423.5	379.4	315.6	223.7
148.6	335.8	245.8	326.8	306.5	321.6	177.4
59.9	227.9	273.3	271.3	276.9	251.1	68.8
29.6	62.3	122.3	175.6	114.8	57	29.1

Fig. 4.80 Distribution of the spheres on the vessel bottom, Q02

QUEOS-03

DISTRIBUTION OF MASS ON GROUND [gr/dm²]

10 kg Mo spheres 4,2 mm dia.   T = 930 K□
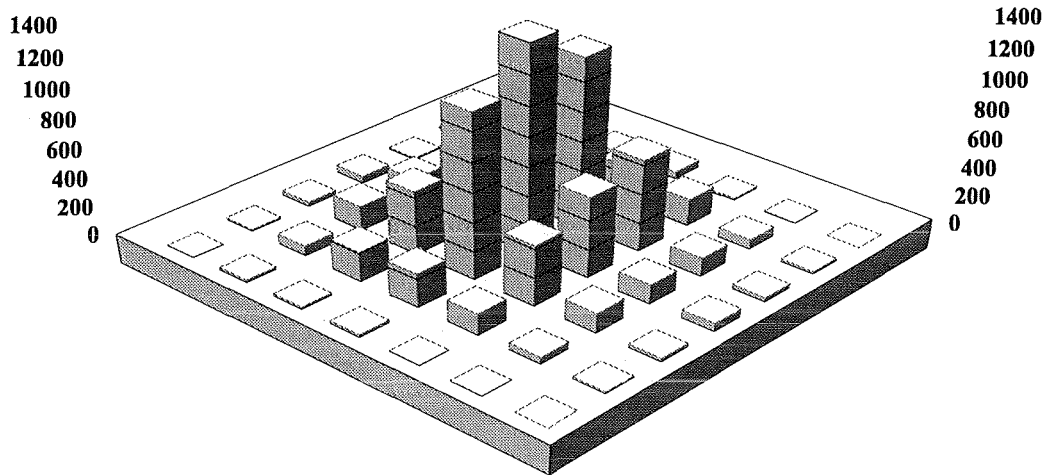
0	4.1	11.1	48.6	30.7	12.8	2.7
11.2	110.4	184.1	188.6	169.9	71.4	17.7
36.1	211.4	347.9	417.3	440.9	209.5	16.8
47.9	252.5	1159.7	1952	1123.8	238	18.5
12.6	186.7	634	559.3	422.2	151.6	2.9
3.7	66.2	129.8	136	139.2	47.7	1.6
0	17.7	30	57.6	23.8	12.8	0

Fig. 4.81 Distribution of the spheres on the vessel bottom, Q03

QUEOS-04

DISTRIBUTION OF MASS ON GROUND [gr/dm²]
10 kg Mo spheres 4,2 mm dia.   T = 1270 K □
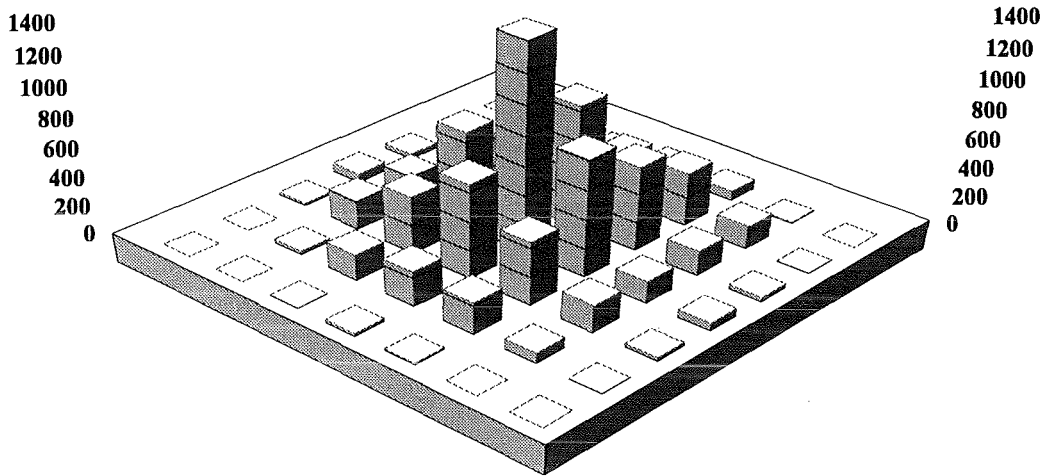
0	0.4	33.1	57.8	18.4	0	0
1.2	82.4	207.6	198.8	203.2	25.8	0
25.5	290.2	408.6	668	398.1	179.4	2.1
70.4	332.2	836.1	1668.9	654.1	244	20.2
65.5	366.7	582.9	807.5	438.2	220.2	11.9
8.3	162	172.1	150.8	190.9	72.1	0
0	2.1	30.2	53.7	23.3	1.3	0

Fig. 4.82 Distribution of the spheres on the vessel bottom, Q04

QUEOS-05
DISTRIBUTION OF MASS ON GROUND [gr/dm²]
7 kg ZrO2 spheres 5 mm dia.   T = 300 K
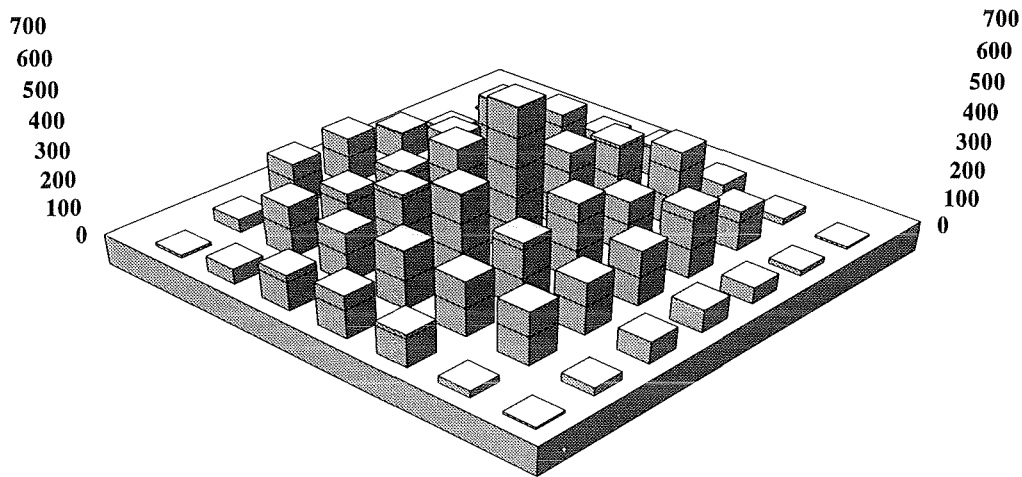
4.3	28.8	103	165.2	157.2	46.1	10.3
28.8	203.1	164.1	125.2	134.8	178.7	52.2
81.8	241.6	186.1	283.3	215.1	172.9	124
107.6	210.5	267.6	501.8	301.9	201.9	149.6
64.3	265.3	179.4	264.2	223.7	190.9	114.3
23.5	137.9	232.7	190.3	180.2	186	24.6
7.3	18.1	56.4	80.2	76.7	29	8.1

Fig. 4.83 Distribution of the spheres on the vessel bottom, Q05

QUEOS-06

DISTRIBUTION OF MASS ON GROUND [gr/dm²]

7 kg ZrO2 spheres 10 mm dia. T = 300 K □
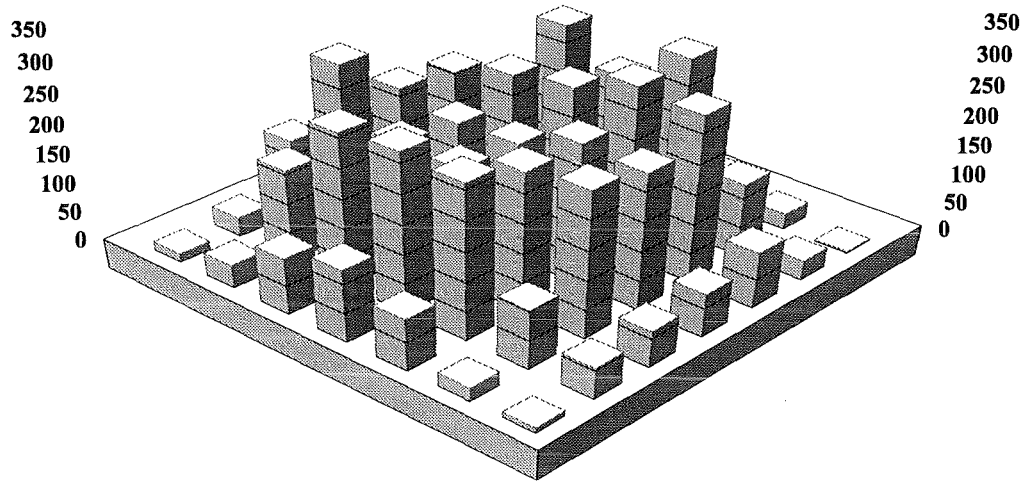
15.1	32.6	124.8	116.2	84.2	42.5	15.1
39.20	155.8	288.7	212.5	202.2	149.4	35.7
95.9	257.3	198.3	191.5	232.4	277.9	78.5
123.1	267	196.8	195.9	247.7	226.6	89.8
88.8	260.4	233.6	235.5	286.9	292.3	51.3
23.8	101.2	245.9	229.2	278.5	123.4	26.7
9	53.9	62.2	73.9	95.3	33.1	2.9

Fig. 4.84 Distribution of the spheres on the vessel bottom, Q06

QUEOS-07

DISTRIBUTION OF MASS ON GROUND [gr/dm²]

7 kg ZrO2 spheres 10 mm dia.   T = 1300 K []
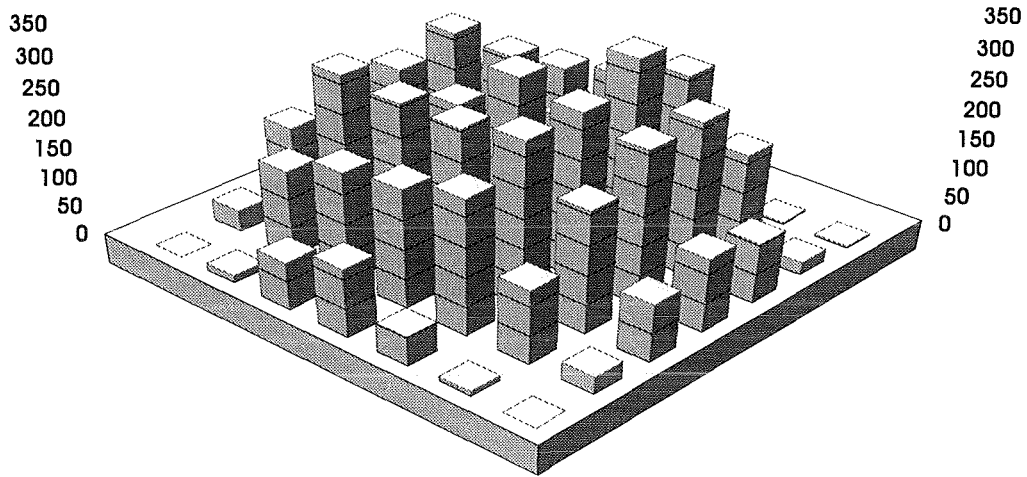
0	35.7	137.9	125.5	145.3	27	0
12.10	146.2	264.2	235.4	259.6	156.2	8.9
81.1	184.7	255.2	214.1	255.3	197.4	53.5
116.3	199.7	253.8	295.3	186.2	220.4	72.3
51	227.4	274.6	277.3	321.5	257.2	47.6
8.9	126	206.1	257.2	259.8	163.7	3
0	29.8	98.9	124.8	102.6	21.1	3.2

Fig. 4.85 Distribution of the spheres on the vessel bottom, Q07

QUEOS-08
DISTRIBUTION OF MASS ON GROUND [gr/dm²]
10 kg Mo spheres 4,2 mm dia.   T = 300 K □
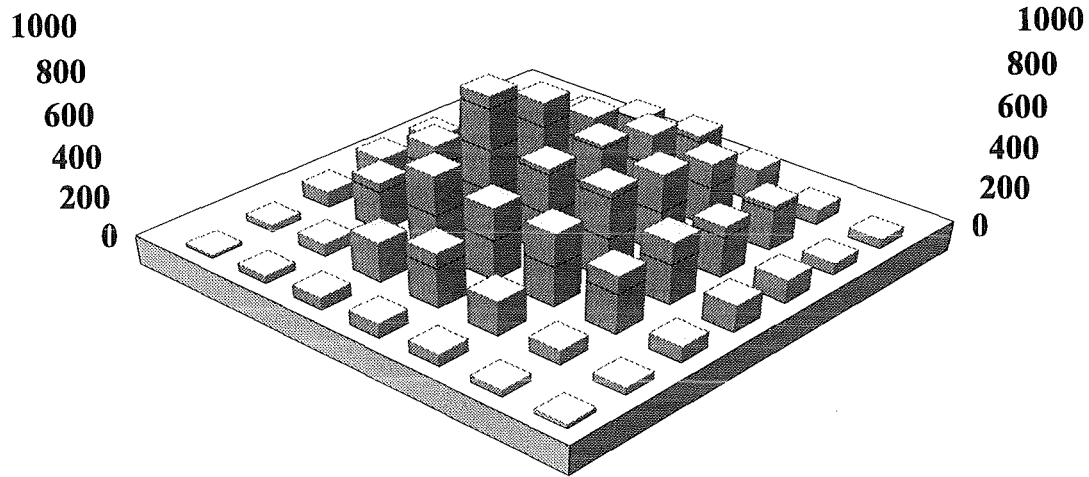
28.6	70	119.8	128.2	78.4	33.3	16.8
116.8	268.2	358.1	304.9	243.9	62.8	37.6
202.7	324.5	516.2	658.4	396.1	197.4	63.4
226	349.1	416.8	424.5	359	271.9	71.8
162	316.5	387.3	431.7	359.9	171.1	60.8
73.9	223.7	251.5	308.7	286.7	73	35
46.2	58.7	115.9	132.5	79	37.4	20.6

Fig. 4.86 Distribution of the spheres on the vessel bottom, Q08

QUEOS-09
DISTRIBUTION OF MASS ON GROUND [gr/dm²]
10 kg ZrO2 spheres 5 mm dia.   T = 1300 K
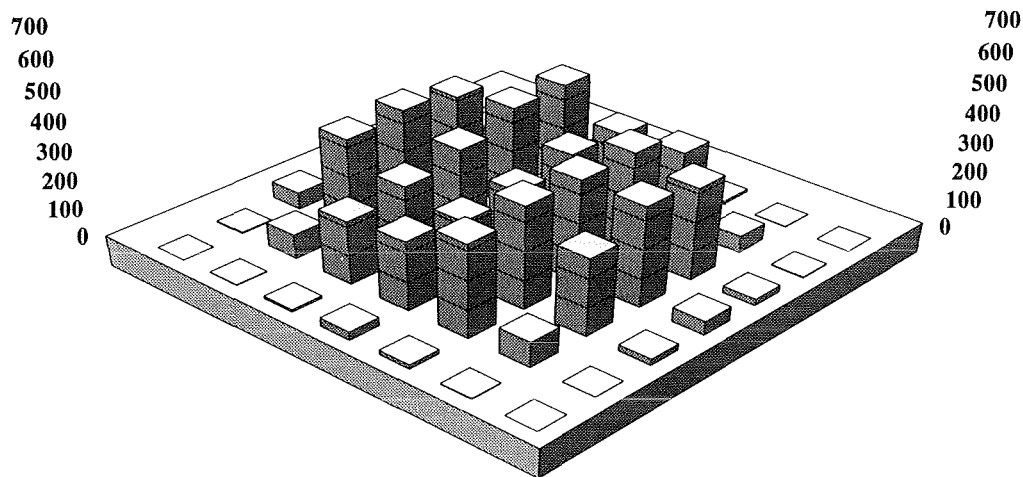
0	3.8	57.9	121.4	71.6	5.5	0
1.6	82.6	326.8	344.6	313.4	88.7	1.7
9.3	218.1	247.1	287.1	349.3	350.5	20.8
29.8	237.9	214	226.2	266.4	254.4	19.6
15	321.1	353	348.3	352.5	268	9.7
3	88.9	267.8	345.7	317.4	58	1.5
0	0.8	22.9	49.1	23.2	3.1	0

Fig. 4.87 Distribution of the spheres on the vessel bottom, Q09

QUEOS-10
DISTRIBUTION OF MASS ON GROUND [gr/dm²]
6,3 kg ZrO2 spheres 10 mm dia.   T = 1780 K
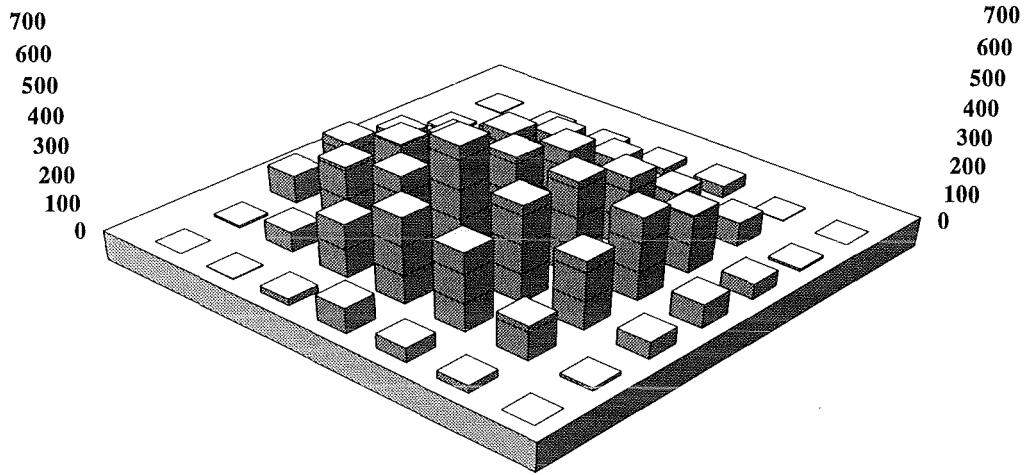
0	8.6	96	131.4	74.4	9	3
2.8	71.4	211.4	205.4	137.6	76.2	9.2
24.2	188.4	261.8	244.6	239.2	143.6	15
89.4	299.4	445.2	321.6	257.8	140.4	24
51	272.4	334.4	323.4	246.6	104	41.4
26.8	121.8	238.2	288.6	203.4	83.8	3
0	11.8	59.6	83.4	53.8	9.4	0

Fig. 4.88 Distribution of the spheres on the vessel bottom, Q10

QUEOS-11

DISTRIBUTION OF MASS ON GROUND [gr/dm²]

5,684 kg Mo spheres 4,2 mm dia.   T = 1780 K
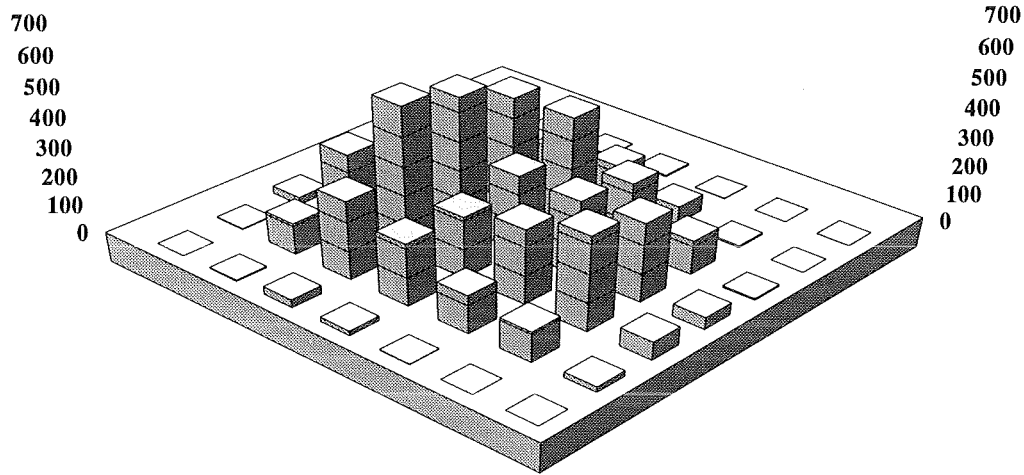
0	3.2	26.2	38.4	10.6	0	0
3.8	108.2	260	210.2	153.2	19.8	0
28.6	271.2	499.8	450.2	368.4	97.2	2.8
16.6	216.2	212 8	263.8	377	123	6.6
2.2	133.4	258.6	261.2	231.8	60	1.6
0	107.4	326.8	273.8	118.4	6.6	0
0	19.6	64.4	43	5.6	0	1

Fig. 4.89 Distribution of the spheres on the vessel bottom, Q11

QUEOS-12
DISTRIBUTION OF MASS ON GROUND [gr/dm²]
6,875 kg Mo spheres 4,2 mm dia.   T = 2250 K
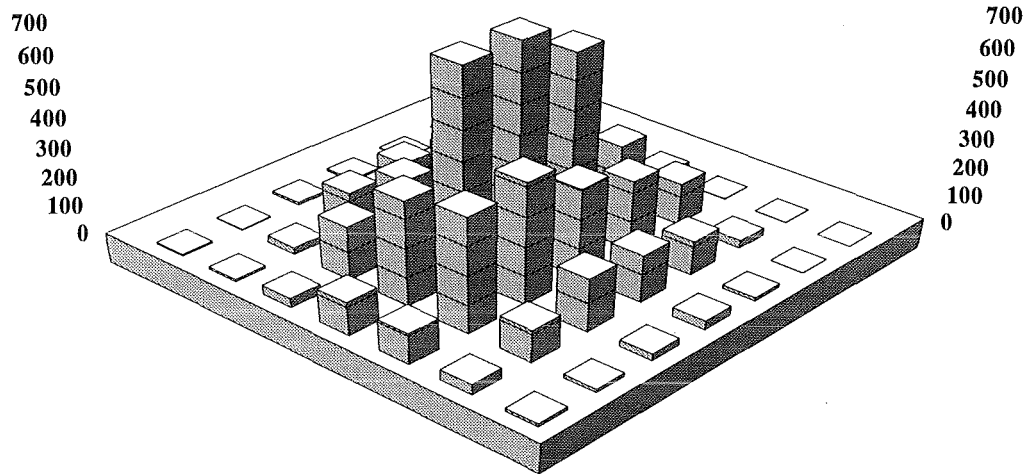
5.6	3.2	8.8	6.8	1.6	0	1.2
7.8	23.2	126.2	144.4	111.2	15.2	1.2
33.2	186	250.6	254.2	392.2	154.6	5.6
116.2	359.2	703	821.4	591.2	195.2	16
107.2	394.6	415	304	240	144	2
36	112.2	184	165.2	117.8	26.6	1.2
10.8	12.2	24.2	31	11.2	1.2	0

Fig. 4.90 Distribution of the spheres on the vessel bottom, Q12

5. CONCLUSION

A first series of experiments with basically three types of spheres has been performed simulating the premixing phase of a steam explosion with molten corium and water. In this series an attempt was made to simulate a compact mass with high solid volume fraction plunging into saturated water.

The main findings are the following:

- the sphere jets take the classical inverted mushroom shape observed for a liquid jet in another liquid;

- especially with small cold spheres a large amount of gas is dragged into the multiphase region;

- the higher the sphere temperature, the faster the leading edge propagates;

- up to 1300 K sphere temperature the evaporation effects are small.

It is obvious that besides the three parameters density, size and temperature of the spheres a fourth parameter, the initial form of the sphere cloud, plays an important role for the further development of the mixing zone. This includes the solid fraction, diameter and length of the pour and uniformity of the cloud. Also the number of spheres changes the mixing process entirely, which might be a a more characteristic parameter than the total mass and diameter of the spheres. For some conditions the test vessel is not deep enough to reach the terminal velocity and to get to the point where the initial gas chimney collapses and does not influence the movement of the spheres anymore. Of course, also the diameter of the vessel has an effect on the form of the mixing zone. There is an upward directed flow around the falling sphere cloud and the velocity of this flow is the larger the smaller the vessel diameter is.

Because of the vast number of parameters it does not seem reasonable to try to set up general laws for the mixing of hot spheres, but rather to describe as accurately as possible the initial and boundary conditions of the experiments and compare the observed results with results from computer simulations, concerning the shape, velocity and the void fraction of the mixing zone, and the steam generation rate.

The series of experiments with a jet diameter of 180 mm is being continued with higher temperatures and higher masses. The temperature of 2500 K has been reached in the meantime. The results of these experiments and the results of the image processing will be published in a separate report.

References:

1. Proceedings of the CSNI Specialists Meeting on Fuel-Coolant Interactions, Santa Barbara, California, USA January 5-8, 1993, NUREG/CP-0127.

2. Nuclear Engineering and Design, Volume 155 (1995), Nos.1-2.

3. C.C. Chu and M.L. Corradini, One-dimensional transient fluid model for fuel/coolant interaction analysis, Nucl. Sci. Eng. 101 (1989), pp. 48-71.

4. W.H. Amarasooriya and T.G. Theofanous, Premixing of steam explosions: a three-fluid model, Nucl. Eng. Des. 126 (1991) 23-39.

5. D.F. Fletcher and A. Thyagaraja, The CHYMES coarse mixing model, Prog. Nucl. Energy 26 (1991), pp 31-61.

6. M.F. Young, Application of the integrated fuel-coolant interaction code to FITS-type pouring mode experiments, Prog. Astronaut. Aeronaut. 134 (1991) pp. 356 - 386.

7. G. Berthoud and M. Valette, Calculations of the premixing phase of an FCI with the TRIO MC code, Proc. CSNI Specialist Meet. On Molten Fuel Coolant Interactions, Santa Barbara, CA, 1993, NUREG/CP-0127, pp.27-36.

8. H. Jacobs, M. Lummer, B. Stehle, K. Thurnay, L. Väth, IVA-KA, a Three-Field Model of Premixing in Steam Explosions; Transactions of the ENC '94 International Nuclear Congress - Atoms for Energy, Lyon, France, 2.-6. 10. 1994, vol. II, p. 542

9. N.I. Kolev, The code IVA-3 for modeling of transient three-phase flows in complicated 3D geometry, Kerntechnik, 58, 147-156 (1993)

10. D. Magallon and H. Hohmann, High pressure corium melt quenching tests in FARO, Nucl. Eng. Design, 155 (1995), Nos.1-2, pp. 253 - 270.

11. H. Hohmann, D. Magallon, H. Schins and A. Yerkess, FCI experiments in the aluminum oxide/water system, Nucl. Eng. Design, 155 (1995), Nos.1-2, pp. 392 - 403.

12. M.K. Denham, A.P. Tyler and D.F. Fletcher, Experiments on the mixing of molten uranium dioxide with water and initial comparisons with CHYMES code calculations, ANS Proc. 5th Int. Topical Meet. On Reactor Thermal Hydraulics (NURETH-5), 1992, pp. 1667-1675.

13. N. Yamano, Y. Maruyama, T. Kudo, A. Hidaka, J. Sugimoto, Phenomenological studies on melt-coolant interactions in the ALPHA program, Nucl. Eng. Design, 155 (1995), Nos.1-2, pp. 369-389.

14. F. Huber, A. Kaiser, W. Schütz, M.Steinbrück, H. Will, Experimental investigation of the premixing behavour of a hot melt in water, Conf. Thermophysics -95, Obninsk, Russia, Nov. 21-24, 1995.

15. S. Angelini, T.G. Theofanous and W.W. Yuen, The mixing of particle clouds plunging into water, NURETH-7, Saratoga Springs, NY, Sept. 10-15, (1995).

16. G. Berthoud, T. Oulmann, M. Valette, Corium-water interaction studies in France, Int. Seminar on Heat and Mass Transfer in Severe Accidents, Cesme, Turkey, May 21-26, 1995.

APPENDIX: Evaluation of the frenquency signals of the volume flow meter

```
/* Programm Name Impulsf1.c..........Datei-Name Impulsf1.c .........
IProgramm-Beschreibung ----MS-C6.0-------------------------------- I
I Durchfluss 100er Rohr !                          I
I Liest aus einer mit TurboLap erstellten ASCII-Datei die        I
I Y-Werte enthaelt. Das Signal muss ein Impulssignal sein, das von   I
I einem Durchflussmesser ( Endres & Hauser ) oder einem Fuellstands-  I
I messer ( Endres & Hauser ) kommt. Die Werte werden gelesen und   I
I in einer Datei, Bildschirm oder Drucker ausgegeben.         I
I 1 Spalte Y-Wert des Signals                    I
I 2 Spalte Gesamt-Zeit des Signals                  I
I 3 Spalte Anzahl der Impulse des Signals               I
I 4 Spalte Impuls Breite ( Anzahl der Sample-Werte )          I
I 5 Spalte Sample-Werte  zwischen zwei Impulsen            I
I 6 Spalte Zeit zwischen zwei Impulsen               I
I 7 Spalte Impuls-Zeit                       I
I 8 Spalte Impuls-Zeit + Zeit zwischen zwei Impulsen          I
I 9 Spalte Sample-Werte zwischen zwei Impulsen + Sample-Impulse   I
I Wenn in Datei geschrieben wird stehen noch folgend Spaltern     I
I zur Verfuegung.                       I
I 1  Spalte Gesamt-Zeit                    I
I 2  Spalte V [l/s]                      I
I 3  Spalte U [m/s]                      I
I 4  Spalte Summe V                       I
I WICHTIG                         I
I Start und Ende der Datei mit TurboLap festlegen dann als ASCII-  I
I Datei abspeichern. ( nur der wichtige Teil der Transiente.  )  I

-----------------------------------------------------------------
I Autor: Kirstahler M.         I              I
I Datum: 11.11.94   I Letzte Bearbeitung      08.02.95     I
---------------------------------------------------------------------*/
#include <process.h>
#include <stdlib.h>
#include <stdio.h>
#include <graph.h>
#include <sys\types.h> /* for creat */
#include <sys\stat.h>  /*   "    */
#include <io.h>      /*   "    */
#include <taste.h>
#include <melib.h>


FILE *stream3;
FILE *stream2;
FILE *stream1;
FILE *drucker;
float  dsz,dt;

char filein [30];    /* Filename Eingabe */
```

```
char  filout [30];    /* Filename  Ausgabe */
char  temp  [30];     /* Filename  Ausgabe */
/*****************************************************************/
main()
 begin

    readf();
    plotdat();
 end
/*****************************************************************/
/*Name fuer Eingabe-Datei eingeben    */
readf()
  begin
       float ywert,alty,frequenz,zl,zi,zg,dz,yh,zgf,zlf,dzf;
       float K,A,d,v,u,pi,gf,vs, dzg, zg_1;
       long int impuls,limpuls,nzeitlow,nzeithigh,il;
       int indatei,aufdrucker,u1,b1;
       long int nzg;


       printf("\n Ergebnise auf Drucker schreiben ja = 1 / nein = 0 :  ");
       scanf("%d",&aufdrucker);


       printf("\n Ausgabe Dateiname :  ");
       scanf("%s",filout);

         if ((stream3 = fopen( filout,"w")) == NULL)
           begin
             fenerr();
           end

       if( aufdrucker == 1 )
         begin
          drucker = fopen( "prn","w");
         end

       printf("\n Siehe TurboLap-ASCII-Datei \n  ");
       printf("\n Eingabe Impuls-Höhe z.B. 9.0 :  ");
       scanf("%f",&yh);

       printf("\n Zeitschritte >= 0.001   :  ");
       scanf("%f",&dt);

       printf("\n Siehe TurboLap-ASCII-Datei \n  ");
       printf("\n Eingabe Impuls-Länge z.B. 4 :  ");
       scanf("%ld",&il);

       printf("\n Siehe TurboLap-ASCII-Datei \n  ");
       printf("\n Eingabe Offset-Start-Zeit 2.0 :  ");
```

```
        scanf("%f",&dsz);

        printf("\n Siehe TurboLap-Ini. \n ");
        printf("\n Eingabe-Frequenz z. B. 30000.0 Hz :  ");
        scanf("%f",&frequenz);

        printf("\n Eingabe-Grenz-Frequenz z. B. 10.0 Hz :  ");
        scanf("%f",&gf);

        printf("\n Von TurboLap erzeugte ASCII-Datei ( Impuls, nur Y- Werte )\n  ");
        printf("\n Eingabe-Datei :  ");
        scanf("%s",filein);

/*************Datei Ende laden ****************************************/
        if ((stream1 = fopen(filein,"r")) == NULL)
         begin
           fenerr();
         end

        limpuls   = 0;
        impuls    = 0;
        nzeitlow  = 0;
        nzeithigh = 0;
        nzg  =     0;
        zg  =      0.0;
        zi  =      0.0;
        zl  =      0.0;
        dz  =      0.0;
        alty =     0.0;
        ywert =      0.0;
        u1 =        0;
        vs =      0.0;
         v=       0.0;
         u=       0.0;
        zg_1 = 0.0;


/***********************************************************************/
      pi = 3.1415927;
      K = 0.9481;      /*  Imp / dm3 */
      d = 1.071;       /* Durchmesser   */
      A = ( d * d ) / 4.0 * pi;  /* Fläche      */
/***********************************************************************/
        if ((stream2 = fopen( "temp.dat","w")) == NULL)
          begin
            fenerr();
          end

      for  ( ;; )
       begin
         fscanf( stream1 , "\ %f\n", &ywert );
```

```
if ( feof ( stream1 ))
  begin
   printf( " File Ende \n " );
   fclose(stream1);
   b1=1;
  end
if ( b1 == 1) break;
if ( ferror ( stream1 ))
  begin
   printf( " File Ende \n " );
   fclose(stream1);
   b1 = 1;
  end
if ( ferror ( stream1 )) break;
nzg++;
if( ywert < yh )
  begin
   nzeitlow++;
  end
 if ( ywert >  yh )
   begin
    limpuls++;
    nzeithigh++;
   end
 if (  limpuls >= il && alty > yh  && ywert < yh )
   begin
       impuls++;
       zg = ( 1.0 / frequenz ) * ((float) nzg ) + dsz;
       zl = ( 1.0 / frequenz ) * ((float) nzeitlow );
       zi = ( 1.0 / frequenz ) * ((float) nzeithigh );
       dz = ( 1.0 / frequenz ) * ((float) (nzeithigh + nzeitlow));
   printf("Y=%7.2fZG=%fl=%6ldIL=%6ldLL=%6ldZL=%fZH=%fDZ=%fNF=%6ld
\n",
          ywert,zg,impuls,limpuls,nzeitlow,zl,zi,dz,nzg);
       v = 1.0 / ( K * dz );
       u = 1.0 / ( K * dz * A * 10.0 );
       dzg =  zg - zg_1;
       zg_1 = zg;
       if ( (( 1.0 / dz )  <  gf)
          || ( impuls == 1  )
          || ( dz > 0.1 ))
         begin
          v = 0.0;
          u = 0.0;
         end
       vs = vs + v * dzg;
       fprintf(stream2," %14.6f %14.6f %14.6f %14.6f\n",
                zg,v,u,vs );
      if( aufdrucker == 1 )
        begin
```

```
            if ( u1 == 0 )
                begin
fprintf(drucker," \n\n ");
fprintf(drucker," 1 Spalte Y-Wert des Signals \n ");
fprintf(drucker," 2 Spalte Gesamt-Zeit des Signals \n");
fprintf(drucker," 3 Spalte Anzahl der Impulse des Signals \n");
fprintf(drucker," 4 Spalte Impuls Breite ( Anzahl der Sample-Werte ) \n");
fprintf(drucker," 5 Spalte Sample-Werte  zwischen zwei Impulsen \n");
fprintf(drucker," 6 Spalte Zeit zwischen zwei Impulsen \n");
fprintf(drucker," 7 Spalte Impuls-Zeit  \n");
fprintf(drucker," 8 Spalte Impuls-Zeit + Zeit zwischen zwei Impulsen \n");
fprintf(drucker," 9 Spalte Sample-Werte zwischen zwei Impulsen + Sample-
Impulse \n");
fprintf(drucker," \n\n ");
                end
    fprintf(drucker," %9.2f %9.6f %6ld %6ld %6ld %9.6f %9.6f %9.6f %6ld \n ",
                    ywert,zg,impuls,limpuls,nzeitlow,zl,zi,dz,nzg);
            end
            limpuls   = 0;
            nzeitlow  = 0;
            nzeithigh = 0;
            u1 = 1;
          end
        alty = ywert;
      end
      if( aufdrucker == 1 ) fclose(drucker);
      fclose(stream2);
      fclose(stream1);
/*****************************************************************/
  end
/*****************************************************************/
  plotdat()
    begin
      float t,vv,v,uu,u,vss,vs,zg,vsumme;

/************Datei Ende laden *************************************/
      if ((stream2 = fopen( "temp.dat","r")) == NULL)
        begin
          fenerr();
        end
/************Datei Ende laden *************************************/
      if ((stream3 = fopen( filout,"w")) == NULL)
        begin
          fenerr();
        end
    t=dsz;
    vsumme = 0.0;

    printf(" UP \n");
    for  ( ;; )
```

```
      begin
        fscanf(stream2," %f %f %f %f\n",&zg,&v,&u,&vs );
        printf(" %14.6f %14.6f %14.6f %14.6f\n",
                  zg,v,u,vs );
         do
           begin
             t = t + dt;
             if( t < zg )
               begin
                 vv = v;
                 uu = u;
                 vss = vs;
                 vsumme = vsumme + v * dt;
                 fprintf(stream3," %14.6f %14.6f %14.6f %14.6f %14.6f\n",
                         t,vv,uu,vss,vsumme);
                 printf(" %14.6f %14.6f %14.6f %14.6f\n",
                         t,vv,uu,vss);
               end
           end
         while ( t < zg );
          t = t - dt;
          if ( feof ( stream2 ))
            begin
             printf( " File Ende \n " );
             fclose(stream2);
             exit(0);
             break;
            end
              if ( ferror ( stream2 ))
            begin
             printf( " File Ende \n " );
             fclose(stream2);
             exit(0);
             break;
            end
      end
          fclose(stream3);
        end
/******************************************************************/


fenerr()
  begin
        _setbkcolor(7L);
        _clearscreen(_GCLEARSCREEN);
        _settextwindow(2,35,7,71);
        _setbkcolor(0L);
        _clearscreen(_GWINDOW);
        _setbkcolor(0L);
        _settextwindow(3,36,6,70);
        _clearscreen(_GWINDOW);
```

```
        printf(" Datei nicht geöffnet ");
        fclose(stream1);
        fclose(stream2);
        while( !kbhit() );
        _setvideomode(_DEFAULTMODE);
        exit(0);
   end
/*******************************************************************/
```

●